

2009

Inhibition of hydroxyapatite growth by osteopontin phosphopeptides

Paul Azzopardi

Follow this and additional works at: <https://ir.lib.uwo.ca/digitizedtheses>

Recommended Citation

Azzopardi, Paul, "Inhibition of hydroxyapatite growth by osteopontin phosphopeptides" (2009). *Digitized Theses*. 4231.

<https://ir.lib.uwo.ca/digitizedtheses/4231>

This Thesis is brought to you for free and open access by the Digitized Special Collections at Scholarship@Western. It has been accepted for inclusion in Digitized Theses by an authorized administrator of Scholarship@Western. For more information, please contact wlsadmin@uwo.ca.

Inhibition of hydroxyapatite growth by osteopontin phosphopeptides

(Spine title: Inhibition of HAP growth by OPN phosphopeptides)

(Thesis format: Monograph)

by

Paul Azzopardi

Graduate Program in Biochemistry

A thesis submitted in partial fulfillment
of the requirements for the degree of
Master of Science

School of Graduate and Postdoctoral Studies
The University of Western Ontario
London, Ontario, Canada

© Paul Azzopardi 2009

ABSTRACT

Biominerals often possess features such as size, shape and crystallinity that are distinct from their abiotically formed equivalents. Organisms are known to achieve this by regulating the crystal growth process. To understand the specific structural features of the phosphoprotein osteopontin (OPN) responsible for its inhibition of hydroxyapatite (HAP) growth, we used a constant-composition seeded-growth assay. In addition to testing the HAP growth-inhibiting effects of the highly phosphorylated bovine milk OPN and the nonphosphorylated rat recombinant OPN, we have also tested the effects of synthetic peptides corresponding to amino acids 220-235 (pSHEpSTEQSDAIDpSAEK) and amino acids 65-80 (pSHDHMDDDDDDDDGD) of rat bone OPN. OPN220-235 was synthesized in triphosphorylated (P3) and nonphosphorylated (P0) forms; OPN65-80 was synthesized in monophosphorylated (P-OPAR) and nonphosphorylated (OPAR) forms. Also studied was poly-L-aspartic acid (poly-Asp) of 11 kDa. Highly acidic and phosphorylated peptides/proteins were observed to be the most potent inhibitors of HAP growth. The 50% inhibitory concentrations measured were: poly-Asp, 1.45 µg/ml; P-OPAR, 1.65 µg/ml; milk OPN, 1.94 µg/ml; P3, 2.03 µg/ml; OPAR, 2.47 µg/ml; recombinant OPN, 5.23 µg/ml; and P0, >75 µg/ml. The thermodynamics of OPN and OPN-sequence-derived peptides adsorbing onto the surface of HAP was probed using isothermal titration calorimetry. At 37°C, adsorption of all strong inhibitors is characterized by an endothermic enthalpy that rapidly diminishes to zero when HAP surface coverage approached 10%. The free energy of adsorption is dominated by large positive entropy change, likely resulting from the liberation of water molecules from the HAP surface. It appears that negative charge, whether contributed by phosphorylated or acidic residues, is a prerequisite for the entropically driven adsorption to and growth inhibition of HAP.

Key Words: phosphoprotein, osteopontin, rat bone osteopontin, bovine milk osteopontin, hydroxyapatite growth, biomineralization, constant-composition, isothermal titration calorimetry, thermodynamics, hydroxyapatite adsorption, protein-mineral interaction.

ACKNOWLEDGMENTS

First and foremost, I would like to thank my family (Mom, Dad, Charlene and Michelle) for their love and support. You were always there whenever I needed help. Thanks Mom and Dad for making your culture a part of my life and exposing me to my heritage. Besides getting to have a relationship with all my extended family I have made many life altering friendships over the years. The islands allowed me to escape from everyday life when I thought it was becoming too much to bear, for me they are truly gems of the Mediterranean.

I would like to thank my supervisors, Dr. Graeme Hunter and Dr. Harvey Goldberg, for their guidance and support; I admire both of you immensely. I have truly enjoyed the time I have spent in your labs and have learned a lot along the way. To my committee members, Dr. James Choy and Dr. Jeffrey Hutter, thanks for your advice and support as well.

A big thank you to the past and present members of the Hunter and Goldberg labs, Gurpreet, Aaron, Krista, Jason, Ron, Erik, Vašek, Brian, Bernd, Hong, Heidi, Kyle, Kamal, Mac, Dave, Susanna and Kari Ann. You were always there when I needed you and were amazing to learn with, work with, and party with. My project would not have existed without the help of Hong, Bernd and Heidi, thanks for your assistance and patience with me. Thanks to my friends/family in Woodbridge (Mike, James, John-Paul, Alex, and Rocco) and Malta (Mark, Shawn, Jerry, Nyam, and Joseph) and roommate Mark, you were always there when I needed to be cheered up or just a break from science. Lee-Ann Briere, thanks for your help and infinite patience with me in the BICF. Dr. Dunn, not only do you manage/head a great scientific facility, the BICF, but my first escapade at the science of wine making would have been a miserable failure without your help, thank you. Thanks to the members of the CIHR group, you were awesome to work

and go to conferences with. Thanks to Dr. Beth Gillies for taking the time to help me synthesize hydroxyapatite crystals. Thanks to Dr. James Choy and Dr. Gary Shaw for letting me use equipment in their labs whenever needed. Anyone else I may have forgotten to mention that has willingly set aside time to assist me, I appreciate your help.

This degree has been an amazing journey. From Ghawdex to Florida, North/South Carolina, Baltimore, Washington D.C., Philadelphia, Montreal, Nicaragua, and soon to be Australia, I've visited more places during the 2 years of my Masters than the preceding 23 years of my life. I am still in awe whenever I think about the fact that I was given a car by a former labmate. I admire your generosity and feel special that you chose to give the car to me, rather than anyone else you could have chosen. Thanks for the never ending adventure as well.

These are relationships that have far surpassed the level of professional acquaintances, we have become great friends. For the last two years you have been my fellow winemakers, drinking partners, wingmen, surfers, SCUBA divers, mechanics, work-out partners, campers, snowboarders, painters, movers, and roommates. We've created a lot of memories in a short time, from knock-outs (unintentional of course!), GC escapades and recreations. The level of friendship we attained I am sure is the envy of most other labs. I hope that I was able to give back even the smallest fraction of what I feel I have received during this time. Science is at a loss for not having more people like you, your sense of humour and carefree spirit was sometimes the only thing I was looking forward to in the lab. You not only made the days fly by, but made them absolutely enjoyable. Thanks to BLACKBIRDS for the opportunity to be a roadie on their tour, you are amazing people that, in just a few short days, changed my life for the better, it was also incredible fun.

TABLE OF CONTENTS

CERTIFICATE OF EXAMINATION.....	ii
ABSTRACT.....	iii
ACKNOWLEDGEMENTS.....	iv
LIST OF TABLES.....	viii
LIST OF FIGURES.....	ix
LIST OF ABBREVIATIONS.....	x
Chapter One – Literature Review.....	1
1.1 Introduction.....	2
1.1.1 Overview of proteins and biomineralization.....	2
1.1.2 SIBLING Proteins.....	6
1.1.3 General introduction to osteopontin.....	7
1.2 Osteopontin Genetic Structure and Expression.....	8
1.2.1 Organization	8
1.2.2 Regulation	8
1.2.3 Isoforms	10
1.2.4 Expression and tissue distribution.....	11
1.3 Osteopontin Protein Structure.....	12
1.3.1 Primary structure and sequence conservation.....	12
1.3.2 Higher-order structure.....	13
1.4 Post-translational Modifications.....	15
1.4.1 Phosphorylation.....	15
1.4.2 Glycosylation.....	19
1.4.3 Transglutamination.....	20
1.4.4 Proteinase cleavage.....	21
1.5 Physiological Roles of Osteopontin.....	22
1.5.1 Bone and tooth development.....	22
1.5.2 Immune system.....	24
1.5.3 Tumour growth and metastasis.....	26
1.5.4 Nephrolithiasis.....	27
1.5.5 Atherosclerosis and native/prosthetic valves.....	30
1.6 Protein-Crystal Interactions.....	32
1.6.1 Crystal formation and growth.....	32
1.6.2 Roles of proteins in biomineralization.....	36
1.6.3 Inhibition/modulation of crystal formation by OPN and other proteins...38	
1.7 Purpose of Thesis.....	42
Chapter Two – Constant Composition Seeded Growth Studies.....	43

2.1	Introduction.....	44
2.2	Materials and Methods.....	46
2.2.1	Chemicals and Reagents.....	46
2.2.2	Synthesis of hydroxyapatite seed crystals.....	47
2.2.3	Characterization of synthesized hydroxyapatite seed crystals.....	48
2.2.4	Constant-composition seeded-growth.....	49
2.2.4.1	Constant-composition seeded-growth assay.....	49
2.2.4.2	Determination of calcium and phosphate concentration.....	51
2.2.5	Protein expression/purification and peptide synthesis/purification.....	51
2.2.6	Circular dichroism of osteopontin peptides.....	52
2.3	Results.....	52
2.3.1	Characterization of synthesized HAP.....	52
2.3.2	Circular dichroism secondary structure prediction.....	55
2.3.3	Constant-composition seeded-growth assay.....	55
2.3.4	Protein/peptide inhibitory potency toward HAP growth.....	73
2.4	Discussion.....	86
2.4.1	Constant-composition seeded-growth assay.....	86
2.4.2	Peptide secondary-structure analysis.....	87
2.4.3	HAP growth inhibition by proteins/peptides.....	88
Chapter Three – Isothermal Titration Calorimetry of the Osteopontin-Hydroxyapatite Interaction.....		93
3.1	Introduction.....	94
3.2	Materials and Methods.....	95
3.2.1	Chemicals and reagents.....	95
3.2.2	Equilibrium adsorption isotherm.....	96
3.2.3	Isothermal titration calorimetry.....	97
3.3	Results.....	98
3.3.1	Equilibrium adsorption isotherm.....	98
3.3.2	Isothermal titration calorimetry.....	109
3.4	Discussion	122
Chapter Four – Summary, Perspectives and Future Directions.....		128
4.1	Summary and Perspectives.....	129
4.2	Future Directions.....	133
References.....		136
Curriculum Vitae.....		157

LIST OF TABLES

Table 2.1	Summary of average fractional secondary structure of P3, P0, OPAR and P-OPAR.....	62
Table 2.2	Summary of constant-composition seeded-growth results.....	85
Table 3.1	Summary of equilibrium adsorption isotherm N_{max} , and K_D for the proteins investigated.....	108
Table 3.2	Summary of isothermal titration calorimetry K , ΔH , ΔS and ΔG for proteins investigated.....	121

LIST OF FIGURES

Figure 1.1	Multiple sequence alignment of OPN amino acid sequence indicating phosphorylated residues.....	17
Figure 1.2	Illustration of topographical features of crystal surfaces.....	33
Figure 2.1	SEM image of synthesized HAP crystals.....	53
Figure 2.2	X-ray powder diffraction pattern of synthesized HAP.....	56
Figure 2.3	Analysis of P3 and P0 by circular dichroism spectroscopy.....	58
Figure 2.4	Analysis of OPAR and P-OPAR by circular dichroism spectroscopy.....	60
Figure 2.5	Schematic of constant-composition seeded-growth assay.....	63
Figure 2.6	Detailed schematic of constant-composition seeded-growth assay.....	65
Figure 2.7	Example HAP growth curve.....	69
Figure 2.8	Rate of HAP growth versus mass of seed HAP crystals.....	71
Figure 2.9	Rate of HAP growth in the presence of increasing concentrations of mOPN.....	74
Figure 2.10	Rate of HAP growth in the presence of mOPN and rOPN.....	76
Figure 2.11	Rate of HAP growth in the presence of P3 and P0.....	78
Figure 2.12	Rate of HAP growth in the presence of P-OPAR and OPAR.....	81
Figure 2.13	Rate of HAP growth in the presence of poly-Asp.....	83
Figure 3.1	Equilibrium Adsorption Isotherm of P3.....	100
Figure 3.2	Equilibrium Adsorption Isotherm of P0.....	102
Figure 3.3	Equilibrium Adsorption Isotherm of rOPN.....	104
Figure 3.4	Equilibrium Adsorption Isotherm of poly-Asp.....	106
Figure 3.5	Calorimetric titration of HAP with rOPN.....	110
Figure 3.6	Calorimetric titration of HAP with mOPN.....	112
Figure 3.7	Calorimetric titration of HAP with poly-Asp.....	115
Figure 3.8	Calorimetric titration of HAP with P3.....	117
Figure 3.9	Calorimetric titration of HAP with P0.....	119

LIST OF ABBREVIATIONS

AARP	Aspartic acid-rich protein
ATR-FTIR	Attenuated total reflection Fourier transform infrared spectroscopy
BAG	Bone-acidic glycoprotein-75
BET	Brunauer-Emmett-Teller
BRCA1	Breast Cancer 1
BRMS1	Breast cancer metastasis suppressor 1
BSP	Bone sialoprotein
BSP I	Bone sialoprotein 1
BSNP	Bone sialoprotein 1
CaOx	Calcium oxalate
CaP	Calcium-phosphate
Cbfa1	Core binding factor alpha 1
CCSG	Constant-composition seeded-growth
CD	Circular dichroism
CK1	Casein kinase 1
CK2	Casein kinase 2
CCSG	Constant-composition seeded-growth
DMP1	Dentin matrix protein 1
DPP	Dentin phosphoprotein
DSP	Dentin sialophosphoprotein
EAI	Equilibrium adsorption isotherm
ECM	Extracellular matrix
ENAM	Enamelin
ePi	Extracellular phosphate
Eta-1	Early T-cell activation-1
FPLC	Fast protein liquid chromatography
FTIR	Fourier-transform infrared
G-CK	Golgi apparatus casein kinase
GRE	Glucocorticoid response element
HAP	Hydroxyapatite
ICP-AES	Inductively coupled plasma-atomic emission spectroscopy
IC ₅₀	50% inhibitory concentration
IL-1 β	Interleukin-1 β
iOPN	Intracellular osteopontin
ITC	Isothermal titration calorimetry
MALDI-TOF	Matrix-assisted laser desorption time-of-flight

MEPE	Matrix extracellular phosphoglycoprotein
MGP	Matrix gla protein
MMP3	Matrix metalloproteinase 3
MMP7	Matrix metalloproteinase 7
MMP9	Matrix metalloproteinase 9
mOPN	Milk osteopontin
NKT	Natural killer T
NMR	Nuclear magnetic resonance
np-OPN	nonphosphorylated osteopontin
NRK	Normal rat kidney
OC	Osteocalcin
ON	Osteonectin
OPAR	Osteopontin poly-Asp region
P-OPAR	Phosphorylated osteopontin poly-Asp region
OPN	Osteopontin
Osx	Osterix
Poly-Asp	Poly-aspartic acid
Poly-Glu	Poly-glutamic acid
PONDR	Predictors of naturally disordered regions
PRP	Proline-rich protein
pS	phosphoserine
pT	phosphothreonine
PTEN	Phosphatase and tensin homologue
PTH	Parathyroid hormone
Ric	Rickettsia resistance
rOPN	Recombinant osteopontin
Runx2	Runt-related transcription factor 2
SEM	Scanning electron microscopy
SIBLING	Small integrin-binding ligand, N-linked glycoprotein
SPP1	Secreted phosphoprotein 1
THP	Tamm-Horsfall protein
TG	Transglutaminase
TGF β	Transforming growth factor β
THP	Tamm-Horsfall protein
TIMP	Tissue inhibitors of metalloproteinases
TNF α	Tumour necrosis factor α
VDRE	Vitamin D response element
5' UTR	5' untranslated region

Chapter One – Literature Review

1.1 Introduction

1.1.1 Overview of proteins and biomineralization

Over the last half a billion years, organisms of many different phyla have evolved the ability to form the over 64 different biominerals known to date (reviewed in [1]). The geological record indicates that biomineralization of many diverse phyla appears to have occurred over a relatively short period. Since these phyla had already diverged before the appearance of biominerals in the fossil records, it is believed to have arisen as a result of the co-optation of an ancestral biomineralization system [2].

Biomineralization refers to the process through which living organisms produce minerals (reviewed in [3]). More specifically, the term biomineral has been coined in order to emphasize the fact that biologically produced minerals are composites that comprise both mineral and organic components that form under exquisitely controlled conditions. Biominerals often possess features such as size, shape and crystallinity that are distinct from their abiotically formed equivalents. This remarkable capability is encoded in the genomes of biomineralizing organisms, which are able to produce biomolecules that induce the nucleation of specific mineral polymorphs and control their subsequent growth.

Early studies on biomineralization revealed two distinct mechanisms through which organisms precipitate mineral salts. These have become known as biologically induced and biologically controlled biomineralization [4, 5]. In biologically induced biomineralization, organisms control the solution composition to favour the precipitation

of particular mineral phases. This indirect control of mineralization results in modest regulation over the type/habit of mineral precipitated [4, 6, 7]. This lack of control has been overcome by organisms that utilize biologically controlled biomineralization. In this process organisms direct the formation and location of biominerals using specific biological molecules tailored to control the nucleation, growth, and morphology of the crystals (discussed in [5, 8, 9]). They may also use cell transport systems, if required, to deposit the precipitated material in its final location. This type of biomineralization can occur extra- or intra-cellularly.

The common characteristics of these molecules, despite all being evolutionarily adapted to precipitate and direct the growth of different crystal phases or polymorphs, are particularly intriguing. For instance, the proteins of magnetotactic bacteria involved in magnetosome production, which consist of 30–50 nm iron oxide (Fe_3O_4) or iron sulfide ($\text{Fe(II)Fe(III)}_2\text{S}_4$) crystals, possess glycine-leucine repeats [10] similar to the repeats in silk fibroin-like proteins involved in the formation of calcium-based minerals in mollusc shells (discussed in [11–13]). Diatoms, the most common type of phytoplankton, are able to create their unique porous silica (SiO_2) cell walls utilizing silaffin peptides that are post-translationally modified with polyamine molecules (discussed in [14]). The rapid formation of supramolecular biomineral assemblies is achieved through silaffin-mediated precipitation of silica, followed by intermolecular interactions between the highly serine-phosphorylated silaffins and polyamines. Echinoderms such as sea urchins and starfish also utilize acidic proteins and several proline-rich proteins (PRPs) during the formation of their calcite (CaCO_3) endoskeletons [15, 16]. In the cases illustrated above, the isolated biomineralization proteins are able to induce the nucleation of their mineral

phases *in vitro*. Furthermore, the nucleation and growth of these minerals occur at physiological temperature and pH, unlike their geological counterparts.

Many plant species are also able to biomineralize crystals within their roots, stems, leaves, flowers, fruits and seeds [17]. These crystals are almost always composed of calcium oxalate (CaOx), and the species-specific morphologies indicate that their nucleation and growth are highly regulated (reviewed in [18]). The protein associated with CaOx precipitation in plants has recently been discovered to be highly acidic in character, although further elucidation of its biochemical properties and mechanism of action require further study [19]. Unsurprisingly, the hydroxyapatite [$\text{Ca}_{10}(\text{PO}_4)_6\text{OH}_2$] crystals of bone and teeth are also believed to be nucleated by poly-anionic proteins such as bone sialoprotein (BSP) and dentin matrix protein 1 (DMP1), respectively [20, 21]. The acidic proteins involved in each of these unique crystallization processes are thought – despite their disordered secondary structure – to provide a template structure that is able to direct the *de novo* formation of specific mineral phases, as was previously shown for aspartic acid-rich mollusc shell matrix proteins [22].

Organisms are also known to possess the ability to influence the morphology, size and orientation of biominerals by regulating the crystal growth process. Several glycoproteins from sea urchin spines have been found to be in contact with crystal planes parallel to the crystallographic *c* axis of growing calcite and are believed to control growth perpendicular to this axis [23]. Similarly, two proteins purified from the aragonite of red abalone nacre, AP7 and AP24, have been shown to restrict the growth of calcite in specific directions [24]. These proteins were found to lack secondary structure. Further study of sea abalone shell proteins led to the identification of perlwapin, a protein

containing acidic domains, which was found to be a potent inhibitor of calcite growth [25]. Perlwapin is also thought to inhibit the growth of certain crystallographic planes as it was found to bind tightly to distinct step edges.

Regulation of crystal growth in humans is known to occur both physiologically and pathologically. The supersaturation of pancreatic juice with calcium carbonate may lead to pancreatic lithiasis. These stones have been observed to contain lithostathine protein, which is able to modify the habit and inhibit the growth of calcite crystals *in vitro* [26]. Remarkably, X-ray crystallographic structures of lithostathine and molecular dynamics simulations suggest that regions of lithostathine progressively unfold as they approach and bind to the surface of calcite.

In the oral cavity, acidic PRPs, statherins, histatins and cystatins in saliva, which is supersaturated with respect to HAP, are believed to prevent the growth of calcium salts on teeth (discussed in [27, 28]). Unlike saliva, human urine is often supersaturated with respect to several mineral phases. These include several forms of calcium phosphate, calcium oxalate and uric acid. Several inhibitors of mineral growth have been discovered in urine, such as nephrocalcin, Tamm-Horsfall protein (THP) and osteopontin (OPN) [29, 30]. Most are predominantly composed of acidic residues and all have been shown to inhibit the *in vivo* growth of several mineral phases. Mice lacking OPN, THP or both have been found to spontaneously form calcium phosphate (CaP) salts in the renal papillae in 10%, 14.3% and 39.3% of animals, respectively [30].

The mineralized matrix of bone also contains several proteins thought to be involved in the regulation of mineralization and growth of HAP, although each protein's specific *in vivo* functions within this organ have yet to be elucidated. These include osteocalcin

(OC), osteonectin (ON), bone-acidic glycoprotein-75 (BAG-75), bone sialoprotein (BSP) and OPN (discussed in [31]). Although each protein is extensively post-translationally modified and contains a high proportion of acidic residues, *in vitro* assays show that BSP, but not OPN, OC or ON, is able to nucleate HAP, whereas OPN and OC, but not BSP or ON, are able to inhibit *de novo* HAP formation [32].

1.1.2 SIBLING Proteins

The Small Integrin-Binding Ligand, N-linked Glycoprotein (SIBLING) protein family is composed of seven genetically related proteins: BSP, OPN, DMP1, dentin sialoprotein (DSP), dentin phosphoprotein (DPP), enamelin (ENAM) and matrix extracellular phosphoglycoprotein (MEPE) [33]. SIBLING proteins are predominantly found in bone and dentin, where they are secreted into the extracellular matrix (ECM) prior to and during tissue mineralization. The genes coding for members of the SIBLING protein family are similarly organized and are all located on human chromosome 4q21-23 [34]. These proteins share several common features: an Arg-Gly-Asp (RGD) cell-binding/signalling motif, acidic nature (rich in Asp and Glu) and presence of post-translational modifications such as phosphorylation, glycosylation and sulfation (for review, see Qin *et al.* [35]).

The fact that SIBLING proteins are abundant in mineralized tissues and supersaturated body fluids such as urine and breast milk suggests that they possess important roles in both physiological and pathological forms of calcification. Several SIBLING proteins have been demonstrated, using both *in vitro* and *in vivo* models, to stabilize solutions supersaturated with respect to particular mineral phases (e.g. HAP)

[36-38]. Others have been shown to promote HAP nucleation *in vitro* (e.g. BSP) [20]. The ability of these proteins to induce and/or inhibit mineralization is often attributed to either their poly-acidic [poly-glutamate (poly-Glu) or poly-aspartate (poly-Asp)] regions or to their numerous phosphoserine residues [37-39].

1.1.3 General introduction to osteopontin

The protein that would eventually come to be known as osteopontin was first described as a protein marker of epithelial cell transformation [40]. OPN was first characterized from mineralized rat bone as a 44-kDa phosphoglycoprotein [41, 42]. This acidic, highly post-translationally modified protein of approximately 300 residues contains an RGD cell-binding motif and conserved poly-Asp region [42-45]. Although bone OPN has a mass spectrometrically determined molecular weight of approximately 38-kDa, the highly acidic nature and substantial post-translational modifications of the native protein cause it to migrate anomalously on SDS-PAGE gels, in which it typically migrates between the 45- and 60-kDa molecular weight markers [41, 42, 46-48].

OPN is a disordered protein [49-52] that is able to bind to calcium ions and mineral faces, the latter with high affinity [44]. In addition to its role in biomineralization OPN is known to be a key regulator of osteoclast differentiation and activity [53]. It is able to interact with a wide range of molecular partners located in the ECM (e.g., fibronectin, collagen), cell-surface integrins (α_v [β_1 , β_2 or β_5] and [α_4 , α_5 , α_8 , α_9] β_1) and several matrix metalloproteinases (MMP2, MMP3, MMP7, MMP9 and MMP12) [53-56].

The scope of the molecule's functions has diversified significantly since its discovery. It is now known to be present in all bodily fluids [57, 58] and is expressed by cells in

bone, kidney, uterus, gastrointestinal tract, and lungs, among others [57, 59-63]. OPN is also involved in many physiological processes such as biomineralization, immunity and apoptosis (reviewed in [64]). Its independent discoveries in diverse tissues has given rise to a multitude of names referring to this single gene product: secreted phosphoprotein 1 (SPP-1) the official gene name, bone sialoprotein I (BSP-I or BNSP), early T-lymphocyte activation 1 (Eta-1), 2ar and Rickettsia resistance (Ric), but the protein is most commonly referred to as OPN [41, 44, 65].

1.2 Osteopontin Genetic Structure and Expression

1.2.1 Organization

Human OPN is encoded by a single-copy gene located on the long arm of chromosome 4 in region 13 (4q13) that codes for a protein 314 amino acids in length [62, 66]. The OPN gene is composed of 7 exons, 6 of which contain coding sequence [62, 67]. Exon 1 and a portion of exon 2 contain the 5' untranslated region (5' UTR) [68]. The majority of OPN is encoded by the last two exons; exons 2, 3, 4, 5, 6 and 7 code for 17, 13, 27, 14, 108 and 134 amino acids, respectively [68]. All intron-exon boundaries in the OPN gene are of the phase 0 type (between two codons), thus any alternative splicing of exons maintains the reading frame of the gene.

1.2.2 Regulation

Regulation of the osteopontin gene is incompletely understood. Furthermore, different cell types may differ in their mechanisms of regulating OPN expression. In

bone, the expression of OPN predominantly occurs by the bone-forming cells (osteoblasts, osteocytes) and bone-resorbing cells (osteoclasts) [69]. The transcription factors Runx2 (aka Cbfa1) and osterix (Osx) are required for the differentiation of osteoblast progenitor cells into mature osteoblasts [70, 71]. Their importance in bone development is exhibited by the complete absence of bone in mice lacking either of the genes coding for these transcription factors [72]. Additionally, *Osx*-null mouse embryos do not express osteoblast marker transcripts, including OPN [71]. Predictably, Runx2 and Osx are able to bind the promoters of osteoblast-specific genes such as *Colla1*, *Bsp* and *Opn* and upregulate transcription [70]. Cells cotransfected with a Runx2 expression vector display a 4-fold increase in OPN expression [70].

Instances that stimulate kidney proximal tubule cells to produce $1\alpha,25$ -dihydroxyvitamin D3 (calcitriol), such as hypocalcemia and hypophosphatemia, lead to increases in OPN transcription, translation and secretion [73]. This occurs as a result of the presence of a high-specificity vitamin D response element (VDRE) in the OPN gene and may be indicative of a role for OPN in bone resorption [74-76].

Recently, extracellular inorganic phosphate (ePi) has also been identified as a modulator of OPN expression [77]. The ePi-responsive region was localized to bases -1454 to -1401 of the OPN promoter in murine cementoblasts. This 53-bp region contains a glucocorticoid response element (GRE) required for the ePi-mediated increase in transcription. Working with cementoblasts transfected with osteopontin luciferase-promoter constructs, Fatherazi *et al.* observed a 63-fold increase in OPN promoter activity in the presence of 3 mM ePi [77]. An increase in the expression of mineralization-associated genes was also exhibited by vascular smooth-muscle cells –

which *in vivo* may undergo ossification – in the presence of elevated levels of ePi [38]. This response may be an adaptive defense against ectopic calcification [38].

Although detailed mechanistic understandings of the regulatory pathways are not yet known, stimulation of OPN transcription has been observed subsequent to exposure of cells to pro-inflammatory cytokines [78], classical mediators of acute inflammation such as tumour necrosis factor α (TNF α) and interleukin-1 β (IL-1 β) [58, 79, 80], as well as angiotensin II, transforming growth factor β (TGF β) and parathyroid hormone (PTH) [81, 82]. Increased OPN expression has also been detected during times of hyperglycemia and hypoxia [81, 83-87]. Evidently more investigations are required to completely understand the mechanistic details involved in the complex regulation of OPN expression.

1.2.3 Isoforms

Most studies on OPN have centred on the fact that it is secreted into the ECM or biological fluids. Recently the extracellular exclusivity of OPN has come into question. Growing evidence demonstrates that intracellular OPN (iOPN) is involved in a number of cellular processes including migration, fusion and motility [88-91]. It appears that the intracellular variant of OPN is generated using an alternative translation start site on the mRNA species used to generate the extracellular isoform [92]. Utilization of the downstream alternative start site produces OPN lacking an N-terminal endoplasmic reticulum-targeting signal sequence, allowing cytoplasmic translation of OPN [92]. Antigen-presenting cells such as dendritic cells and macrophages have been shown to be particularly rich in iOPN, which has been found to activate podosome formation in

plasmacytoid dendritic cells [92], although further research is required to fully understand its role within cells.

Genes providing a survival advantage to cancer cells are typically dysregulated by aberrant expression or splicing [93, 94]. Multiple splice variants of OPN have been observed to be expressed by various human breast cancers both *in vivo* and *in vitro* [95, 96]. These cancer specific splice variants have been termed osteopontin-a, osteopontin-b and osteopontin-c. Osteopontin-b lacks exon 5 whereas osteopontin-c lacks exon 4 [95]. OPN-c, which remains soluble as a result of its inability to associate with the ECM, has been found to be a highly specific marker for transformed cells [95]. This ability to remain soluble has been suggested to facilitate the anchorage-independent phenotype of some human breast cancer cells [95].

1.2.4 Expression and tissue distribution

Unlike other members of the SIBLING protein family, osteopontin is expressed by a diverse array of tissues and found in all bodily fluids [57]. Early studies revealed that in addition to bone, OPN mRNA is expressed in tissues such as the kidney, ovary and uterus [59-63]. Subsequently, OPN was shown to be secreted by epithelial cells and present in biological fluids such as plasma [97], milk [98], saliva, bile and urine [99] (reviewed in [58]). In humans, the protein is found as a prominent layer on the luminal surfaces of populations of epithelial cells in the gastrointestinal tract, gall bladder, pancreas, lung, breast, salivary glands, sweat glands and urinary/reproductive tracts [57]. In spite of its widespread incidence in the human body, OPN was not detected in several sites, including lymph nodes, spleen and skeletal muscle [57].

Consistent with its proposed involvement in the regulation of biomineralization, OPN is localized to osteogenic tissues during mouse embryogenesis [60]. Merry *et al.* showed that osteoclasts actively resorbing bone display the highest level of OPN expression. Preosteoblasts were observed to express slightly lower levels than active osteoclasts [69]. Within mature bone, OPN is found concentrated at the surfaces of bone trabeculae and in cement lines, sites where new bone is deposited onto older bone during remodeling [100].

1.3 Osteopontin Protein Structure

1.3.1 Primary structure and sequence conservation

The primary sequence of osteopontin reveals a copious amount of charged residues, few hydrophobic residues and a high proportion of disorder-promoting residues (D, M, K, R, S, Q, P and E) [101]. Serine, glutamic acid, glutamine, aspartic acid and asparagine comprise approximately one half of OPN's amino acid content [44]. 26 of 55 serine residues and 26 of 33 glutamic acid residues in rat OPN appear in S-X-E *O*-glycosylation motifs [44].

Osteopontin possesses several conserved regions including an RGD motif that binds the $\alpha_v\beta_3$ integrin cell-surface receptor, a poly-Asp region and a thrombin-cleavage site [102]. Mammalian osteopontins are identical in approximately 40% of their amino acid residues. A comparison of human and mouse OPN reveals they are identical at approximately 63% of their amino-acid positions [103]. Serine residues are among the most highly conserved (24%), followed by the acidic residues aspartate (19%) and glutamate (17%) [104]. The high prevalence of conserved acidic amino acids suggests

negative charge may play an important role in osteopontin function. The conservation of serine residues even in less well-conserved areas of OPN suggests site-specific phosphorylations may be critical for the function of the protein [105]. Mass spectrometric analysis of OPN phosphorylation sites has revealed that, of the residues located in either a casein kinase 2 (CK2) or golgi apparatus casein kinase (G-CK) consensus site, approximately 20% satisfy the CK2 consensus sequence whereas 80% possess a G-CK consensus sequence [46, 106-108].

1.3.2 Higher-order structure

Although the three-dimensional structure of osteopontin was not known during the early years of its study, the historical view that protein structure is a prerequisite for function led to the assumption that OPN possesses secondary and tertiary structure. In 1989, Prince used five computer models to predict the structure of OPN based on its amino-acid sequence [43]. His results suggested that up to 41% of the protein exists in α -helices [43]. Polymeric OPN, created through transglutaminase cross-linking of OPN monomers, has also been observed to possess a more ordered structure than monomeric OPN, with disorder decreasing by ~13% [54]. Gorski *et al.* were the first to provide evidence that rat bone OPN is an unstructured protein [50]. Using circular dichroism (CD) spectropolarimetry and Fourier-transform infrared (FTIR) spectroscopy, they showed that soluble rat bone OPN possesses a disordered structure, with the amount of disorder escalating with increasing calcium concentration [50]. It was also shown that at high concentrations (>15 mg/ml) OPN exhibits a more-organized structure, although the

in vivo relevance of this finding is uncertain. To date OPN has not been crystallized, precluding X-ray diffraction analysis.

The results suggesting the disordered nature of OPN have more recently been supported by the findings of Fisher *et al.* [49]. At a concentration of 15 mg/ml, recombinant OPN was found to be devoid of fixed tertiary structure in solution using one-dimensional nuclear magnetic resonance (NMR) spectroscopy [49]. Recent advances in the understanding of protein folding have increased the accuracy of computationally predicted protein structures. One such neural network known as Predictors of Natural Disordered Regions (PONDR) [51] also supports the experimental evidence that OPN is a disordered protein, predicting that the overwhelming majority of the length of OPN lacks defined secondary and tertiary structure.

Most recently, using attenuated total reflection Fourier transform infrared spectroscopy (ATR-FTIR), Gericke *et al.* measured the effect of calcium-ion concentration and adsorption to HAP on the structure of bovine milk and rat bone OPN [52]. This group observed no change in the random-coil structure of either protein analyzed under conditions of increasing calcium ion concentrations. Upon adsorption to HAP crystals, the results indicated a slight increase (several percent) in β -strand content of bovine milk, but not rat bone, OPN. As noted by Gericke *et al.*, the observed shift to lower wave numbers actually occurred beyond the limit of secondary-structure change detectable by current ATR-FTIR technology [52]. Nevertheless, in agreement with previous structural data on OPN, the ATR-FTIR datum reveals the structure remains largely disordered in the presence of HAP.

After reviewing recurrent α -helical motifs in naturally unfolded proteins, Zetina discovered their striking similarity to CK2 consensus sequences [109]. This suggests that although OPN has been shown to lack secondary structure, CK2 phosphorylation of OPN may act to promote helix unfolding, which has already been experimentally confirmed to occur in several proteins [109, 110].

Disordered proteins' lack of structure is thought to endow several advantages such as (1) a greater interaction surface area, (2) flexibility to interact with several different binding partners, (3) elements that fold upon binding, (4) maintenance of accessibility of post-translational modification sites and (5) the availability of short linear interaction motifs [111-114]. The evidence of OPN's disordered structure in both the presence and absence of HAP may be an important aspect of its ability to adsorb to several different calcium-rich minerals whilst mediating matrix-cell interactions [49].

1.4 Post-translational Modifications

1.4.1 Phosphorylation

Nemir *et al.* have provided evidence that normal rat kidney (NRK) cells secrete two distinct forms of OPN [115]. In addition to the phosphorylated OPN molecule known to be secreted by osteoblasts, NRK cells were found to express nonphosphorylated OPN (np-OPN). It was subsequently discovered that phosphorylated OPN associated with cell-surface bound fibronectin in a heat-stable complex, whereas np-OPN formed a heat-dissociable complex with soluble fibronectin [116]. Thus, phosphorylated OPN may form a component of the ECM of NRK cells [116].

Tissue-specific differences in global OPN phosphorylation levels have also been revealed. Its post-translational phosphorylation is considered a major form of regulation of OPN function. The OPN isoforms analyzed for post-translational phosphorylations thus far include human milk, bovine milk, human urine and rat bone [46, 106-108]. Studies of the global phosphate content of full-length OPN have revealed the average number of phosphate residues per molecule is highly dependent on the tissue of origin - even though they contain the same number of consensus phosphorylation sites - but less so on the species of origin [35, 117]. For example, the phosphorylation status of human milk OPN [106] is similar to bovine milk OPN [105] and both possess higher phosphate contents than rat bone and bovine bone OPN [42, 46, 118].

OPN from human milk, human urine, bovine milk and rat bone have been characterized by mass spectrometry and found to possess 36, 30, 28 and 29 phospho-sites, respectively (Figure 1.1) [46, 105, 106, 108]. These numbers represent the maximum number of phosphorylations possible, but in all cases heterogeneity in the phosphorylated residues has been observed. This heterogeneity is likely due to incomplete phosphorylation of each consensus site by endogenous kinases [106]. The average number of phosphates detected per OPN molecule from rat bone, bovine bone, bovine milk, human milk and human urine is 11 [42, 46, 119], 8 [118], 28 [105], 32 [120] and 8 [108], respectively. Potential phospho-sites are often organized in groups of approximately 3, separated by longer stretches of amino acids (11-32 residues) [105].

Many of osteopontin's phosphorylated serine and threonine residues reside within the consensus sequences of G-CK (S/T-X-E/D/pS/pT) and CK2 (S/T-X-X-E/D/pS/pT)

Figure 1.1 Multiple sequence alignment of OPN amino acid sequence indicating phosphorylated residues.

The sequences of *Homo sapiens*, *Bos taurus* and *Rattus norvegicus* OPN proteins were obtained from gene bank (sp/P10451/OSTP_Human, sp/P31096/OSTP_Bovin and sp/P08721/OSTP_Rat, respectively). Sequences were aligned using ClustalW (version 2.0) [121]. *In vivo* phosphorylated residues of human milk, human urine, bovine milk and rat bone OPN are indicated in red [46, 105, 106, 108]. Isoforms are indicated by superscripts, m = milk, u = urine and b = bone. The underlined portion of rat bone OPN indicates the sequence not analyzed for phosphorylated residues. Introduced gaps are indicated by dashes, asterisks represent positions where all amino acids are identical in the alignment, colons represent conserved amino acid substitutions and periods represent semi-conservative amino acid substitutions.

* . * * * * . * . * * * *

(where pS and pT denote phosphoserine and phosphothreonine, respectively) [106, 122-127]. *In vitro* phosphorylation studies indicate that both casein kinase 1 (CK1) and CK2 are inferior to G-CK at phosphorylating OPN [127]. G-CK has additionally been shown to carry out minor phosphorylation of CK2 consensus motifs, suggesting it is the predominant kinase responsible for OPN phosphorylation [126]. Several other kinases, such as protein kinase C (PKC) and cGMP-dependent protein kinase have been found to play a minor role in OPN phosphorylation, introducing one phosphate each onto OPN [118].

1.4.2 Glycosylation

In addition to the phosphorylated OPN and np-OPN, Singh *et al.* have discovered that these differentially phosphorylated forms of OPN also represent different glyco-forms of OPN [116]. This group was able to show that np-OPN, but not phosphorylated OPN, is *N*-glycosylated. Additionally, treating cells with tunicamycin, an inhibitor of *N*-glycosylation, destroys np-OPN's ability to associate with soluble fibronectin [116]. Although *N*-linked glycosylation is imperative for this complex to form, it is presently unknown whether the lack of *N*-glycosylation of np-OPN, fibronectin or both is responsible. Moreover, this may be a rat kidney-specific post-translational modification of OPN as characterization of other OPN isoforms from other tissues and species have not detected *N*-glycosylations.

Considerable *O*-glycosylation of OPN takes place in nearly all tissues [128]. The cDNA of rat OPN indicates that the primary sequence of OPN contains one consensus site for modification by *N*-linked glycosylation (N-X-S/T) and 26 potential *O*-

glycosylation sites (S/T-X-E) [44, 128]. Approximately 17% of the mass of rat bone OPN has been found to correspond to carbohydrate modifications [42]. These were originally determined to comprise a single *N*-glycosylation and 5 or 6 *O*-linked oligosaccharides. More recent analysis of rat bone OPN using proteolytic digestion and tandem MALDI-TOF mass spectrometry has identified 4 *O*-glycosylation sites (T¹⁰⁷, T¹¹⁰, T¹¹⁶, T¹²¹) and no *N*-glycosylations [46]. Bovine milk and human urine OPN possess 3 *O*-glycosylated threonines (T¹¹⁵, T¹²⁴ and T¹²⁹) and 5 *O*-glycosylated threonines (T¹¹⁸, T¹²², T¹²⁷, T¹³¹ and T¹³⁶), respectively [105, 108]. Similar to rat bone OPN, both lack *N*-glycosylations. While OPN has a considerable quantity of glycosylated residues *in vivo*, uncertainty remains regarding their specific purpose.

1.4.3 Transglutamination

Prince *et al.* originally discovered that OPN was a substrate for transglutaminase (TG), although the residue(s) susceptible to transglutamination and substrates to which OPN was cross-linked were unknown [129]. The reactive residues in bovine OPN were subsequently identified as Q34 and Q36 [130]. OPN polymers produced by TG linkages between OPN molecules and OPN cross-linked to fibronectin were detected in the ECM of cultured NRK cells [131, 132]. OPN polymers, like monomeric OPN, are able to bind to HAP [107] and exhibit increased collagen-binding properties [54]. While substantial evidence exists for the TG reactivity of OPN in the ECM, the *in vivo* significance of these findings is presently unknown, necessitating further studies.

1.4.4 Proteinase cleavage

The first OPN cleavage products discovered were 23-kDa and 20-kDa fragments purified from demineralized porcine bone extracts [133]. *In vitro* thrombin-cleavage of OPN produced similarly sized fragments, both possessing a sequence identical to the 23-kDa fragment purified from bone extracts. This fragment corresponds to the carboxy-terminal half of OPN, the cleavage localized to Arg¹³⁷-Ser¹³⁸ in rat OPN [134]. Conservation of the thrombin-cleavage site among mammals suggests physiological relevance. Indeed, circulating OPN is cleaved by thrombin subsequent to induction of the blood-coagulation cascade and the generated OPN fragments have been shown to increase cell attachment and spreading [134].

In vitro evidence of OPN fragments in human tumour cell lines and postpartum uterus led Agnihotri *et al.* to hypothesize that the co-expressed MMP3 (stromelysin-1) and/or MMP7 (matrilysin) were responsible for the OPN cleavage [135]. Analysis revealed that, indeed, both MMP3 and MMP7 were able to cleave OPN, the affected peptide bonds being Gly¹⁶⁶-Leu¹⁶⁷, Ala²⁰¹-Tyr²⁰² (MMP-3 only) and Asp²¹⁰-Leu²¹¹ [135]. The Gly¹⁵¹-Leu¹⁵² MMP cleavage site is the only one conserved in rat OPN. Further studies involving mutational analysis of OPN and the generation of recombinant OPN fragments of the corresponding MMP-cleavage products revealed that the 40-kDa fragment possessed stronger adhesive and migratory activity than full-length OPN and this activity was dependent on the SVVYG¹⁶²⁻¹⁶⁶ motif [136]. The SVVYGLR sequence, a cryptic integrin-binding site, has been previously characterized to bind the β 1 integrins [137-139]. Thus, these cleavage products possess properties distinct from the full-length

parent OPN molecule and the extent of their ability to affect cell adhesion and migration *in vivo* requires further investigation.

1.5 Physiological Roles of Osteopontin

Consistent with its diverse expression, OPN is known to participate in numerous physiological and pathological processes, including: biomineralization, cancer metastasis, wound repair, inflammation, immunity and apoptosis (reviewed in [64]). Several of these processes involve the deposition of calcium salts. Physiological or “normal” calcification occurs in skeletal tissues whereas pathological or “abnormal” calcifications refer to those occurring in functional soft tissues [140]. Dystrophic calcification refers to pathological calcifications occurring in individuals with normal circulating levels of calcium [140].

1.5.1 Bone and tooth development

Biomineralization is the physiological process through which living organisms deposit salts in order to stiffen existing soft tissues and occurs in both human health and disease. The major mineralized tissues within the mammalian body are bones and teeth. Bone provides motility, strength and protection of vital organs, while teeth are used to tear and chew food. Bone is a dynamic organ that is constantly remodelled. This remodelling process involves the breakdown of old bone (mineral and matrix) and its replacement with new osteoid matrix, which is then mineralized. HAP is a calcium phosphate mineral that is the major inorganic constituent of this organ. Regulation of the mineralization process is known to involve acidic phosphoproteins that induce and/or inhibit the growth of the HAP crystals in bone [20, 32, 36, 141].

With regard to biomineralization, OPN is thought to perform several functions depending on its location, all of which pertain to the inhibition of mineralization. At physiological sites of biomineralization, OPN has been found to be involved in the inhibition of HAP formation and growth [141-144]. Within bone, osteopontin is found at especially high concentrations in cement lines, sites where new bone is deposited onto older bone during remodeling [100]. In this context, OPN is thought to coat HAP in the newly mineralized bone to inhibit its further growth and maintain close contact between the older bone and newly deposited osteoid matrix by mediating matrix-mineral interactions [100]. *Opn*-null mice, although indistinguishable from littermates, develop bones with a higher than normal density and contain HAP with increased crystallinity [141]. Moreover, these mice are resistant to ovariectomy-induced bone loss, demonstrating that OPN is necessary for the rapid bone loss provoked by estrogen depletion [142, 145].

OPN, one of the more abundant noncollagenous proteins in bone matrix, is synthesized by preosteoblasts, osteoblasts and osteocytes [146-148]. It is then secreted into the osteoid, becoming incorporated into mineralized bone [147, 148]. Cementoblasts of the oral cavity secrete cementum, whose components are similar to the osteoid of bone [149]. In fact, cementoblasts possess many characteristics that are similar to those of osteoblasts. *Runx2*- and *Osx*-positive cementoblasts express OPN, analogous to osteoblasts [149]. A subcutaneous implantation study by Salih *et al.* suggests that osteogenesis induction by BSP is dependent on the extent of both OPN and BSP phosphorylation [117]. Overall *in vivo* biomineralization was maximal when the

phospho-BSP/phospho-OPN ratio was approximately 3-4:1, whereas no mineral was deposited at a ratio of approximately 1.2:1 [117].

Osteopontin has a high affinity for HAP [41] and is able to mediate the attachment of osteoblasts (bone forming cells) and osteoclasts (bone resorbing cells) to bone [150-152]. Cell-culture and gene-ablation experiments have shown OPN to be important for the differentiation, recruitment [142, 145, 153] and promotion of osteoclast function through its interaction with the $\alpha_v\beta_3$ integrin receptor [36, 58]. Active osteoclastic bone resorption is confined to the acidic milieu within the ruffled border area. A prerequisite to the creation of the acidic microenvironment is the formation of an isolated sealing zone between the osteoclast and bone, known as the clear zone [154, 155]. High concentrations of OPN have been localized to the sealing zone of actively resorbing osteoclasts, while much lower concentrations were observed in the resorption pit itself [152]. Furthermore, bone resorption can be blocked by monoclonal antibodies directed against OPN or its RGD domain [150]. This suggests OPN is an important component in the creation/maintenance of the tight osteoclast-bone interaction, which is a prerequisite for bone resorption. Similarly, OPN is thought to be involved in the maintenance of teeth in their sockets through a resorption and apposition process analogous to that which occurs in bone [156].

1.5.2 Immune system

The expression of the early T-lymphocyte activation-1 (Eta-1) gene was identified as a predominant transcript in activated but not resting CD4⁺ cells [65]. Eta-1 was localized to the murine chromosome-5 locus, *Ric*, which confers immunity to *Rickettsia*

tsutsugamushi infection [65]. Its expression is part of a rapid T cell-dependent immunity [65]. It was later recognized that this highly acidic secreted protein was identical to OPN (and will hereafter be referred to as OPN).

Further study indicated OPN is secreted by various immune cells including activated T-cells, dendritic cells, natural killer T (NKT) cells, macrophages and platelets [53, 102, 157-160]. It is the most abundantly expressed transcript in activated T-cells, stimulating antibody secretion by B-lymphocytes, proliferation of mast cells, bone marrow production of granulocytes/macrophages and is a macrophage chemoattractant [58, 79, 157, 161, 162]. Disregulation of OPN expression may also contribute in the onset and severity of autoimmune diseases [163].

Intradermal injection of OPN results in an inflammatory cellular infiltrate within 24 hours that is predominantly composed of macrophages [164]. Its ability to induce macrophage chemotaxis has been localized to the C-terminal domain of OPN, which is able to interact with the cell-surface receptor CD44 [165]. Binding of a non-overlapping N-terminal region of OPN to $\alpha_v\beta_3$ -integrin receptors induces cell spreading and activation [165].

In addition to immune cell attraction and activation, OPN also plays an important role in protecting host cells from lysis by the alternative complement pathway, an evolutionarily older complement-activation pathway [166]. This is possible through OPN's ability to link the complement-control protein, Factor H, to $\alpha_v\beta_3$ or CD44 [166].

1.5.3 Tumour growth and metastasis

Cancer progression often involves the neoplastic transformation of cells, followed by their interaction with the ECM to create additional space to grow. The cancer cells subsequently proliferate to occupy the newly created void. Several alterations in cell physiology are essential for the ability of cells to achieve the characteristics of transformed cells, including growth signal self-sufficiency, growth-inhibition signal insensitivity, evasion of apoptosis, unlimited replicative potential, sustained angiogenesis, tissue invasion and metastasis [167].

In 1989, 2ar, the mouse transformation-associated phosphoprotein whose expression is correlated with tumorigenicity was reported to be identical to OPN [168]. Since this discovery, OPN and various combinations of SIBLING proteins have been found to be significantly upregulated in many tumours that exhibit tendencies to calcify and/or metastasize to bone [48, 169-177]. Evidence has also been provided showing that the OPN gene is also inducible by tumour promoters and growth factors, including breast cancer 1 (BRCA1), phosphatase and tensin homologue (PTEN) and breast cancer metastasis suppressor 1 (BRMS1) [48, 178]. Gene-expression analyses have determined OPN is among the most strongly upregulated genes in several mouse and human cancers [48]. Its expression often directly correlates with specific stages of clinical progression [179], such as metastasis [172, 180, 181].

The ability of cancer cells to metastasize is often attributed to enhanced cell motility and increased expression/activity of proteinases capable of degrading the ECM [182, 183]. SIBLINGs, being multifunctional ECM proteins, are expected to have key roles in metastasis. OPN has been shown to enhance cancer cells' ability to intravasate into

blood vessels [180]. Furthermore, the carboxy-terminal fragment of thrombin-cleaved OPN has been shown to increase both invasion and tumorigenesis [184]. Likewise, matrix metalloproteinase 9 (MMP9)-directed cleavage of OPN produces OPN fragments that increase the cell-invasion properties of hepatocellular carcinoma [185]. Takafuji *et al.* also found that the pathological upregulation of OPN and MMP9 are coregulated *in vivo* in humans [185]. OPN has been reported to bind pro-MMP3 and convert it to the enzymatically active MMP3 and also has the capacity to reactivate TIMP (tissue inhibitor of metalloproteinases)-inhibited MMP3 [186]. This MMP activation and reactivation capability has been observed for other SIBLINGs acting on various other MMPs [186].

Several *in vivo* models provide evidence that OPN contributes to the generation of new capillaries (angiogenesis) infiltrating cancerous lesions [187, 188] and that this ability is dependent on its RGD motif [187]. Given OPN's diverse effects on both cancer cells and ECM-degrading enzymes, it is unsurprising that OPN expression has been shown to be a predictor of outcome for numerous cancer types [189-192]. Increased OPN expression always correlates with a worse clinical outcome. With regard to ovarian carcinoma, survival for 36 months post-diagnosis is predicted to be less than 5% for patients with increased OPN expression and 75% for those with no OPN increase [189].

1.5.4 Nephrolithiasis

Kidneys are responsible for the regulation of whole-body salt balance. This necessitates the urinary excretion of salts including calcium and phosphate [193]. The obligatory solute output often produces urine that exceeds the solubility limit of calcium salts [193]. This metastable supersaturation often occurs in the renal distal tubule and

collecting ducts [193]. Urinary stones are formed through a phase change where dissolved salts, driven by their supersaturation, condense into solids [194].

Calcium oxalate stones often develop on surfaces of renal papillae on collections of interstitial suburothelial CaP particles referred to as Randall's plaques [195]. The number of CaOx stones formed has been shown to vary directly with plaque surface coverage of the renal papillae, suggesting this surface promotes CaOx overgrowth [196]. These interstitial nidi, which represent the most minimal plaque lesions, have been found to be exclusively composed of HAP and are believed to initiate the precipitation of CaOx or grow to become HAP stones [195].

Although the solubility product for CaOx and CaP salts is frequently exceeded in normal human urine, most people do not form stones [193]. Nearly 5% of American women and 12% of men will develop a kidney stone during their lives and the prevalence of developing stones has been increasing over the last 30 years [197]. Approximately 80% of stones are composed of CaOx and/or CaP [197]. HAP comprises the core of one-third of all CaOx monohydrate stones and is found as the major phase in 18% of all kidney stones [198].

Urinary stones are aggregates of crystals and possess an organic matrix that is approximately 2-5% of the total stone weight [99]. This organic matrix is predominantly composed of OPN [199]. Early experiments on normal urine revealed that the majority of its crystal growth-inhibitory properties were contributed by macromolecules rather than the lower-molecular-weight molecules [200, 201]. Since then, many inhibitors of mineral precipitation and growth have been discovered in urine: osteopontin [202], prothrombin F1 fragment [203], inter- α -trypsin inhibitor [204], calgranulin [205], THP

glycoprotein [206], albumin, RNA fragments, DNA fragments and glycosaminoglycans [193]. Known inhibitors all possess poly-anionic segments. The overall compositions of proteins extracted from CaOx stones exhibit a high proportion of acidic amino acids [207-209], yet the role of acidic residues is not well understood.

Osteopontin is present in all bodily fluids, especially milk, saliva and urine, which possess high concentrations of calcium salts. Considerable amounts of both *in vitro* and *in vivo* data suggest that OPN is able to inhibit the spontaneous precipitation and/or aggregation of several calcium-rich mineral phases, hence decreasing the overall size of pathological precipitations [30, 210-212]. OPN was found to be highly expressed by rat kidney epithelial cells of distal tubules after induction of urolithiasis via sodium glyoxylate administration [99]. The increase in OPN mRNA expression was proportional to the dosage and duration of glyoxylic acid [99]. OPN concentration was also observed to be inversely proportional to urine volume by Chalko *et al.* [213]; thus, the more concentrated urine is, the higher the OPN concentration. This is a characteristic suggested to favour inhibition of solute precipitation [213]. Moreover, OPN is found as a major organic constituent of growing renal calculi [199].

At concentrations typically found in normal human urine ($\sim 0.1 \mu\text{M}$), OPN is a very potent inhibitor of CaOx crystallization and subsequent aggregation *in vitro* [202, 213-215]. This concentration is too low for the inhibitory potency to be due to ion chelation [216]. This suggests that OPN inhibits crystal formation and growth through interaction with the nascent crystal surface, although the exact nature of the protein-crystal interaction has not been defined [216]. Compelling *in vivo* evidence of OPN's crystal

growth inhibitory function is observed in *Opn*-null mice, which have a predisposition to forming kidney stones and other ectopic calcifications [30, 212].

1.5.5 Atherosclerosis and native/prosthetic valves

Ectopic calcification represents a prominent characteristic of various cardiovascular diseases [217]. Atherosclerosis, commonly referred to as hardening of the arteries, is a chronic inflammatory response in arterial walls (reviewed in [218]). This occurs due to a buildup of low-density lipoproteins resulting in the accretion of macrophages. The progression following chronic inflammation typically includes arterial enlargement, plaque rupture and arterial stenosis or complete closure. The final outcome is either a reduction in downstream blood supply or aneurysm potentially leading to severe hemorrhage. Calcification often occurs at the outer base of advanced atherosclerotic lesions [219]. In addition, ectopic mineralization of native human and porcine xenograft bioprosthetic (both glutaraldehyde-treated/-untreated) heart valves continues to be an intractable source of valve failure [220-223].

Human atherosclerotic lesions have been found to contain proteins typically involved in bone development and maintenance [224-227]. Normal soft tissues do not express OPN, although it is induced in response to injurious stimuli such as atherosclerotic lesions [228-234] and prosthetic valves [235-237]. Adult aortas increase their OPN mRNA expression levels throughout the stages of atherosclerotic progression [232]. In fact OPN content and expression level are related to coronary artery disease severity and the degree of calcification, respectively [232, 238].

OPN is highly localized to the surfaces of calcified deposits in arteries and valves, although a thorough mechanistic understanding of the biological process is lacking [100, 234]. The situation is further complicated by conflicting data. For example, the findings of Kadoglou *et al.* suggest that while OPN decreases plaque calcification it may additionally promote plaque instability [239], yet Burke *et al.* have found that calcification itself is a reliable marker of plaque instability [240]. Analysis of porcine bioprosthetic heart valves and human heart valves revealed that increased OPN content correlates with increased calcification [237]. A comparison to noncalcified valves showed higher noncollagenous-protein mRNA levels, including OPN, in calcified valves. Based on this result Srivatsa *et al.* suggest that a therapeutic approach to the prevention of valve failure may be to modulate the expression of mineralization-related proteins such as OPN [237]. More recent investigations, however, show OPN coating arterial mineral deposits in mice lacking matrix gla protein (MGP), a high-affinity calcium-binding protein, but not in wild-type or $MGP^{-/-}OPN^{-/-}$ mice [241]. Furthermore, not only did $MGP^{-/-}OPN^{+/+}$ mice outlive $MGP^{-/-}OPN^{-/-}$ double knockouts, they contained one-half and one-third as much mineral deposits as the double knockouts at two and three weeks of age, respectively. Thus, Speer *et al.* have shown that OPN is an inducible inhibitor of dystrophic vascular calcification *in vivo* [241], suggesting the enhanced OPN expression observed with increased vascular calcification is a physiological adaptation aimed at preventing further calcification.

1.6 Protein-Crystal Interactions

1.6.1 Crystal formation and growth

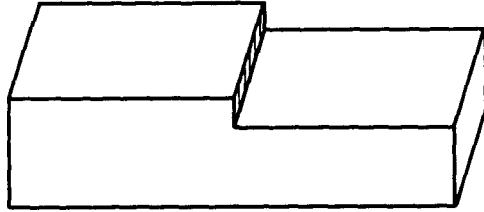
A crystal is a solid body possessing a regular repeating internal arrangement of constituent molecules, atoms or ions (reviewed in [242]). Nucleation is the initial event during the precipitation of an inorganic crystal from dissolved ions. The process occurs through the aggregation of individual solution-phase ions to form a small cluster, known as a nucleus. The stability of a nucleus is dependent upon its size, which in turn is dependent on the supersaturation level of the solution [243]; nuclei larger than the critical radius tend to grow larger, whereas those below the lower limit of the critical radius tend to dissolve. The formation of a nucleus in a pure solution is known as homogeneous nucleation. In contrast, organisms facilitate biomineralization through heterogeneous nucleation on preexisting nuclei or seed crystals (which have a similar but different composition from the newly formed nucleus) [242]. This occurs due to the presence of impurities and other organic molecules in solution, which reduces the free energy barrier typically hindering nucleation.

After the formation of a supra critical nucleus, the rate of growth is dependent on the rate of transport, or diffusion, of lattice ions to the surface of the crystal. Growth of a crystal in a supersaturated solution occurs due to the flux of ionic constituents attaching to the crystal surface exceeding the flux of these constituents leaving the surface. The surface of a crystal typically possesses several distinct features including terraces, steps and kinks [244]. Terraces comprise the flat areas of the crystal, over which new layers can form through the extension of raised layers, called steps (see Figure 1.2). The steps

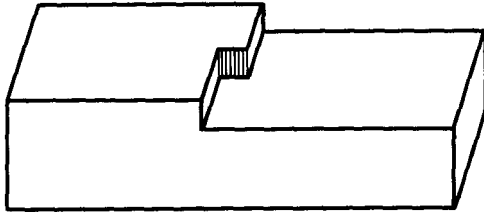
Figure 1.2 Illustration of topographical features of crystal surfaces.

(A) Depiction of a step (hashed region) on a terrace/crystal face. (B) Depiction of a kink within a step. (C) Depiction of a screw dislocation/growth hillock.

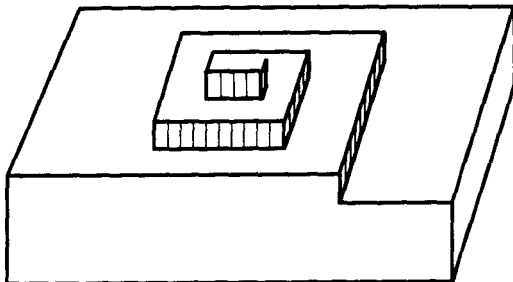
A



B



C



are either complete or incomplete, the latter being more common and referred to as kinks. New areas of crystal growth typically occur at kinks as incoming ions can form more bonds at kinks than on terraces or at step edges. Thus, addition of ionic crystal constituents to kinks propagates steps, which grow to the crystal edge, forming a new terrace/crystal face. There must be a mechanism to create new steps and/or kinks on the crystal surface, since growth would quickly cease once each extends to a crystal edge. There are two ways for this to be accomplished. The first method involves the growth of a 2-dimensional nucleus on the preexisting crystal surface, which, although more favourable than the creation of a 3-dimensional nucleus, is exceedingly rare unless growth is occurring in very highly supersaturated solutions [245]. More commonly, spiral arrangements of steps are created at crystal lattice dislocations (breaks in the crystal lattice), referred to as screw dislocations or growth hillocks [246]. By growing in spiral fashion, these provide a perpetual source of steps and kinks.

Crystal growth inhibition is predominantly thought to occur by step-pinning, which is a model describing the adsorption of inhibitory molecules to the terraces of a crystal [247]. Growing steps then encounter these adsorbed molecules. Strongly bound inhibitory molecules preclude the incorporation of ions directly beneath them, thus preventing the advancement of a step edge. These 'pinned' steps are able to grow around the blocked sites if the concentration of adsorbed inhibitors is sufficiently low. If the average spacing between adsorbed inhibitors is similar to the critical radius of curvature of a step, growth is inhibited. Furthermore, if the amount of adsorbed inhibitor is sufficiently high, the curvature of the growing bulges falls below the critical radius of curvature of a step and growth effectively ceases.

1.6.2 Roles of proteins in biomineralization

Biomineralization involves the exquisite control of nucleation, growth and morphology by living organisms [248]. Apart from arthropod exoskeletons, it is a universal means of producing high stiffness [249]. Animals may use one or both of two strategies to promote the nucleation of inorganic minerals. The first is accomplished by increasing the supersaturation level of parent ions in a solution thereby increasing the probability of nucleation [250, 251]. The second involves using biological macromolecules, such as proteins or polysaccharides, as templates that mimic the crystal lattice of a particular crystal face, thereby offsetting the unfavourable entropy associated with the solution-solid phase transition [252, 253].

The incorporation of organic constituents within or between the growing crystals is an adaptive solution to the brittleness (lack of toughness) that typically accompanies stiffness. These biogenic composite materials have properties vastly different from those of pure crystals [249]. For instance, the nacreous layer of abalone shell (mother of pearl) possesses a fracture resistance ~3,000 times greater than the pure mineral from which it is formed, aragonite (calcium carbonate) [254-256]. This remarkable difference in fracture resistance is attributable to the degree of mineralization and ability of the organic components, which in the case of abalone shell comprise only 1-5% of total mass, to resist tension [249, 254, 255].

While the individual crystals of composite biominerals provide stiffness, water and the organic components – namely protein or carbohydrates –contribute resistance to impact loads and crack elongation [249]. Moreover, organisms are able to modulate the stiffness of biominerals to suit particular functions. Water and organic material can

comprise a significant portion of biomineral mass, with the most flexible bones encompassing approximately equal masses of water/organic material and mineral [249]. The elasticity contributed by the organic matrix of bones is easily observed with a demineralized fibula, as it is easily tied in a knot [257].

Calcium is the predominant cationic component found in most biominerals, some of which include HAP, CaOx and calcium carbonate (as aragonite or calcite) [252]. The most common types of biological macromolecules able to modulate crystal growth are acidic polysaccharides and ECM proteins [252]. Organisms have evolved an exquisite control over the ability to both nucleate and direct the growth of particular mineral phases. For instance, mollusk shell organic extracts from either aragonite- or calcite-containing layers induce the formation of their respective biomineral phases under identical *in vitro* conditions [258].

The highly acidic ECM proteins are thought to control the precipitation and growth of minerals in the vertebrate skeleton. In teeth, DPP and DMP1 have been shown to initiate HAP nucleation and growth *in vitro* [32, 259, 260]. Similarly, BSP, a mineralized tissue-specific collagen-binding protein [261, 262], is believed to initiate HAP nucleation in the ECM of bone [20, 32]. In addition to its *in vitro* HAP-nucleating properties, BSP has been found to be recruited to prebiomineralization foci just prior to mineralization *in vivo* [263]. OPN is a major component of the calcium carbonate-containing egg shell [264]. It is expressed only during the period of egg shell calcification, although its specific role and mechanism of action in this process is yet to be elucidated, as are the roles of many other mineralization-associated proteins [265].

1.6.3 Inhibition/modulation of crystal formation by OPN and other proteins

Proteins with neutral or positively charged residues generally exhibit a low affinity for the surface of HAP [266]. Salivary proteins able to adsorb to the HAP surface of teeth with high affinity have been observed to possess negative residues in specific regions of the molecule. Principal among the multitude of organic molecules within biological systems able to modify inorganic crystallization is a class of poly-anionic proteins, to which OPN belongs. These proteins possess relatively high proportions of aspartic acid, glutamic acid, serine and phosphorylated residues. OPN has been shown, *in vitro*, to inhibit the nucleation of a multitude of inorganic crystal species commonly found in organisms, including HAP, calcite, and CaOx [36, 37, 216, 267-269]. Extensions of these nucleation-inhibition studies have also shown OPN to be an effective inhibitor of crystal growth [32, 36, 37, 270]. This ability of OPN to inhibit crystal growth has also been confirmed *in vivo* [241, 271]. Furthermore, a study of the inhibitory potency toward HAP formation of several mineralized-tissue proteins revealed that, compared to OC, BSP, chondrocalcin, and ON, OPN was the most potent inhibitor [37].

More recently, peptide-based studies using amino-acid sequences derived from known inhibitors have become common in an effort to further elucidate the specific requirements and mechanistic process of crystal growth inhibition. Using synthetic peptides and phosphopeptides corresponding to sequences of OPN, Hoyer *et al.* showed that the full protein is not required for inhibitory activity. The OPN-derived peptides, some comprising only 14 residues, were able to inhibit CaOx crystal growth to varying degrees [272]. A similar study performed on HAP nucleation by Pampena *et al.* reported that OPN peptides with sequences corresponding to 41-52 and 290-301 of rat bone OPN

were 4 times more potent HAP nucleation inhibitors compared to sequences derived from residues 7-17 and 248-264 [269]. Both studies showed that particular sequences of OPN were particularly suited to inhibition of nucleation or growth of the respective minerals used in the study.

Several studies have been directed towards the significance of acidic amino-acid residues in mineral-binding proteins since many members of this class are poly-anionic. CaOx crystal growth was not found to be decreased by two OPN peptides with evenly distributed acidic residues, but two other peptides with aspartic acid clusters were able to inhibit its growth [272]. Furthermore, the inhibitory potencies of all peptides tested by Hoyer *et al.* were drastically increased by phosphorylation [272]. Studies using synthetic poly-Asp or poly-Glu have revealed that poly-Asp's effect on calcium mineral growth was similar to those of aspartic acid-rich proteins (AARP) [22, 37], whereas the equally acidic poly-Glu merely exhibited a nonspecific effect on crystallization, having an inhibition potency ~1000 times lower. This result may be explained by the finding of Taller *et al.*, who developed a technique to visualize adsorbed protein on the surface of minerals [273]. Poly-Asp was observed to adsorb preferentially to a specific face of CaOx crystals, whereas poly-Glu was found to adsorb nonspecifically to all faces. Further investigation is required to elucidate by what method poly-Glu is able to adsorb to several faces yet be a poorer crystal growth inhibitor than poly-Asp. This may possibly be rationalized on a structural basis since at physiological pH poly-Asp is disordered, whereas poly-Glu exists as an extended helix [274, 275]. Interestingly, both molecules, when immobilized/adsorbed to germanium surfaces, act as HAP nucleators [276]. The observed importance of acidic clusters in the inhibition of crystal growth led

Butler to propose that the conserved poly-Asp region of OPN was responsible for its mineral-binding properties [104]. Yet this is inconsistent with studies showing dephosphorylated native osteopontin does not inhibit *in vitro* HAP growth or vascular smooth muscle cell calcification [37, 38]. This suggests that phosphorylation may be the major modulator of OPN's ability to inhibit mineral growth since all other post-translational modifications are still present on dephosphorylated native osteopontin.

The importance of post-translational phosphorylation on the regulation of biomineralization by proteins is suggested by the observation that HAP- and CaOx-inhibiting properties of several proteins are altered by dephosphorylation [36, 37, 270, 277, 278]. Early studies demonstrated that dephosphorylated bovine bone OPN binds to HAP with less affinity than the native protein [36]. Furthermore, nonphosphorylated polypeptides have been correlated with decreased inhibitory potency [36, 38, 52, 269]. A constant-composition study comparing the influence of a 5-residue fragment of statherin on HAP growth/dissolution revealed that the N-terminally phosphorylated pentapeptide was superior to the nonphosphorylated peptides at inhibiting both processes [279].

Recent studies performed by Gericke *et al.* have shown that highly phosphorylated milk OPN promotes HAP formation [52]. Although other proteins involved in HAP nucleation are known to be affected by phosphorylation, the significant quantities of OPN, calcium and phosphate in milk [280, 281], coupled with the rarity of mineral precipitates in milk, calls this finding into question.

Several recent studies of face-specific adsorption to CaOx by differentially phosphorylated OPN and OPN-derived peptides have revealed that each peptide or protein preferentially binds to specific faces of the crystals. Their findings suggest that

phosphorylated macromolecules adsorb to Ca^{2+} -rich crystal faces of CaOx through nonspecific electrostatic interactions between the phosphate groups and Ca^{2+} ions [282, 283]. Based on the accumulated data, it is evident that phosphate groups present in OPN and other biomineral-associated proteins are required for efficient inhibition of crystal formation and growth. Despite this, relatively little is known regarding the mechanism through which anionic proteins are able to adsorb to biominerals since a comprehensive understanding of their behaviour at this liquid-solid interface is lacking.

The combination of the importance of acidic residues and post-translational phosphorylations to biomineral adsorption indicate that negative charge is imperative to the ability of these proteins to perform their function. The propensity and clustering of these negative charges suggests that the high affinity of these AARPs toward calcium-rich minerals is derived from their ability to electrostatically interact with calcium ions. Equilibrium and kinetic studies on the association of the salivary PRPs, PRP1 and PRP3, as well as poly-Asp, revealed that the adsorption process is entropically, and not enthalpically, driven [284]. Thus, although electrostatic interactions seem to be a prerequisite for protein-mineral interactions, the driving force of adsorption – or greatest contributor of free energy – is increased entropy of the system. Recently, Goobes *et al.* has similarly demonstrated, using isothermal titration calorimetry (ITC), that the mechanism of adsorption of salivary statherin to HAP is driven by entropy, a process reminiscent of the hydrophobic effect driving protein folding [285]. This finding suggests that this entropic adsorption process may be a common mechanism exploited by biomineral associated anionic proteins.

1.7 Purpose of Thesis

Although OPN is known to inhibit HAP growth both *in vitro* and *in vivo*, the specific structural features responsible for its effect on HAP growth and its mechanism of adsorption are not fully understood. The ability of the synthetic polymer poly-Asp to inhibit HAP growth has led to the notion that the poly-Asp region of OPN is the mineral-binding region [104], although this has never been directly investigated.

To elucidate the role of the poly-Asp sequence in the inhibition of HAP growth, we have used a 16mer peptide containing the poly-Asp sequence of rat OPN. To examine the effects of phosphate groups, both phosphorylated and nonphosphorylated peptides were synthesized. Additional peptides allowed for the elucidation of inhibitory potency of OPN sequences containing ~30% acidic residues (the average proportion of acidic residues in OPN) with and without naturally occurring phosphate groups.

The HAP-inhibiting potencies of these OPN-derived peptides were compared with that of the full-length protein using an *in vitro* constant-composition seeded-growth (CCSG) assay, which allows for prolonged steady-state crystal growth at physiological pH, temperature and ionic strength. Furthermore, the mechanism of adsorption of OPN to HAP was probed using isothermal titration calorimetry, a technique able to provide a full thermodynamic characterization of the adsorption process. Elucidation of the thermodynamic driving force of HAP adsorption of model compounds and OPN was coupled to the analysis of their inhibitory potency. These studies expand the current body of knowledge concerning interactions between organic molecules and inorganic mineral phases and the mechanisms by which biomolecules exert their exquisite control on mineral growth.

Chapter Two – Constant Composition Seeded Growth Studies

2.1 Introduction

Attempts to elucidate factors affecting the precipitation of the biologically relevant mineral HAP have produced various assays with which to assess its rate of growth. This was initially performed by simply preparing supersaturated calcium phosphate solutions and analyzing the drop in concentration of the respective ions over time. This technique was superseded by the development of a pH-stat method, which enabled experiments to be conducted in the presence of a constant hydrogen ion activity [286]. These methods possessed two major disadvantages: 1) the concentration of mineral constituents, such as calcium and phosphate, decrease over the course of the experiment thus decreasing the driving force for precipitation, and 2) due to the incessant decrease in the concentration of constituent ions, the experiments had to begin at supersaturation levels at which several mineral phases other than HAP were stable, including tricalcium phosphate $[\text{Ca}_3(\text{PO}_4)_2]$, octacalcium phosphate $[\text{Ca}_8\text{H}_2(\text{PO}_4)_6 \cdot 5\text{H}_2\text{O}]$, anhydrous dicalcium phosphate (CaHPO_4), and dicalcium phosphate dihydrate ($\text{CaHPO}_4 \cdot 2\text{H}_2\text{O}$). These issues were solved with the development of the constant-composition/seeded-growth method, in which the pH and concentrations of both calcium and phosphate were maintained at constant levels for the duration of the experiment [287]. This new method thus enabled the conduction of experiments with initial calcium phosphate concentrations at which HAP was the sole thermodynamically favourable mineral phase. Studies of factors affecting the rate of mineralization of HAP at very low supersaturations could then be conducted [288]. Furthermore, when coupled with the use of well-characterized HAP seed crystals, this technique eliminates the kinetic uncertainty of nucleation assays,

allowing for the elucidation of the effects on the HAP growth rate of any molecule under study.

In the present study, a constant-composition seeded-growth assay was utilized to assess the HAP-inhibiting potency of nonphosphorylated rat recombinant OPN (rOPN), highly phosphorylated bovine milk OPN (mOPN) and four synthetic 16mer peptides whose sequences are derived from two distinct regions of rat bone OPN. The first set of peptides is derived from residues 220-235, and is used as a representative of the phospho-clusters composing the majority of the OPN sequence. P3 (pSHEpSTEQSDAIDpSAEK) contains three phosphoserine residues, whereas P0 (SHESTEQSDAIDSAEK) possesses an identical amino acid sequence but lacks phosphorylations. The second set of peptides is derived from residues 65-80, which contains the OPN poly-Asp region. This peptide was synthesized with and without a phosphate group on the N-terminal serine: OPAR (SHDHMDDDDDDDDDDGD) and P-OPAR (pSHDHMDDDDDDDDDDGD). This peptide was used to elucidate whether the short poly-Asp sequence within OPN (9 consecutive Asp residues in rat OPN) is capable of adsorbing to HAP and inhibiting crystal growth, as has been suggested in the literature on OPN [104].

Full-length OPN has been shown to lack secondary structure through several techniques such as NMR, CD spectroscopy and ATR-FTIR [43, 49, 52]. Structural information on the four novel peptides used in this study was not available and, since these 16mer sequences would be studied out of the context of the full-length OPN molecule, it was of interest to determine whether they possess secondary structure. CD spectroscopy is a quantitative spectroscopic technique that can be used to estimate the fraction of residues in α -helix, β -strand, β -turn, and disordered secondary structure. Thus,

CD spectroscopy was utilized to estimate the secondary structure of the 4 OPN-sequence-derived 16mer peptides in order to ascertain whether any differences in their effects on HAP growth rate were structurally based.

2.2 Materials and Methods

2.2.1 Chemicals and Reagents

Ca(NO ₃) ₂ · 4 · H ₂ O (>99.0%)	Sigma-Aldrich (St. Louis, MO)
Na ₂ HPO ₄ (>99.0%)	EMD Chemical Inc. (Gibbstown, NJ)
NaCl (>99.5%)	Sigma-Aldrich (St. Louis, MO)
NaOH (>98%)	EMD Chemical Inc. (Gibbstown, NJ)
HCl (36.5-38%)	EMD Chemical Inc. (Gibbstown, NJ)
NH ₄ OH (NH ₃ content 28-30%)	Sigma-Aldrich (St. Louis, MO)
Acetone (HPLC grade)	Sigma-Aldrich (St. Louis, MO)
HEPES (>99.5%)	Sigma Aldrich (St. Louis, MO)
N ₂ (medical grade)	Praxair (Mississauga, ON)
Poly-L-Aspartic acid (sodium salt) 11,000 MW	Sigma (St.Louis, MO)
0.2-µm Acrodisc Syringe Filter (polyethersulfone)	PALL Corp. (Ann Arbor, MI)
Quanti-Chrom™ Calcium Assay Kit	BioAssay Systems (Hayward, CA)
ALS P _i ColorLock™ P _i Detection Reagent	Innova Biosciences (Hamburg, Germany)
150 mm Single Tube Rotameter	AALBORG (Orangeburg, New York)
IUPAC Buffer pH 7.000	Radiometer Analytical (Villeurbanne, FR)

IUPAC Buffer pH 10.012	Radiometer Analytical (Villeurbanne, FR)
Calomel pH4006 electrode	Radiometer Analytical (Villeurbanne, FR)
TIM900 Titration Manager	Radiometer Analytical (Villeurbanne, FR)
ABU93 Triburette	Radiometer Analytical (Villeurbanne, FR)
TimTalk 9 version 2.1 software	LabSoft (Tampa, FL)
96-well Flat-Bottom Immuno Plate	NalgeNunc International (Rochester, NY)
Safire Microplate Reader	Tecan (Männedorf, Switzerland)
Bruker D8 μ XRD	Laboratory for X-ray Diffraction and Microdiffraction (University of Western Ontario)
ICP-AES Geochemistry Laboratories	Biodome (UWO)
Micrometrics ASAP 2010 BET SA Analyzer	Control and Crystallization of Pharmaceutical Laboratory (UWO)
LEO 1540XB SEM	The Nanofabrication Laboratory (UWO)
Jasco J-810 Spectropolarimeter	Biomolecular Interactions and Conformations Facility (UWO)
Water was Milli-Q quality with 18 Mega ohms resistance	

2.2.2 Synthesis of hydroxyapatite seed crystals

Hydroxyapatite for use in the constant-composition seeded-growth assay was synthesized using a modification of the protocol described by Nancollas and Mohan (1970) [286]. Briefly, 250 ml of 0.5 M $\text{Ca}(\text{NO}_3)_2$ was added drop-wise to a magnetically

stirred 250-ml solution of 0.3 M Na_2HPO_4 , which was maintained between pH 8.5 and 10.0 by the addition of concentrated NH_4OH (28-30% solution). The Na_2HPO_4 solution was also maintained at 70°C whilst being bubbled with water-saturated nitrogen. The precipitate was washed with dH_2O , and then resuspended in the mother liquor and refluxed for 24 h. The crystals were then washed in a medium sintered-glass funnel under vacuum, first with pH 10.0 dH_2O , then with acetone. The crystals were dried in a sealed Büchner flask under vacuum, and stored at room temperature in a desiccator.

2.2.3 Characterization of synthesized hydroxyapatite seed crystals

X-ray powder diffraction of the synthesized HAP was utilized to verify the absence of other calcium phosphate phases. Spectra were collected on a Bruker D8 microdiffractometer. Specific surface area measurements on synthesized HAP were performed using a Micrometrics ASAP 2010 BET Surface Area Analyzer to measure the volume of adsorbed nitrogen gas.

Scanning electron microscopy (SEM) was performed on a LEO 1540XB SEM. Synthetic HAP was mounted on a carbon strip prior to SEM analysis. For HAP samples obtained after CCSG experiments, the metastable calcium phosphate solution was removed by vacuum filtration through a 0.2- μm polyethersulfone filter after which a carbon strip was blotted onto the filter to facilitate transfer of HAP crystals to the strip.

The ratio of calcium to phosphate (detected as phosphorus) of the synthesized HAP was determined using inductively coupled plasma – atomic emission spectroscopy (ICP-AES). 2 mg of HAP was dissolved in 50 ml of 0.1 M HCl solution overnight on a rotator prior to ICP-AES analysis.

2.2.4 Constant-composition seeded-growth

2.2.4.1 Constant-composition seeded-growth assay

A modification of the constant-composition seeded-growth assay originally developed by Nancollas and Koutsoukos (1978) was used [287]. Metastable calcium phosphate solutions were prepared by combining 1.25 ml of dH₂O (minus polypeptide volume), 2 ml of 1.2 mM Na₂HPO₄, 4 ml of 1 mM Ca(NO₃)₂/300 mM NaCl solution (in the order listed), and the test inhibitor (dissolved in dH₂O) in a custom-made double-walled pyrex vessel with agitation using a magnetic stirrer to minimize localized regions of high supersaturation. The solution was maintained at $37 \pm 0.1^\circ\text{C}$ using a circulating water bath connected to the Pyrex vessel. All solutions were previously vacuum-filtered through 0.2 μm -pore-size polyethersulfone membranes. A calomel pHC4006 electrode connected to a TIM900 titration manager was immersed into the reaction solution. The electrode was calibrated before each experiment with standard IUPAC buffer solutions ($\text{pH } 7.000 \pm 0.01$ and $\text{pH } 10.012 \pm 0.01$) at 37°C . To exclude atmospheric carbon dioxide, a single flow tube rotameter was used to bubble 18.3 ml/min of water-saturated nitrogen through the solution. To provide adequate time to reach equilibrium, nitrogen flow began one hour prior to the addition of seed crystals. Prior to the addition of HAP seed crystals, the pH of the metastable solution was adjusted to between 7.400 and 7.410 by the addition of small aliquots of 25 mM NaOH.

The titrant solutions were empirically determined for the maintenance of constant solution composition by varying the concentration of NaOH in the Na₂HPO₄/NaOH titrant solution. An ABU93 triburette was customized so that two of its 5-ml burettes operated in the 'master-slave' mode. The 'master' burette contained 3.5 mM

$\text{Ca}(\text{NO}_3)_2$ /300 mM NaCl and the 'slave' burette contained 2.1 mM Na_2HPO_4 /1.6 mM NaOH. Titrant addition was controlled using TimTalk 9 in pH-stat mode with an endpoint pH of 7.400 and proportional band pH of 0.100. The burettes were limited to a minimum speed of 1.0%/min and a maximum speed of 3.0%/min.

Using the auto-titration setup described, the fluctuation in pH generally did not exceed 7.400 ± 0.003 . The titration manager was programmed to maintain a pH of 7.400 for 240 minutes after the crystal growth reaction began. The reaction was initiated by the addition of 750 μl of a freshly made HAP slurry in dH_2O (2 mg HAP, unless otherwise stated), giving a final reaction solution composition of 0.5 mM $\text{Ca}(\text{NO}_3)_2$, 0.3 mM Na_2HPO_4 and 150 mM NaCl (total volume, 8 ml).

Aliquots (0.4 ml) were removed from the reaction immediately after the addition of the hydroxyapatite slurry (0 min) and immediately prior to the termination of the assay (240 min). Aliquots were immediately filtered through 0.2- μm polyethersulfone membrane syringe filters. The calcium and phosphate concentrations were determined spectrophotometrically (see below) to ensure constant composition was maintained within $\pm 5\%$ of their initial concentrations. The linear portion of the slope of titrant addition against time, which occurred within ~ 60 minutes after addition of seed crystals until termination of the experiment, was used to calculate the HAP growth rate. The HAP growth rate was expressed as a percentage of growth compared to that observed in the absence of inhibitor; growth rate (%) = $[G_i/G_0] \times 100$, where G_i is the growth rate in the presence of inhibitor and G_0 is the growth rate in the absence of inhibitor.

2.2.4.2 Determination of calcium and phosphate concentration

Calcium and inorganic phosphate ions were detected spectrophotometrically and their concentrations were calculated using standard curves of known concentrations. Calcium was detected using the QuantiChrom™ Calcium Assay Kit (612 nm) whereas inorganic phosphate was detected using the Innova Biosciences PiColorLock™ Phosphate Assay Kit (635 nm) according to protocols recommended by the respective manufacturers. Spectrophotometer readings were performed on a Safire microplate reader.

2.2.5 Protein expression/purification and peptide synthesis/purification

P3, P0, OPAR and P-OPAR peptides were synthesized and purified by Yinyin (Heidi) Liao and Kari Ann Orlay. Briefly, peptides were synthesized by a batch method with free amino and carboxyl termini using Fmoc chemistry and purified by high-performance liquid chromatography on a C18 column, as previously described [269]. Peptide purity was determined by mass spectrometry and amino acid analysis (Institute for Biomolecular Design, U of A/Advanced Protein Technology Centre, SickKids).

Milk OPN was supplied by Esben S. Sørensen (Protein Chemistry Laboratory, Department of Molecular Biology, University of Århus, Denmark) [289]. Briefly, bovine milk OPN was purified by Sephadex G-75 gel chromatography, Q-Sepharose ion-exchange followed again with an additional Sephadex G-75 gel chromatography in the presence of urea.

Recombinant OPN was expressed and purified by Hong Hong Chen (Goldberg lab, UWO, London, Ontario). Briefly, *Escherichia coli* BL21 cells were transformed with a pET28a expression vector containing rat OPN cDNA. The expressed protein was

purified by nickel affinity chromatography followed with fast protein liquid chromatography (FPLC) as previously described for BSP [39].

2.2.6 Circular dichroism of osteopontin peptides

CD studies were performed using a Jasco J-810 specropolarimeter equipped with a Peltier temperature-control system. Scans were recorded at 37°C from 250 to 190 nm, with a step size of 0.5 nm and a scan speed of 100 nm/min. A cell with a path length of 0.1 mm was used. Each peptide solution was scanned 30 times and the resulting spectra averaged. Blank buffer scans were subtracted from the raw data, which were then converted to mean residue ellipticity (θ) in units of degree $\text{cm}^2 \text{dmol}^{-1}$ by standard procedures. CDSSTR and CONTINLL algorithms for the estimation of protein secondary structure from UV CD spectra were used to analyze the CD spectra generated [290, 291]. Each peptide was resuspended at a concentration of 0.4 mM in either Ca/PO_4 [500 μM $\text{Ca}(\text{NO}_3)_2$, 300 μM Na_2HPO_4 , 150 mM NaCl, pH 7.4] or HEPES (10 mM HEPES, 100 mM NaCl, 10 mM KCl, pH 7.4) buffer.

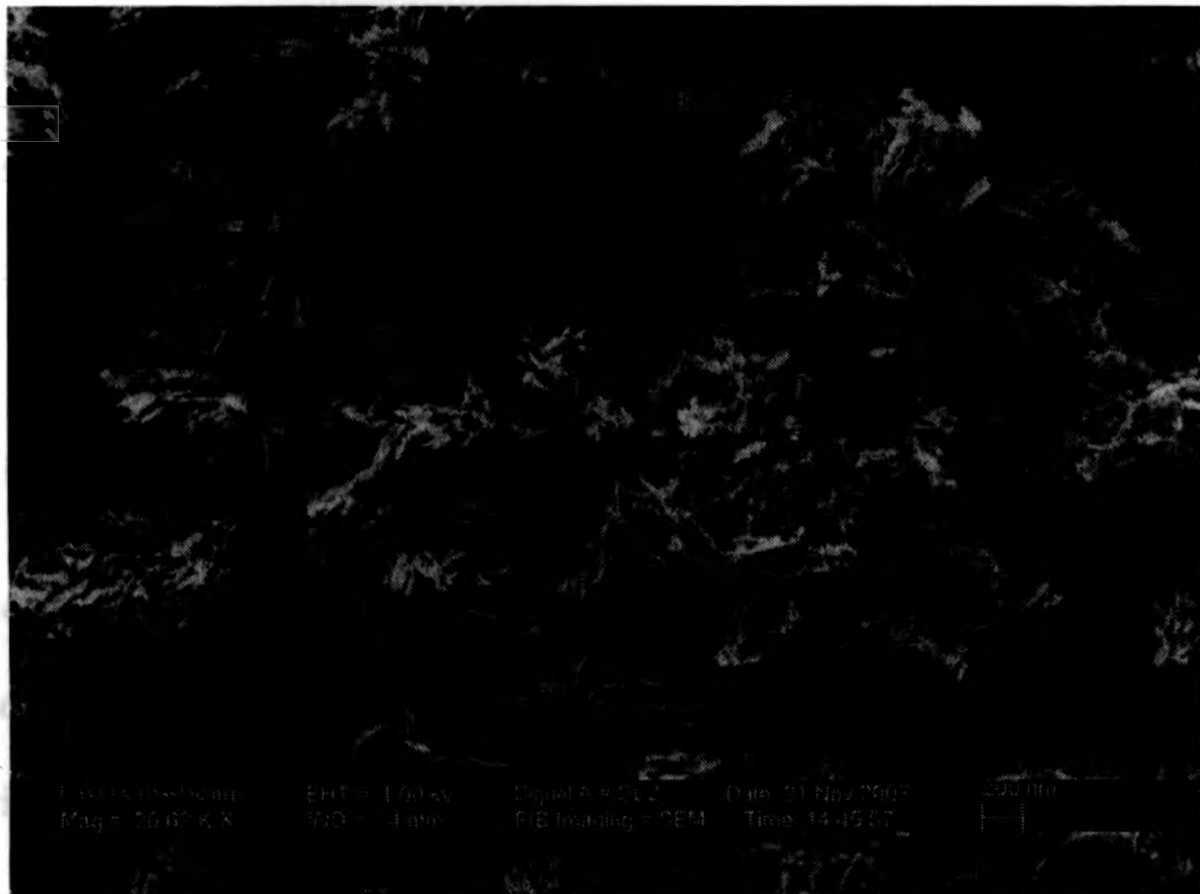
2.3 Results

2.3.1 Characterization of synthesized HAP

The mineral phase of bone is a calcium-deficient and poorly crystalline analogue of the geologically occurring hydroxyapatite [$\text{Ca}_{10}(\text{PO}_4)_6\text{OH}_2$]. SEM of the synthesized HAP revealed aggregates of plate-like crystals with apparent dimensions of approximately 2 nm in thickness, 40 to 200 nm in length and variable width (Figure 2.1).

Figure 2.1 SEM images of synthesized HAP crystals.

Images are representative of the morphology of the synthesized HAP crystals before (A) and after (B) 4 hours of growth in the constant-composition seeded-growth assay.

A**B**

X-ray powder diffraction was also utilized to ensure the absence of other calcium phosphate mineral phases (Figure 2.2). The synthesized HAP exhibited a Brunauer-Emmett-Teller (BET) surface area of $84.126 \pm 0.094 \text{ m}^2/\text{g}$ and a Langmuir surface area of $115.290 \pm 2.347 \text{ m}^2/\text{g}$. ICP-AES analysis revealed the calcium/phosphorus molar ratio to be 1.612 ± 0.013 , in comparison to the theoretical ratio of 1.67 for HAP.

2.3.2 Circular dichroism secondary structure prediction

The secondary structures of the peptides were determined at 37°C in both Ca/PO_4 buffer and HEPES buffer. All four peptides analyzed by CD spectroscopy displayed the characteristic spectrum of a 'random coil' secondary structure (Figures 2.3 and 2.4). Secondary-structure prediction algorithms estimated P3 and P0 to possess ~70% disorder while OPAR and P-OPAR were estimated to possess ~50% disorder over their 16 residue sequences (Table 2.1). P3/P0 were also estimated to possess between 12-17% β -strand and approximately 10% β -turn structure, whereas OPAR/P-OPAR peptides were predicted to possess between 24-30% β -strand and 13-17% β -turn.

2.3.3 Constant-composition seeded-growth assay

Hydroxyapatite growth in a calcium/phosphate solution slows and then ceases as the calcium, phosphate and hydroxide ions are depleted from the solution. In the constant-composition seeded-growth assay the incorporated growth constituents are continuously replenished, allowing for hydroxyapatite growth to continue under a constant driving force for extended periods (see CCSG assay schematic Figures 2.5 and 2.6). This can be

Figure 2.2 X-ray powder diffraction pattern of synthesized HAP.

X-ray powder diffraction pattern of synthesized HAP crystals showing the characteristic peaks of HAP. Prominent diffraction peaks corresponding to reflections from (002), (211), (310), (311), (113) and (222) planes of HAP are labeled. A 'stick-figure' spectrum for HAP is set below the experimental spectrum for comparison.

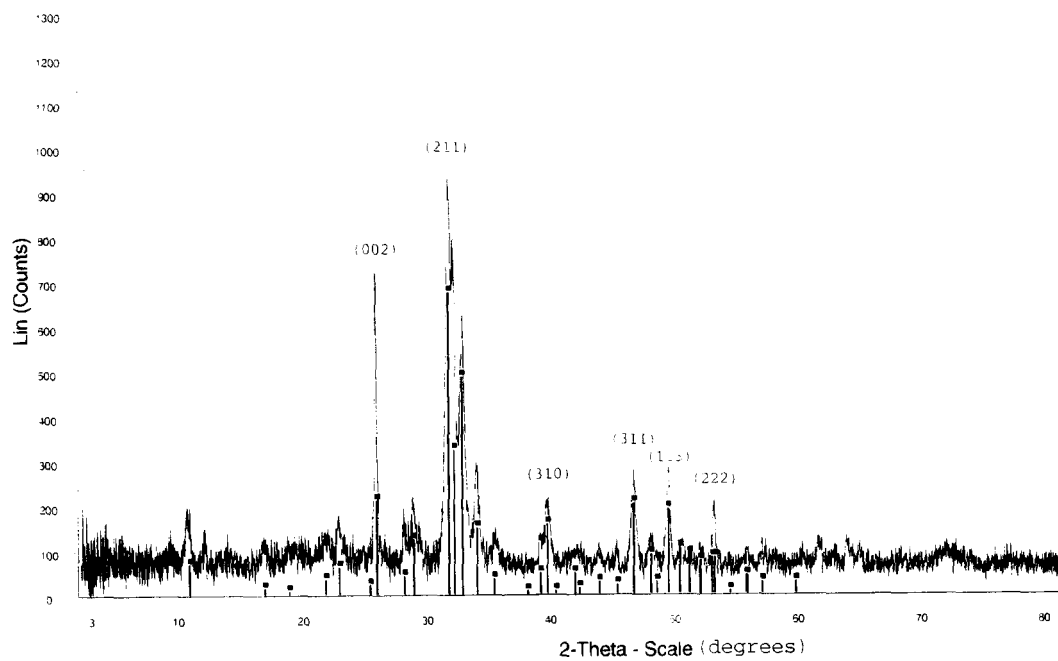
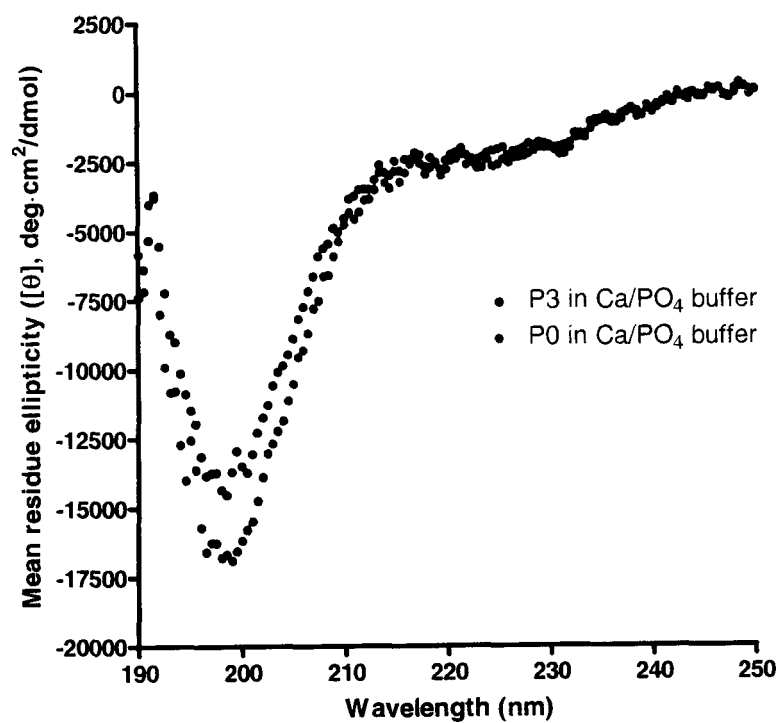


Figure 2.3 Analysis of P3 and P0 by circular dichroism spectroscopy.

(A) P3 and P0 dissolved in Ca/PO_4 buffer used in CCSG experiments. (B) P3 and P0 dissolved in HEPES buffer used in ITC experiments. Each peptide was resuspended at a concentration of 0.4 mM. CD spectra were collected at 37°C in 0.5-nm steps at a scan speed of 100 nm/min. Ca/PO_4 buffer composition: 500 μM $\text{Ca}(\text{NO}_3)_2$, 300 μM Na_2HPO_4 , 150 mM NaCl, pH 7.4. HEPES buffer composition: 10 mM HEPES, 100 mM NaCl, 10 mM KCl, pH 7.4.

A



B

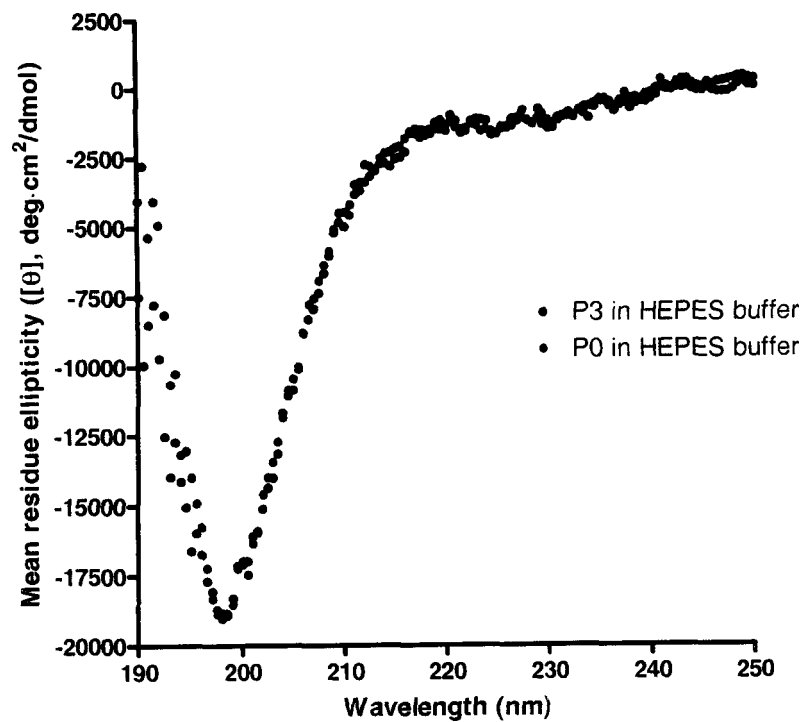
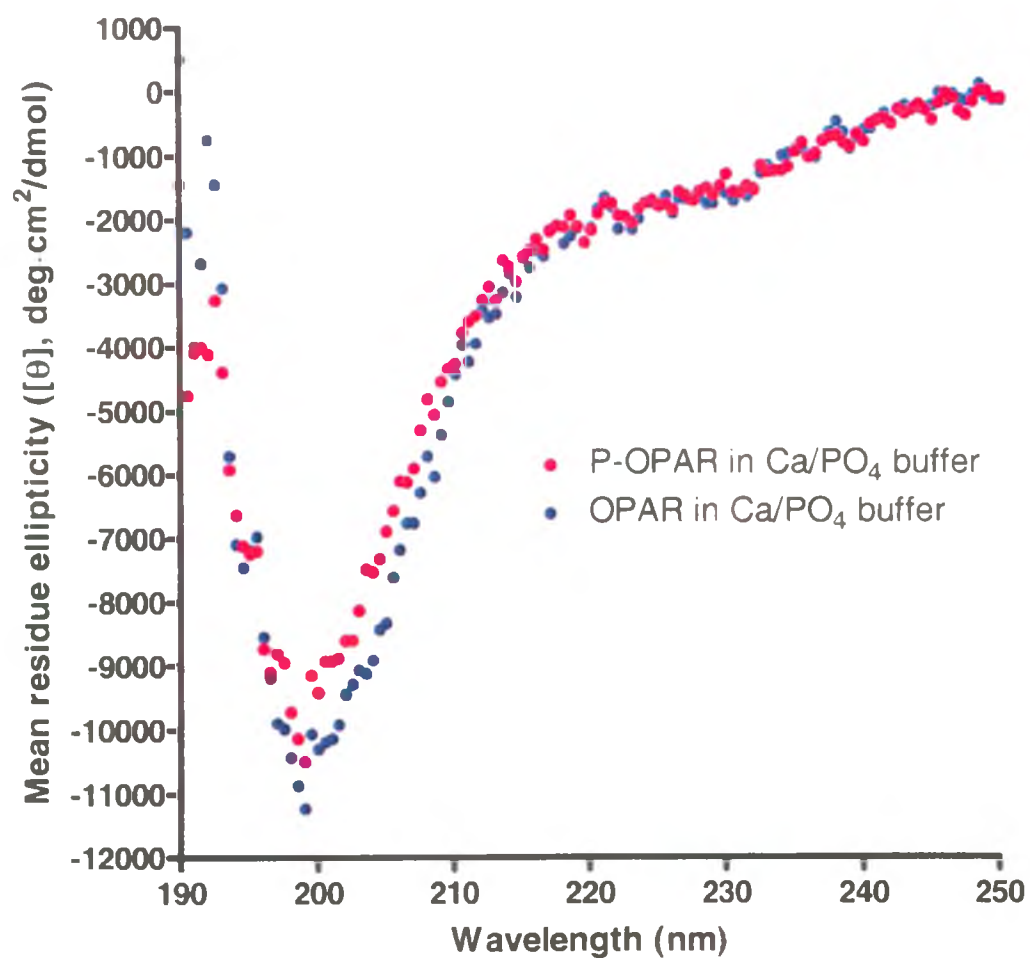


Figure 2.4 Analysis of OPAR and P-OPAR by circular dichroism spectroscopy.

(A) OPAR and P-OPAR dissolved in Ca/PO_4 buffer used in CCSG experiments. (B) OPAR and P-OPAR dissolved in HEPES buffer used in ITC experiments. Each peptide was resuspended at a concentration of 0.4 mM. CD spectra were collected at 37°C in 0.5-nm steps at a scan speed of 100 nm/min. Ca/PO_4 buffer composition: 500 μM $\text{Ca}(\text{NO}_3)_2$, 300 μM Na_2HPO_4 , 150 mM NaCl, pH 7.4. HEPES buffer composition: 10 mM HEPES, 100 mM NaCl, 10 mM KCl, pH 7.4.

A



B

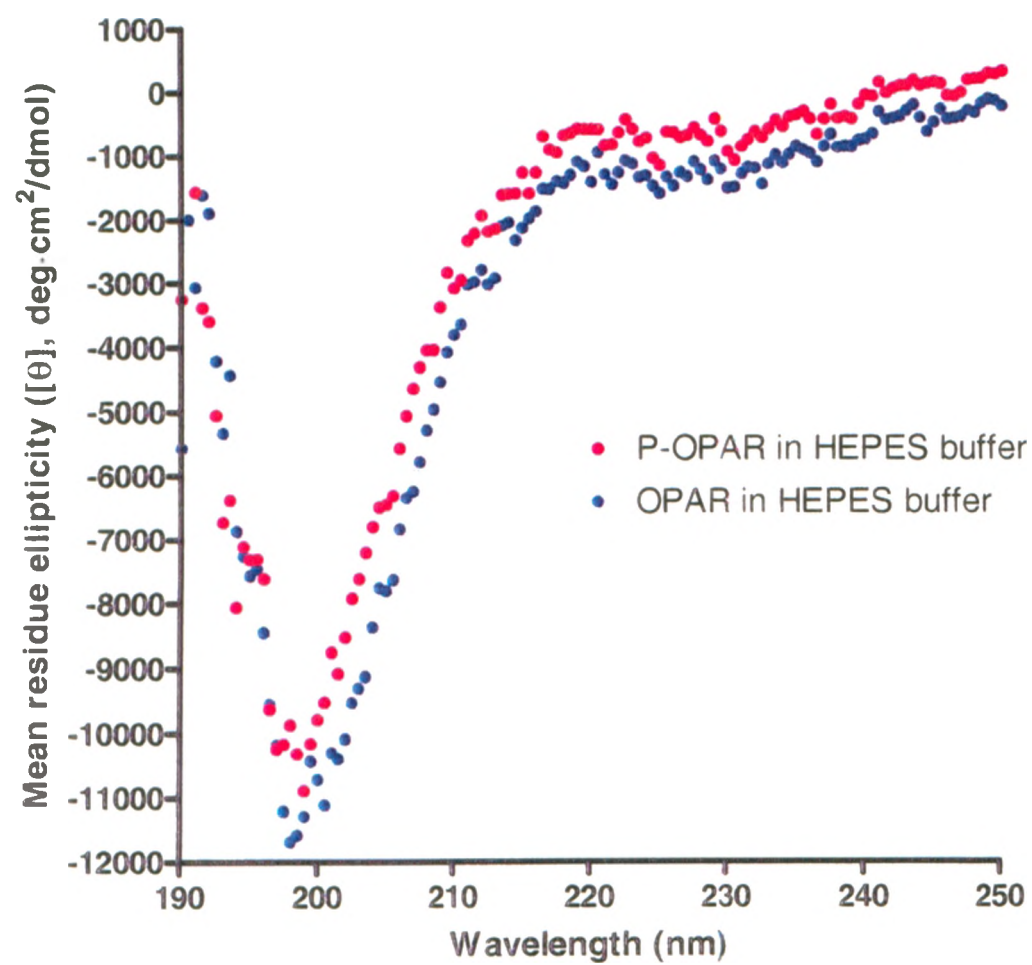


Table 2.1 Summary of the average fractional secondary structure of P3, P0, OPAR and P-OPAR.

Peptide	Buffer*	Average Fractional Secondary Structure Prediction [†]			
		α -Helix	β -strand	β -turn	Unordered
P3	Ca/PO ₄	3.6	15.2	9.2	71.5
	HEPES	2.3	15.9	9.2	72.1
P0	Ca/PO ₄	3.6	12.2	7.4	76.1
	HEPES	3.1	17.3	9.6	69.8
OPAR	Ca/PO ₄	4.1	27.6	14.6	53.0
	HEPES	3.5	23.1	13.1	59.7
P-OPAR	Ca/PO ₄	3.7	28.9	18.0	48.6
	HEPES	2.4	30.4	17.1	49.2

* Ca/PO₄ buffer composition: 500 μ M Ca(NO₃)₂, 300 μ M Na₂HPO₄ and 150 mM NaCl, pH 7.40. HEPES buffer composition: 10 mM HEPES, 100 mM NaCl, 10 mM KCl, and pH 7.4.

[†] Reported fractional secondary structures are the average of those calculated using the CDSSTR and CONTINLL algorithms.

Figure 2.5 Schematic of constant-composition seeded-growth assay.

Seed crystals (2 mg) were grown in a solution composed of 500 μM $\text{Ca}(\text{NO}_3)_2$, 300 μM Na_2HPO_4 and 150 mM NaCl (pH 7.40, 37°C). The two titrant solutions were composed of 3.5 mM $\text{Ca}(\text{NO}_3)_2$ /300 mM NaCl and 2.1 mM Na_2HPO_4 /1.6 mM NaOH and were housed separately. The HAP crystals were kept suspended by a rotating Teflon-coated bar magnet (not shown). Figure not to scale.

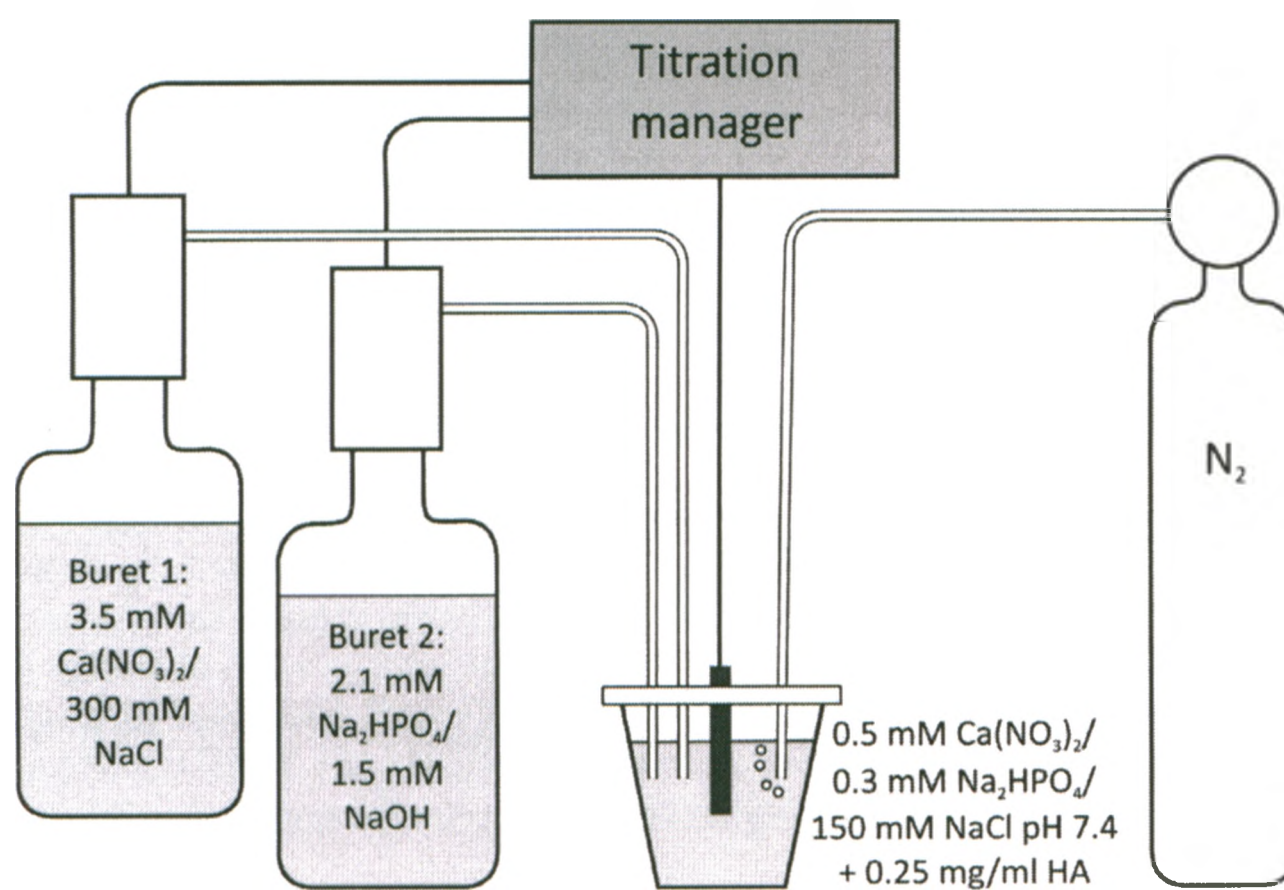
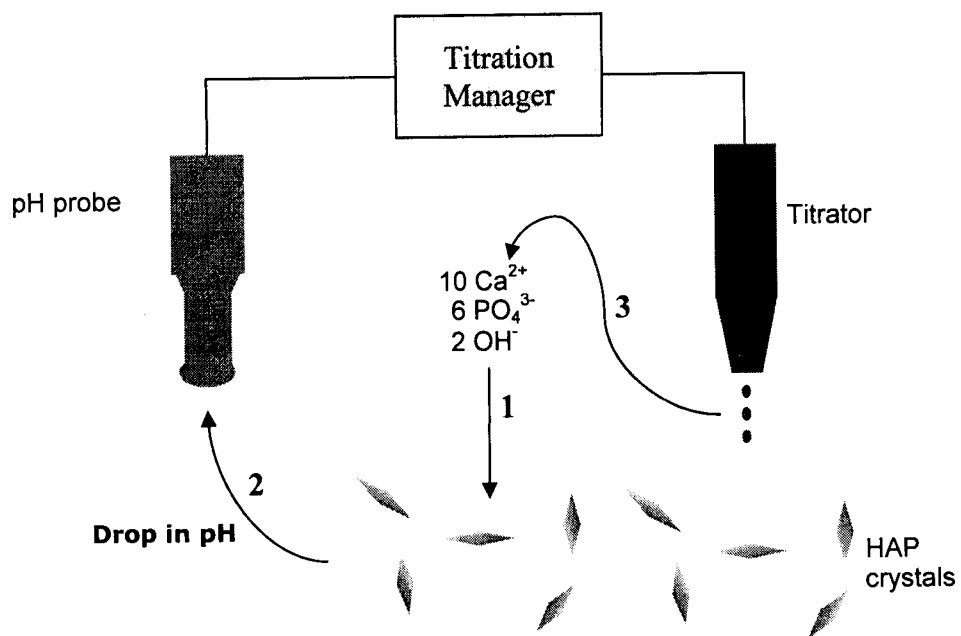


Figure 2.6 Detailed schematic of constant-composition seeded-growth assay.

1) HAP crystal growth results in a pH drop (due to incorporation of OH^- into the growing crystal lattice), 2) which is detected by the pH probe, which is interfaced to a computer. 3) In response to the pH drop, software (TimTalk) activates titrators that deliver concentrated $\text{Ca}(\text{NO}_3)_2/\text{NaCl}$ and $\text{Na}_2\text{HPO}_4/\text{NaOH}$ solutions to reconstitute the starting Ca/PO_4 concentrations and restore the pH to 7.400. The stoichiometry of hydroxyapatite is $\text{Ca}_5(\text{PO}_4)_3(\text{OH})$. The two titrant solutions were composed of 3.5 mM $\text{Ca}(\text{NO}_3)_2/300$ mM NaCl and 2.1 mM $\text{Na}_2\text{HPO}_4/1.6$ mM NaOH and were housed separately. Figure not to scale.



accomplished by taking advantage of the increasing acidity of the calcium phosphate solution as hydroxide ions are incorporated into the crystal lattice of the growing HAP. Any drop in pH below 7.400 detected by the pH probe activates the titrator to administer solutions containing calcium, phosphate and hydroxide in the ratios occurring in HAP (5:3:1). Titrant addition ceases once the pH of the solution returns to 7.400, and is resumed each time the pH drops below 7.400 for the duration of the assay. As the ratio of $\text{Ca}/\text{PO}_4/\text{OH}$ is the same in the titrants as in the growing crystals, a constant supersaturation will be maintained in the reaction solution. Alternatively, the pH of the solution can be maintained using a pH electrode, while the calcium and phosphate concentrations are controlled using a calcium-specific electrode.

The constant-composition seeded-growth assay used here involves an autotitration apparatus in which a pH electrode controls two burets. The “master” buret contains sodium phosphate and sodium hydroxide, the “slave” buret contains calcium nitrate and sodium chloride. The experimental variables include the concentrations of calcium and phosphate in the reaction solution, the pH of titrant 1 and the concentrations of calcium and phosphate in the titrants. To determine values for these variables that maintained a constant composition, a large number of exploratory studies were performed. For example, if concentrations of calcium and phosphate were observed to rise during the assay, the amount of NaOH in the phosphate titrant was increased for subsequent constant-composition trials. Our goal was to maintain the calcium and phosphate concentrations of the reaction solution within 5% of initial values throughout the assay period. A related goal was to achieve a linear rate of titrant addition: if reaction-solution

supersaturation increases, titrant addition becomes exponential; if supersaturation decreases, addition becomes hyperbolic.

During this empirical determination of appropriate titrant concentrations to achieve constant composition, it was discovered that a constant flow of nitrogen through the reaction solution was essential to achieving a linear rate of crystal growth. If nitrogen flow is not constant, variable amounts of atmospheric carbon dioxide will dissolve into the reaction solution, altering the rate of titrant addition in response to crystal growth. This was accomplished by the use of a single-tube flow meter through which the flow of nitrogen could be controlled with adequate precision.

The conditions determined empirically to maintain linear HAP growth at constant supersaturation are described above (section 2.2.4.1). Under these conditions, it was observed that the growth of HAP was composed of two phases, an initial phase of exponential growth followed by an extended period of linear growth (Figure 2.7). The linear growth rate observed after 60 min of growth was used as a measure of the HAP growth rate. The rate of growth was found to be linearly proportional to the mass of HAP (Figure 2.8).

Figure 2.7 Example HAP growth curve.

Ca²⁺ addition required to maintain constant solution composition during the course of a CCSG assay. Seeded with 2 mg of hydroxyapatite.

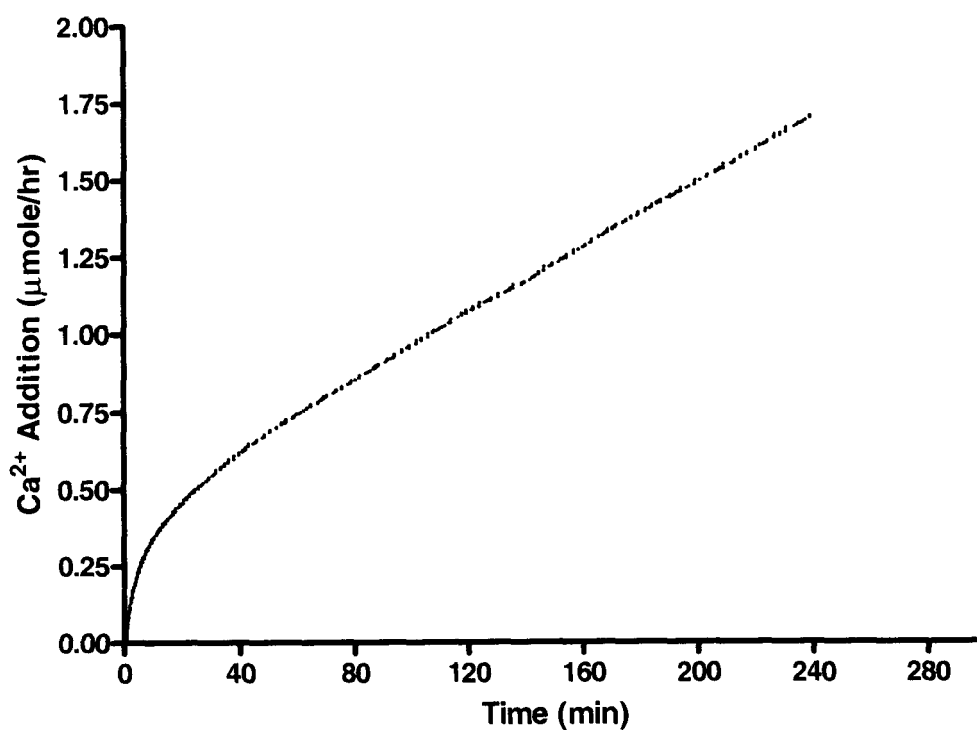
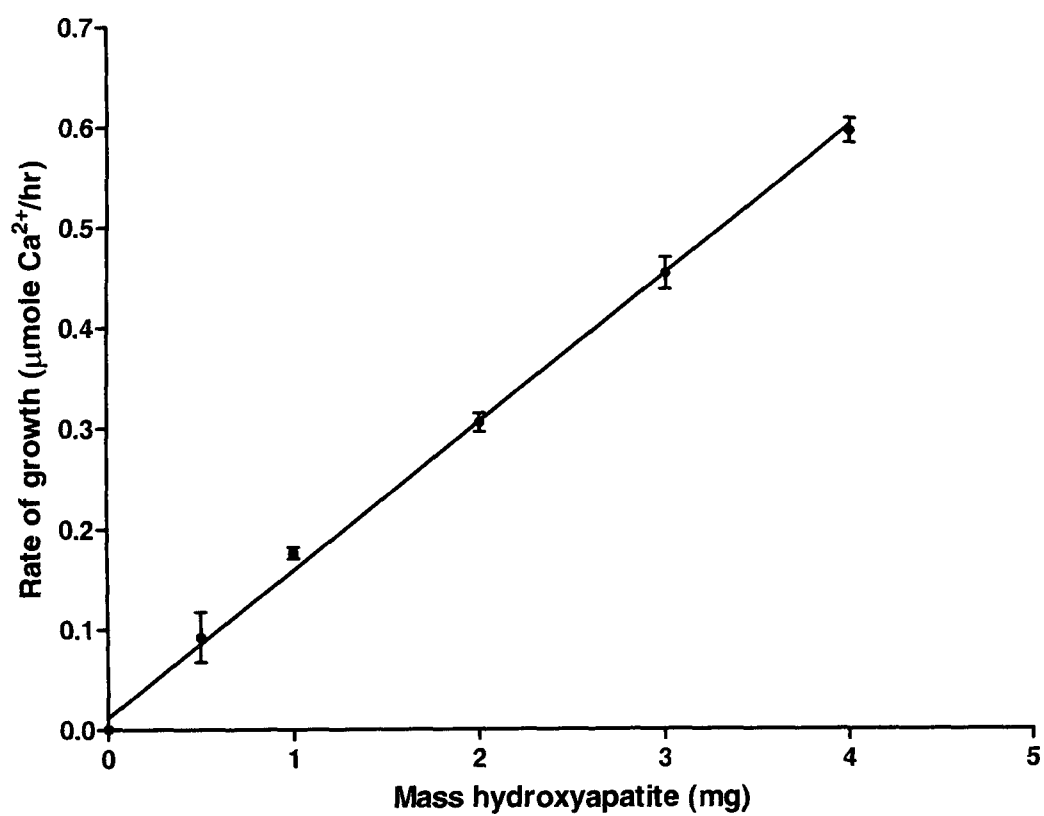


Figure 2.8 Rate of HAP growth versus mass of seed HAP crystals.

HAP growth rate was observed to be linearly proportional to the mass of HAP seed crystals added to the CCSG assay. The linear relation demonstrates that primary nucleation does not occur during the course of the experiment. Thus, consumption of calcium, phosphate and hydroxide from solution occurs solely due to incorporation of these ions into the growing crystal lattice of HAP seed crystals. $n = 3$.



2.3.4 Protein/peptide inhibitory potency toward HAP Growth

The effects of rat rOPN, bovine mOPN, rat OPN-sequence-derived peptides and the model compound poly-Asp upon HAP growth were evaluated using the constant-composition assay. HAP growth rates, expressed as a percentage of standard (no added protein/peptide) rates, were plotted against protein/peptide concentration. The data for all peptides/proteins (except P0) were fitted to exponential decay curves in order that the proteins could be compared on the basis of their 50% inhibitory concentrations (IC_{50}).

A representative example of a family of titration curves of HAP growth rate in the presence of increasing concentrations of mOPN is illustrated in Figure 2.9. The slope of the linear portion of the HAP growth assay (1h to 4h) decreased when higher concentrations of mOPN were used in the crystal growth assay. The IC_{50} for mOPN was observed to be 1.94 $\mu\text{g/ml}$ and complete inhibition of HAP crystal growth was achieved with 4.6 $\mu\text{g/ml}$ (Figure 2.10A). In contrast, the unmodified rOPN's IC_{50} for HAP growth was 5.23 $\mu\text{g/ml}$ and the growth was reduced to approximately 40% of the uninhibited crystal growth rate at the highest concentration tested (13 $\mu\text{g/ml}$) (Figure 2.10B).

P3 exhibited an IC_{50} of 2.03 $\mu\text{g/ml}$ and the crystal growth rate was reduced by approximately 80% at the highest concentration of peptide tested (10 $\mu\text{g/ml}$) (Figure 2.11A). The IC_{50} of P0 could not be measured as this peptide exhibited considerably reduced inhibition compared to P3. At a concentration of 15 $\mu\text{g/ml}$ P0 inhibited crystal growth by approximately 10% and extrapolation of the curve gave an IC_{50} of >75 $\mu\text{g/ml}$ (Figure 2.11B).

Figure 2.9 Rate of HAP growth in the presence of increasing concentrations of mOPN.

HAP seed crystals (0.25 mg/ml) were grown in a solution composed of 500 μM $\text{Ca}(\text{NO}_3)_2$, 300 μM Na_2HPO_4 and 150 mM NaCl (pH 7.40, 37°C). Samples were removed periodically, filtered to remove the HAP crystals, and the concentrations of calcium and phosphate were determined to ensure constant composition was maintained. A dose-dependent inhibition was observed with increasing concentrations of mOPN decreasing the HAP growth rate. $n = 1$.

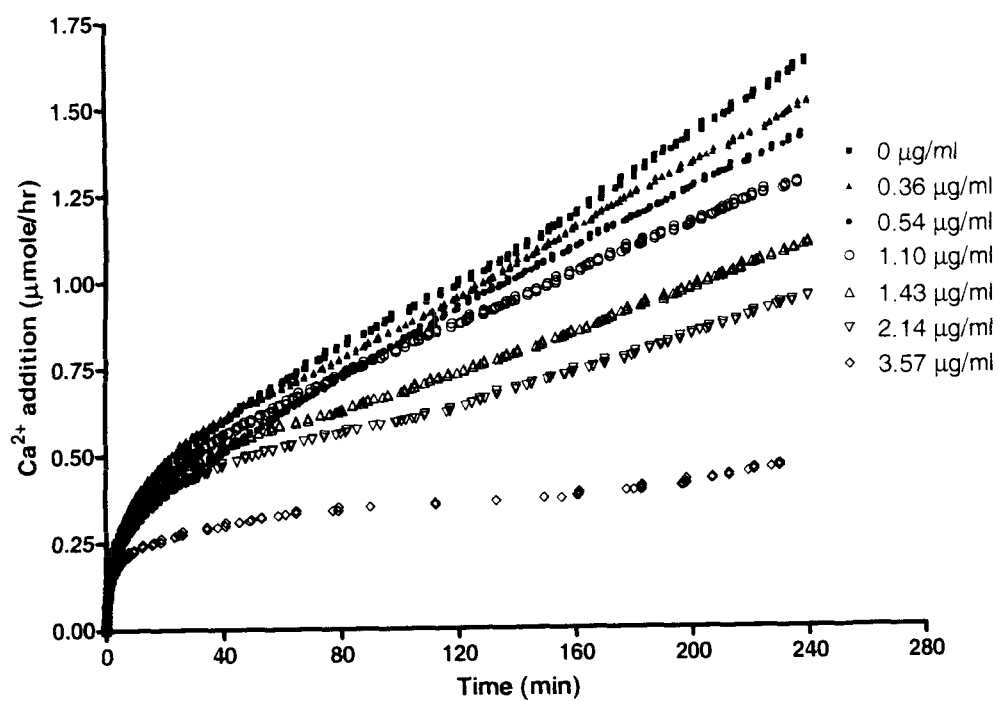
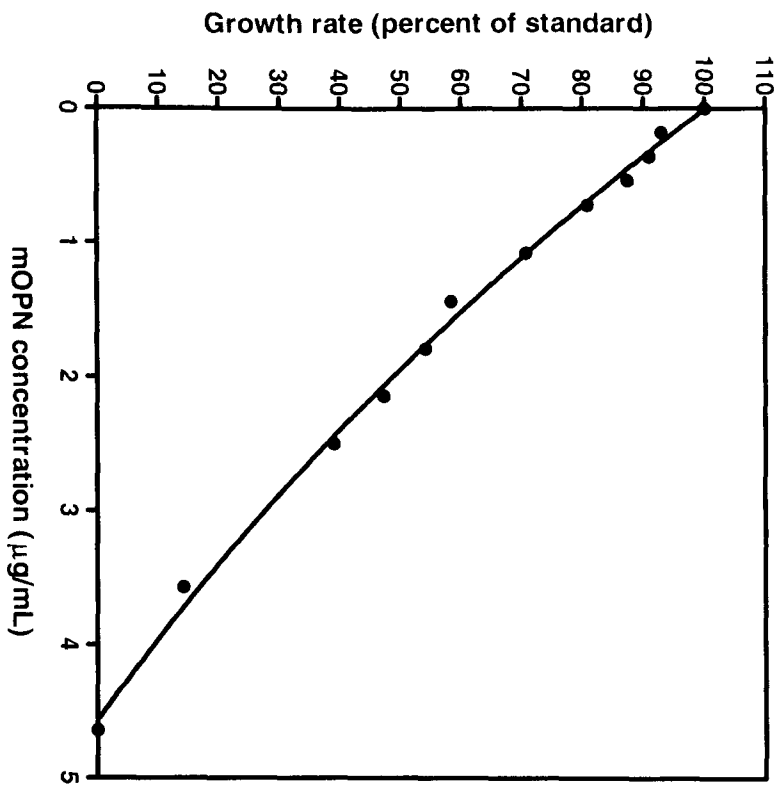


Figure 2.10 Rate of HAP growth in the presence of mOPN and rOPN.

HAP seed crystals (0.25 mg/ml) were grown in a solution composed of 500 μM $\text{Ca}(\text{NO}_3)_2$, 300 μM Na_2HPO_4 and 150 mM NaCl (pH 7.40, 37°C). Samples were removed periodically, filtered to remove the HAP crystals, and the concentrations of calcium and phosphate were determined to ensure constant composition was maintained. (A) The IC_{50} for mOPN was observed to be 1.94 $\mu\text{g/ml}$ and HAP growth was completely inhibited with $\sim 4.6 \mu\text{g/ml}$ [$K = 0.1374$, $r^2 = 0.990$], whereas (B) the IC_{50} for rOPN was observed to be 5.23 $\mu\text{g/ml}$ and the HAP growth rate was reduced to approximately 40% of the uninhibited growth rate (at highest concentration tested, 13 $\mu\text{g/ml}$) [$K = 2912$, $r^2 = 0.978$]. $n = 1$.

A



B

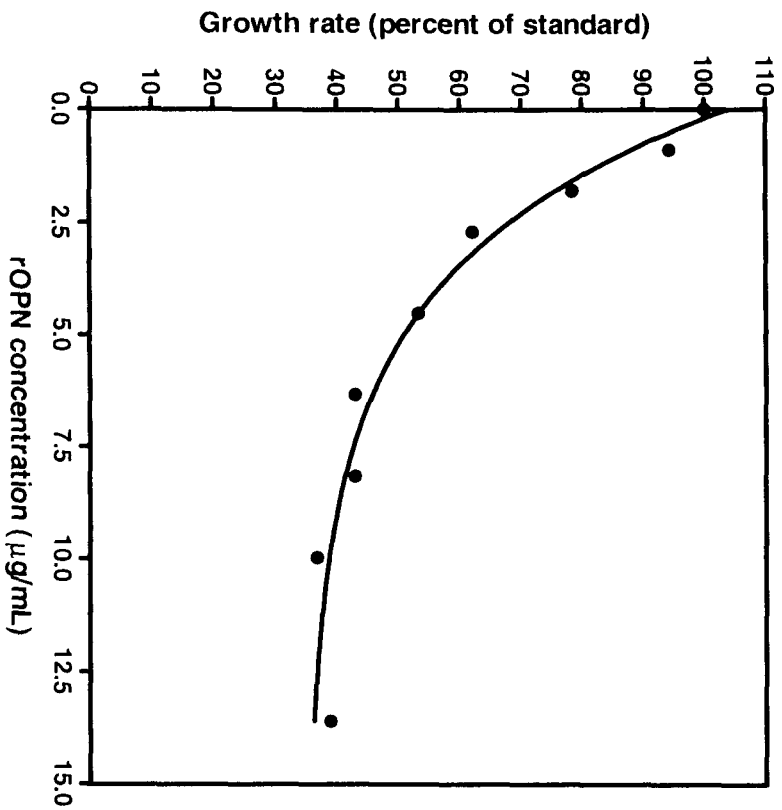
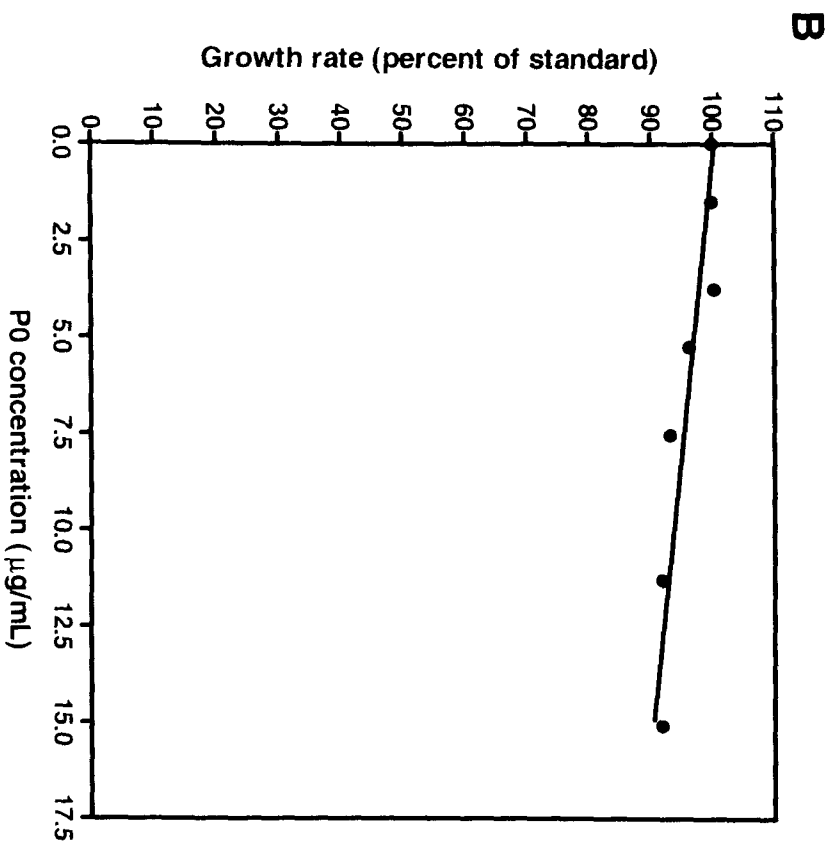
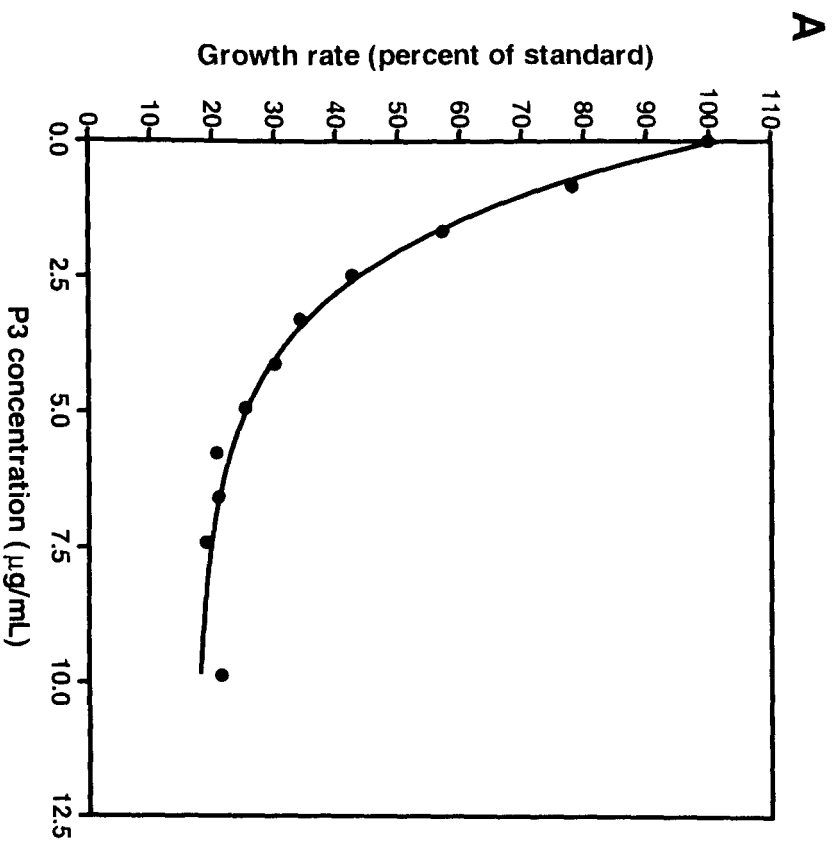


Figure 2.11 Rate of HAP growth in the presence of P3 and P0.

HAP seed crystals (0.25 mg/ml) were grown in a solution composed of 500 μM $\text{Ca}(\text{NO}_3)_2$, 300 μM Na_2HPO_4 and 150 mM NaCl (pH 7.40, 37°C). Samples were removed periodically, filtered to remove the HAP crystals, and the concentration of calcium and phosphate were determined to ensure constant composition was maintained. The 16mer P3 corresponds to residues 220-235 of rat OPN (pSHEpSTEQSDAIDpSAEK, where pS denotes phosphoserine). The 16mer P0 corresponds to residues 220-235 of rat OPN (SHESTEQSDAIDSAEK). (A) The IC_{50} of P3 was observed to be 2.03 $\mu\text{g}/\text{ml}$ and HAP growth was reduced approximately 80% at the highest concentration tested (10 $\mu\text{g}/\text{ml}$) [$K = 0.4682$, $r^2 = 0.995$], whereas (B) the IC_{50} of P0 was extrapolated to be greater than 75 $\mu\text{g}/\text{ml}$ [$y = -0.6650x + 100.4$, $r^2 = 0.840$]. $n = 1$.



P-OPAR and OPAR exhibited IC_{50} 's of 1.65 $\mu\text{g/ml}$ and 2.47 $\mu\text{g/ml}$, respectively (Figure 2.12A and B). Complete inhibition of HAP growth was achieved with a concentration of 7.4 $\mu\text{g/ml}$ P-OPAR and 9.2 $\mu\text{g/ml}$ OPAR.

Poly-Asp (11,000 Da) was observed to possess an IC_{50} of 1.45 $\mu\text{g/ml}$ and completely inhibited crystal growth at a concentration of approximately 5.5 $\mu\text{g/ml}$ (Figure 2.13).

See Table 2.2 for a summary of results obtained from CCSG experiments.

Figure 2.12 Rate of HAP growth in the presence of P-OPAR and OPAR.

HAP seed crystals (0.25 mg/ml) were grown in a solution composed of 500 μM $\text{Ca}(\text{NO}_3)_2$, 300 μM Na_2HPO_4 and 150 mM NaCl (pH 7.40, 37°C). Samples were removed periodically, filtered to remove the HAP crystals, and the concentration of Ca and PO_4 were determined to ensure constant composition was maintained. P-OPAR = phosphorylated OPN poly-aspartic acid region corresponds to residues 65-80 of rat OPN (pSHDHMDDDDDDDDDDGD, where pS denotes phosphoserine). OPAR = osteopontin poly-aspartic acid region corresponds to residues 65-80 of rat OPN (SHDHMDDDDDDDDDDGD). (A) The IC_{50} for P-OPAR was observed to be 1.65 $\mu\text{g}/\text{ml}$ and HAP growth was completely inhibited at ~ 7.4 $\mu\text{g}/\text{ml}$ [$K = 0.3588$, $r^2 = 0.995$], whereas (B) the IC_{50} for OPAR was observed to be 2.47 $\mu\text{g}/\text{ml}$ and HAP growth was completely inhibited at ~ 9.2 $\mu\text{g}/\text{ml}$ [$K = 0.2334$, $r^2 = 0.997$]. $n = 1$.

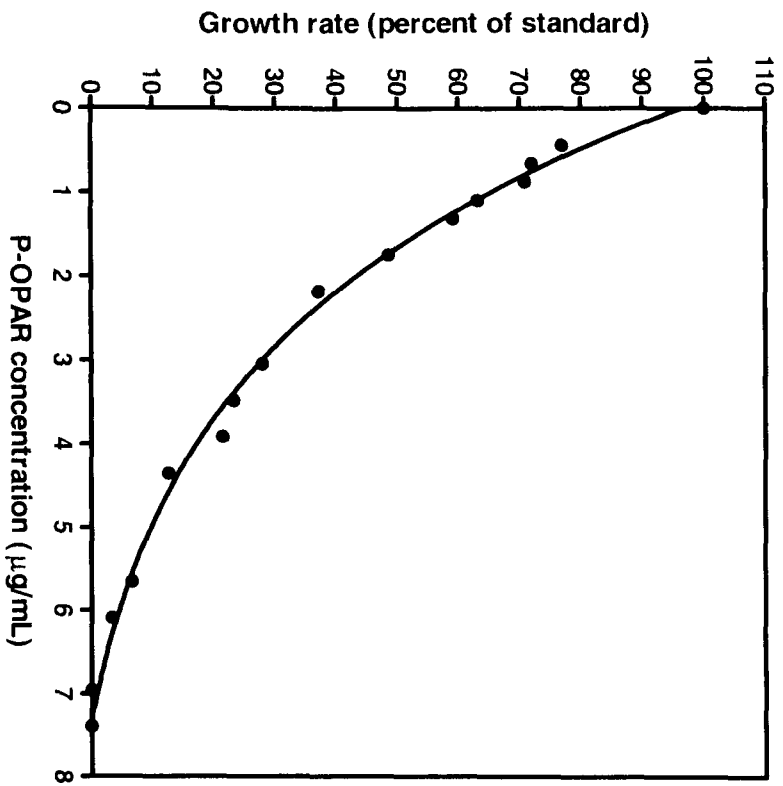
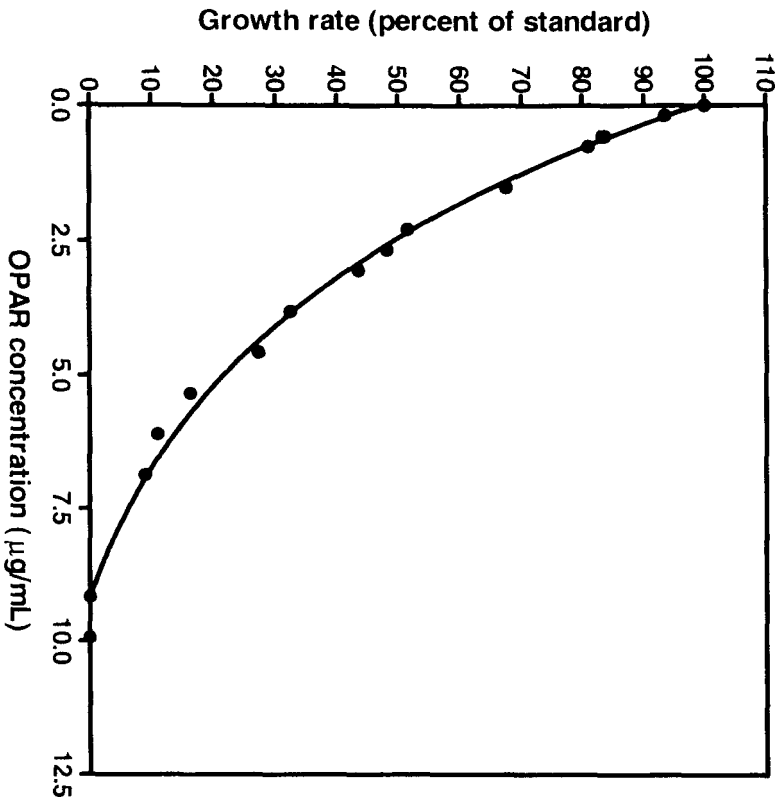
A**B**

Figure 2.13 Rate of HAP growth in the presence of poly-Asp.

HAP seed crystals (0.25 mg/ml) were grown in a solution composed of 500 μM $\text{Ca}(\text{NO}_3)_2$, 300 μM Na_2HPO_4 and 150 mM NaCl (pH 7.40, 37°C). Samples were removed periodically, filtered to remove the HAP crystals, and the concentration of calcium and phosphate were determined to ensure constant composition was maintained. MW of poly-Asp = 11,000 (Sigma). The IC_{50} was observed to be 1.45 $\mu\text{g}/\text{ml}$ and HAP growth was completely inhibited at ~ 5.5 $\mu\text{g}/\text{ml}$ [$K = 0.3893$, $r^2 = 0.994$]. $n = 1$.

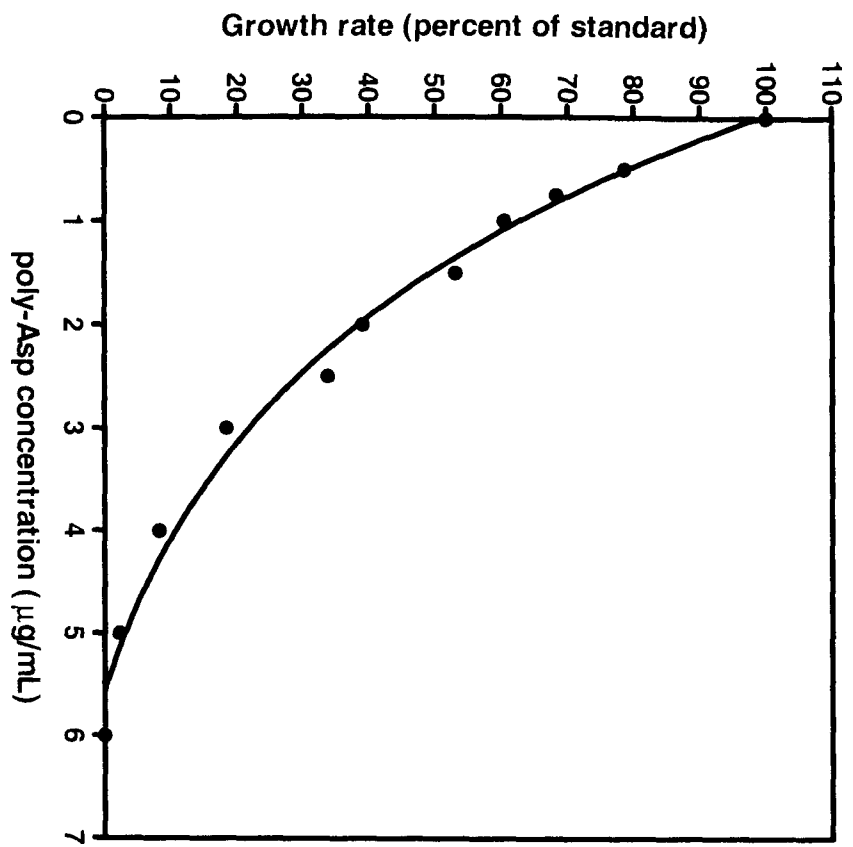


Table 2.2 Summary of constant-composition seeded-growth results.

Peptide/ Protein	# Residues	# PO ₄	# Acidic Residues	# Basic Residues	Net Charge ^y	Net Charge/ Residue	IC ₅₀ (μg/ml)	IC ₅₀ (nM)
Poly- Asp ^Δ	~95	0	~95	0	~ -95	-1	1.45	131.8
P- OPAR	16	1	11	0	-13	-0.81	1.65	867.3
mOPN ^β	262	25	62	28	-84	-0.32	1.94	57.5
P3	16	3	5	1	-10	-0.63	2.03	1033.3
OPAR	16	0	11	0	-11	-0.69	2.47	1353.8
rOPN	301	0	75	27	-48	-0.16	5.23	157.3
P0	16	0	5	1	-4	-0.25	>75	>42597

^y Net charge = (-1 x # acidic residues) + (1 x # basic residues) + (-2 x # phosphorylated residues). Charge of phosphoserine was determined based on the average of the pKa values obtained from [292-294].

^Δ Poly-Asp of 11,000 MW possesses an average of 95 residues per polymer.

^β Phosphate content and molecular mass (for μM IC₅₀ calculation) obtained from [105].

2.4 Discussion

2.4.1 Constant-composition seeded-growth assay

CCSG experiments revealed that the HAP growth was composed of two distinct phases: an initial rapid growth rate that slowed over the course of the first 60 min, after which a constant rate of growth was observed. Previous studies have shown that the initial rapid growth phase results from crystal growth at several different types of crystal surface imperfections [295, 296]. These include steps, kinks and screw dislocations (see Figure 1.2). Whereas the growth of steps and kinks leads to their disappearance, growth at screw dislocations does not [246]. Thus, over time crystal growth slows to a constant rate at which point growth predominantly takes place at screw dislocations. The transition to constant growth was found to occur within the first 60 minutes at the supersaturation level chosen for these studies and has been observed by others utilizing the constant-composition seeded-growth assay [297, 298]. The slope of the linear growth curve (representing the amount of calcium ions incorporated into the growing crystals) from 1 h through 4 h was used to calculate the HAP growth rate in the peptide and protein inhibition experiments.

The linear relationship observed between the HAP growth rate and the mass of seed crystals used, as shown in Fig 2.8, indicates that primary crystal nucleation does not occur during the course of a CCSG experiment at the supersaturation level chosen. Thus, the measured growth rate was due solely to growth of the HAP seed crystals. Growth

inhibition experiments were thus performed using a constant mass of 2 mg seed HAP and increasing concentrations of protein/peptide.

2.4.2 Peptide secondary-structure analysis

Although calcium is known to affect the secondary and tertiary structures of many proteins (e.g. [299]), no major structural differences were observed in any of the peptides studied between the two buffers tested. Each peptide displayed very low levels of α -helical structure ($< 5\%$). Even though α -helices are typically 4 to 12 residues in length [300], this is unsurprising as it is well known that short peptides do not typically exhibit significant α -helical structure in solution. This results from the inability of a short peptide to generate a sufficient number of stabilizing interactions to offset the entropic cost of folding into an α -helix [301].

The α -helix is a highly constrained structure in that it generally shows very small variations in the geometry of its psi and phi bond angles [302]. Unfortunately, the same is not true for β -turns and β -sheets, which are often bent/twisted and show a much larger variation in ψ/ϕ angles. The observed variation in CD spectra of β -structures results in variable ability of spectral-analysis algorithms to estimate the β -content of proteins [303]. Both secondary structure prediction algorithms used here estimated approximately 10% β -turn structure in P3/P0 and 13%-18% in OPAR/P-OPAR. Furthermore, β -strand secondary structure was estimated to be ~15% and ~30% in P3/P0 and OPAR/P-OPAR peptides, respectively. All peptides used in this study were 16 residues in length. This would correspond to β -turns of less than 2 residues in the P3/P0 peptides and less than 3 residues for OPAR/P-OPAR. The 4 types of turns identified in proteins thus far, α -, β -,

γ - and π -turns, require 5, 4, 3, and 6 residues, respectively [304]. Thus, it is unlikely that the reported percentages represent the true β -turn content of the peptides under study.

The β -strand is typically comprised of 5-10 amino acids, the majority of which exist in a hydrogen bond network with other adjacent β -strands, referred to as a β -sheet [305]. The β -strand percentages reported by the CD spectrum analysis algorithms would consist of less than 3 residues for the P3/P0 peptides, and 4 to 5 residues for the OPAR/P-OPAR peptides. The high preponderance of disorder-promoting residues D, M, K, S, Q and E [101], which constitute 69% and 82% of P3/P0 and OPAR/P-OPAR, respectively, coupled to the qualitative observation that each spectrum possesses the strong negative band near 200 nm which is characteristic of disordered polypeptides [306], puts the calculated β -strand content in question. This is further supported by the total lack of the bands characteristic of β -strands (negative at 216 and 175 nm and positive between 195 and 200 nm) [306]. Therefore, it is likely that these 4 peptides exist predominantly in the disordered state in solution.

2.4.3 HAP growth inhibition by proteins/peptides

Of the proteins and peptides examined in this study, mOPN, P3, OPAR and P-OPAR displayed a strong potency toward HAP growth inhibition, with each having an IC_{50} below 2.5 $\mu\text{g/ml}$. The model compound poly-Asp, composed of consecutive acidic residues, was observed to have the greatest inhibitory potency toward HAP growth and required the lowest concentration to achieve complete inhibition of crystal growth. This is in agreement with the findings of Tsortos and Nancollas who, using a constant-composition assay with similar supersaturation levels, reported that complete inhibition

of HAP growth occurred at a poly-Asp concentration of approximately 5 $\mu\text{g/ml}$, compared to approximately 5.5 $\mu\text{g/ml}$ found in this study [276]. Similarly, the consecutive short sequence of aspartic acidic residues found in OPAR seems to confer a high degree of inhibitory potency. In the presence of P-OPAR the inhibition of HAP crystal growth increased only slightly. Of the macromolecules studied, rOPN possesses the highest IC_{50} . P0 essentially lacks inhibitory activity at concentrations at which the other compounds elicit significant reductions in HAP growth rate.

Of the strong inhibitors, the inhibition potency of poly-Asp > P-OPAR > mOPN > P3 > OPAR when ranked according to their IC_{50} (by weight). The promotion of HAP growth by low concentrations of mOPN reported by Gericke *et al.* was not observed [52]. It is possible that differences in experimental setup are responsible for the observed difference. Gericke *et al.* utilized a steady-state double-diffusion gelatin-gel system. The results of the current study align with the prevailing theory that increased phosphorylation of inhibitory macromolecules yields more potent crystal growth inhibitors and parallel the findings of Wikiel *et al.* [279]. This group utilized a constant-composition seeded-growth assay to study differentially phosphorylated pentapeptides derived from the salivary protein statherin. Furthermore, the results observed by Gericke *et al.* describing a complete lack of HAP growth inhibitory effect by rOPN was also not observed in this study [52]. In addition to the above stated differences in experimental procedure that may be responsible for the observed differences, the sensitivity of the gelatin-gel system appears to be an order of magnitude below that of the CCSG assay. Gericke *et al.* report that at least 10 $\mu\text{g/ml}$ of bovine mOPN was required for detection of HAP growth inhibition, and at 25 $\mu\text{g/ml}$ growth was reduced by approximately 40% [52].

In contrast, the CCSG assays performed in this study resulted in HAP growth being decreased by 50% in the presence of $\sim 1.94 \mu\text{g/ml}$ mOPN and complete inhibition of growth in the presence of $\sim 4.6 \mu\text{g/ml}$. Considering mOPN was observed to possess a much higher inhibitory potency than rOPN in the CCSG assay, the maximum concentration of rOPN used by Gericke *et al.* in the gelatin-gel system ($25 \mu\text{g/ml}$) may be an order of magnitude too low to observe significant reductions in HAP growth [52].

The concentration of OPN in the urine of healthy adults has been reported to be approximately $3.5 \mu\text{g/ml}$ [214]. Thus, since the strong HAP growth inhibitors reported in this study each displayed an IC_{50} at least 1.5-fold lower than the physiological concentration of OPN in urine, they would likely inhibit HAP growth in urine as well. Furthermore, these results provide evidence that the OPN concentration present in the urine of healthy adults is capable of reducing the rate of HAP growth within urine, corroborating the findings that OPN is able to inhibit the spontaneous formation of CaP mineral phases *in vivo* [30].

Acidic residues are known to be important in conferring inhibitory potency to peptides and proteins [32, 36, 37, 269]. Lacking all post-translational modifications, rOPN was observed to be a relatively poor inhibitor of HAP crystal growth. The inhibitory potency of rOPN, which is composed of approximately 30% acidic residues, was markedly greater than the equally acidic P0 which possessed the lowest degree of HAP growth inhibition. This suggests that regions within rOPN similar in composition to P0 do not effectively inhibit HAP growth. If this were true, OPAR, as the only significantly acidic region within rOPN, would be expected to be providing the majority of rOPN's inhibitory potency. Yet, this is refuted by the finding that OPAR's molar IC_{50}

is much greater than that of rOPN. Thus, although P0 is a weak inhibitor of HAP growth, it is evident that regions adjacent to the poly-aspartic acid region within rOPN contribute to its inhibitory potency. This implies that the length of a polypeptide inhibitor is an important variable contributing to HAP growth inhibition, with increasing length producing greater inhibitory potency.

The 25 phosphoserine residues present in bovine mOPN produced a much more potent inhibitor, exhibiting an IC_{50} approximately three times lower than rOPN. Thus, post-translational phosphorylation is able to increase the potency of weak inhibitors. In agreement with this, the inhibitory potency of P0 was markedly increased by the addition of the 3 phosphoserine residues present in P3. These 3 phosphoserines collectively increase the magnitude of the negative charge by approximately six (net charge of ~ -10). Thus, the observation that phosphate clusters and blocks of consecutive aspartic acid residues are both able to effectively inhibit HAP growth suggests that regions possessing concentrated negative charge are required to produce a robust inhibitor. It should also be noted that the tissue-specific post-translational phosphorylations may be evolutionarily adapted phospho-forms of OPN possessing optimal crystal growth inhibition properties tailored to their unique physiological environments.

Of the polypeptides tested, the strong inhibitors all possess a relatively high average net negative charge per residue, except for mOPN, which possesses a much higher inhibitory potency than would be predicted based on this measure (Table 2.2). Franzen and Heinegard (1985) reported that bovine mOPN possesses $\sim 5\%$ (of dry weight) sialic acid content [41]. Taking these sialic acid moieties into account increases the magnitude of average net negative charge per residue marginally, to ~ -0.35 from ~ -0.32 , and

remains approximately one-half the magnitude of the average net negative charge per residue of the other strong inhibitors observed in this study. Thus, assuming the *O*-linked glycosylations present on mOPN do not possess a high affinity for the surface of HAP – suggested by the fact that dephosphorylated OPN loses most of its inhibitory potency – the higher-than-expected inhibitory potency of mOPN is likely not due to the increased negativity contributed by the sialic acid moieties. Unlike the other strong HAP growth inhibitors investigated in this study such as the homo-polymer poly-Asp and the relatively short 16mer peptides, mOPN is a relatively large and complex molecule with regard to its sequence and the number of anionic clusters (both phospho-clusters and poly-acidic regions). Thus, a synergistic effect between the affinities of each anionic cluster is hypothesized to be responsible for the greater-than-expected inhibitory potency. This effect would produce a much stronger avidity for the mOPN molecule toward the surface of HAP than the sum of the anionic clusters' individual affinities. This effect may also explain the difference in molar inhibitory potency between rOPN, OPAR, and P0. Although this suggestion accounts for the observations of the present study, future experiments are required for its validation.

Chapter Three – Isothermal Titration Calorimetry of the Osteopontin-Hydroxyapatite Interaction

3.1 Introduction

Almost all chemical reactions and physical adsorption processes exhibit some exo- or endothermic enthalpy change (ΔH) that can be directly measured through isothermal titration calorimetry (ITC). ITC is also able to measure the full binding isotherm of an interaction, from which the binding/equilibrium constant K_b can be deduced. Thus, ITC can provide a full thermodynamic characterization of an interaction, and is unique in its ability to do so without the need to chemically modify the interacting molecules (reviewed in [307]).

ITC has been used to assess the thermodynamics of the salivary protein statherin and HAP interaction [285]. Mutational studies can also be performed to reveal the role of specific residues on the adsorption process to mineral, as was shown with statherin [308]. The thermodynamics of OPN adsorption to HAP was previously unknown and was characterized using ITC in this study. This approach was also used to study the peptides P0, P3 and the homopolymer poly-Asp in order to elucidate the effects of acidic residues and phosphorylation on the thermodynamics of peptide/protein adsorption to HAP.

ITC experiments are typically performed on interactions with a quantitative relationship between the interacting molecules. For example, protein A may interact with protein B with a 1:1 stoichiometry. However, a heterogeneous population of HAP crystals poses a unique problem to the thermodynamic characterization of peptide-crystal adsorption. Since each peptide/protein, as suggested by the CCSG inhibition experiments, likely has a distinct number of binding sites for the HAP crystals utilized in this study, it was necessary to elucidate the stoichiometry of each adsorbate-HAP interaction prior to analysis by ITC. This was performed with a series of equilibrium

adsorption isotherm (EAI) experiments in which increasing amounts of peptide/protein were equilibrated with a defined mass of HAP crystals. The thermodynamic characterization of each adsorption interaction was thus performed subsequent to the elucidation of the maximum number of binding sites (N_{\max}) per unit surface area of HAP for each polypeptide.

3.2 Materials and Methods

3.2.1 Chemicals and reagents

Ca(NO ₃) ₂ 4·H ₂ O (>99.0%)	Sigma-Aldrich (St. Louis, MO)
Na ₂ HPO ₄ (>99.0%)	EMD Chemical Inc. (Gibbstown, NJ)
NaCl (>99.5%)	Sigma-Aldrich (St. Louis, MO)
NaOH (>98%)	EMD Chemical Inc. (Gibbstown, NJ)
Microcal VP high-sensitivity ITC	MicroCal (Northampton, MA)
ThermoVac	MicroCal (Northampton, MA)
Origin Software	MicroCal (Northampton, MA)
0.2-μm Acrodisc Syringe Filter (polyethersulfone)	PALL Corp. (Ann Arbor, MI)
Poly-L-Aspartic acid (sodium salt) 11,000 MW	Sigma (St. Louis, MO)
IUPAC Buffer pH 7.000	Radiometer Analytical (Villeurbanne, FR)
IUPAC Buffer pH 10.012	Radiometer Analytical (Villeurbanne, FR)
Calomel pH4006 electrode	Radiometer Analytical (Villeurbanne, FR)
Fluoraldehyde reagent solution	Pierce (Rockford, IL)

96-well Flat-Bottom Immuno Plate

Nalge Nunc International (Rochester, NY)

Safire Microplate Reader

Tecan (Männedorf, Switzerland)

Water was Milli-Q quality with 18 Mega ohms resistance

3.2.2 Equilibrium adsorption isotherm

A concentration series of peptide/protein (0 to 220 $\mu\text{g/ml}$, unless otherwise noted) was incubated with stirring at 37 °C in 0.5 ml of 1 mg/ml HAP (for synthesis and characterization see sections 2.2.2 and 2.3.1, respectively) slurry in HEPES buffer (10 mM HEPES, 100 mM NaCl, 10 mM KCl, pH 7.40). After 4 h the HAP was pelleted from the slurry by centrifugation at 16,100 g for 5 min. 350 μl of the supernatant was then removed and assayed for the concentration of free (unbound) peptide/protein. Protein concentration was measured using fluoraldhyde reagent solution following the Microassay protocol with an appropriate ratio of sample-to-reagent volume (determined by trial and error for each peptide/protein). The sample/reagent solution was then excited at 340 nm and the fluorescence measured at 450 nm using a Safire microplate reader. The concentration of peptide/protein was determined by comparison of unknowns with a standard curve created using a known quantity of purified sample protein as determined by amino acid analysis (Institute for Biomolecular Design, U of A/Advanced Protein Technology Centre, SickKids). The free peptide/protein concentration was then subtracted from total protein added to slurry to calculate the mass of protein bound to the HAP.

3.2.3 Isothermal titration calorimetry

Thermodynamic effects were measured with a Microcal VP high-sensitivity isothermal titration calorimeter using a protocol adapted from Goobes *et al.* (2006) [285]. The probe solutions were degassed under vacuum (ThermoVac) for 10 min at 37°C prior to loading into the ITC cell (1.4 ml) and syringe (300 µl). Data were acquired and analyzed with Origin software developed by Microcal. HEPES/HAP slurry (2 mg/ml) was prepared and left on a rotator at least 12 hours prior to running an ITC experiment to equilibrate. One ml of this slurry was removed immediately prior to the ITC experiment to be performed and the HAP was removed using a 0.2-µm filter. This HAP-equilibrated HEPES buffer was then used to resuspend the peptide/protein in the appropriate volume minus 5 µl. The pH of the peptide/protein solution (595 µl) was then adjusted to that of the HAP slurry (approximately pH 7.5) using less than 5 µl of 62 mM NaOH. The solution was then brought to a final volume of 600 µl to achieve the appropriate concentration. Binding constants and reaction enthalpies were measured by injection of peptide into 2 mg/ml HAP/HEPES slurry. The injections were 10 µl of 100 µg/ml peptide/protein solution into the sample cell spaced at 7-min intervals (unless otherwise stated). A 2-µl initial injection was discarded from the analysis to minimize error associated with diffusion of peptide/protein from the syringe prior to the first injection. Control measurements were made by injecting the corresponding polypeptide into the calorimeter cell filled with 0.2 µm-filtered HEPES buffer that had been previously equilibrated with HAP crystals for at least 12 h. Prior to data analysis, the heat value determined from the corresponding control experiment was subtracted to correct for heat contributed by polypeptide dilution caused by injection of the syringe solution into the

cell. Peptide/protein injection produced an endothermic heat of reaction that was determined by integration of the heat flow tracings. For all conditions studied, at least two independent experiments were performed.

3.3 Results

3.3.1 Equilibrium adsorption isotherm

The EAI for the polypeptides adsorbing onto HAP (for synthesis and characterization see sections 2.2.2 and 2.3.1, respectively) at 37°C are expressed as the number of moles adsorbed per unit of surface area (N) versus the equilibrium concentration of free peptide/protein in solution (Figures 3.1 to 3.4, Table 3.1). The measured data points were collected after allowing 4 h for equilibration at each concentration, after which the concentration of protein in the supernatant was determined. This value was then used to calculate the mass of protein bound to the HAP. The data were fitted to a first-order Langmuir model.

It was observed that the maximum number of binding sites (N_{\max}) for peptides P3 and P0 were $4.69 \pm 0.46 \times 10^{-7}$ and $8.92 \pm 2.30 \times 10^{-8}$ mole/m², respectively (Figure 3.1 and 3.2, Table 3.1). This corresponds to mass per area coverage of 921 ± 90 µg/m² for P3 and 154 ± 41 µg/m² for P0. When comparing these peptides on a molar ratio, approximately six times more P3 binds to an equal mass of HAP than P0.

The maximum number of binding sites for rOPN (Figure 3.3) and poly-Asp (Figure 3.4) were $7.10 \pm 0.36 \times 10^{-8}$ and $7.35 \pm 0.53 \times 10^{-8}$ mole/m², respectively. Thus, approximately the same number of molecules bound to equal surface areas of HAP. The

poly-Asp used in this study is approximately one-third the length of rOPN (~95 vs. 301 residues, respectively). A comparison of mass per area coverage of both polymers reveals that $2,361 \pm 120 \mu\text{g}$ of rOPN adsorbs to one square meter of HAP, whereas only $809 \pm 68 \mu\text{g}$ of poly-Asp is required to cover the equivalent area.

Figure 3.1 Equilibrium Adsorption Isotherm of P3.

P3 was allowed to equilibrate in 0.5 mg HAP (1 mg/mL) in HEPES buffer at 37°C for 4 h. N_{\max} was observed to be $4.69 \pm 0.46 \times 10^{-7}$ mole P3 per m^2 HAP and the $K_D = 2.94 \pm 0.71 \times 10^{-5}$. Data points were fit to a one-site binding model. $n = 2$.

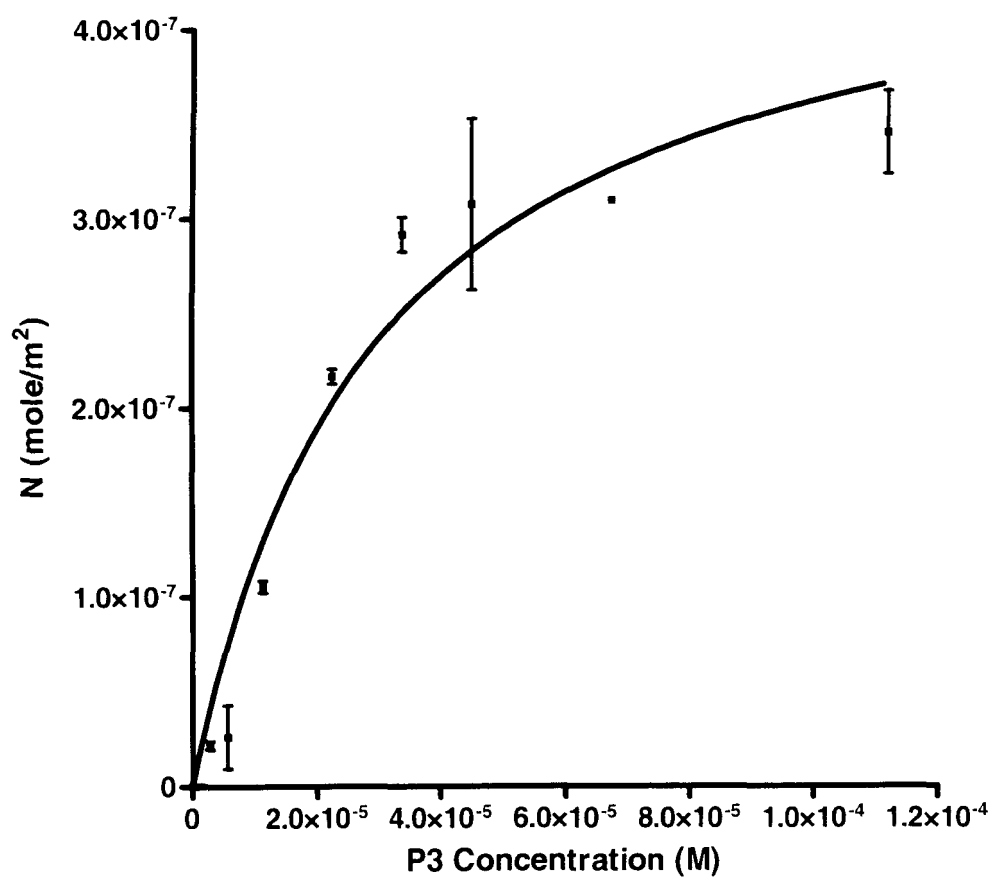


Figure 3.2 Equilibrium Adsorption Isotherm of P0.

P0 was allowed to equilibrate in 0.5 mg HAP (1 mg/mL) in HEPES buffer at 37°C for 4 h. N_{\max} was observed to be $8.92 \pm 2.30 \times 10^{-8}$ mole P0 per m^2 HAP and the $K_D = 1.58 \pm 0.93 \times 10^{-5}$. Data points were fit to a one-site binding model. $n = 2$.

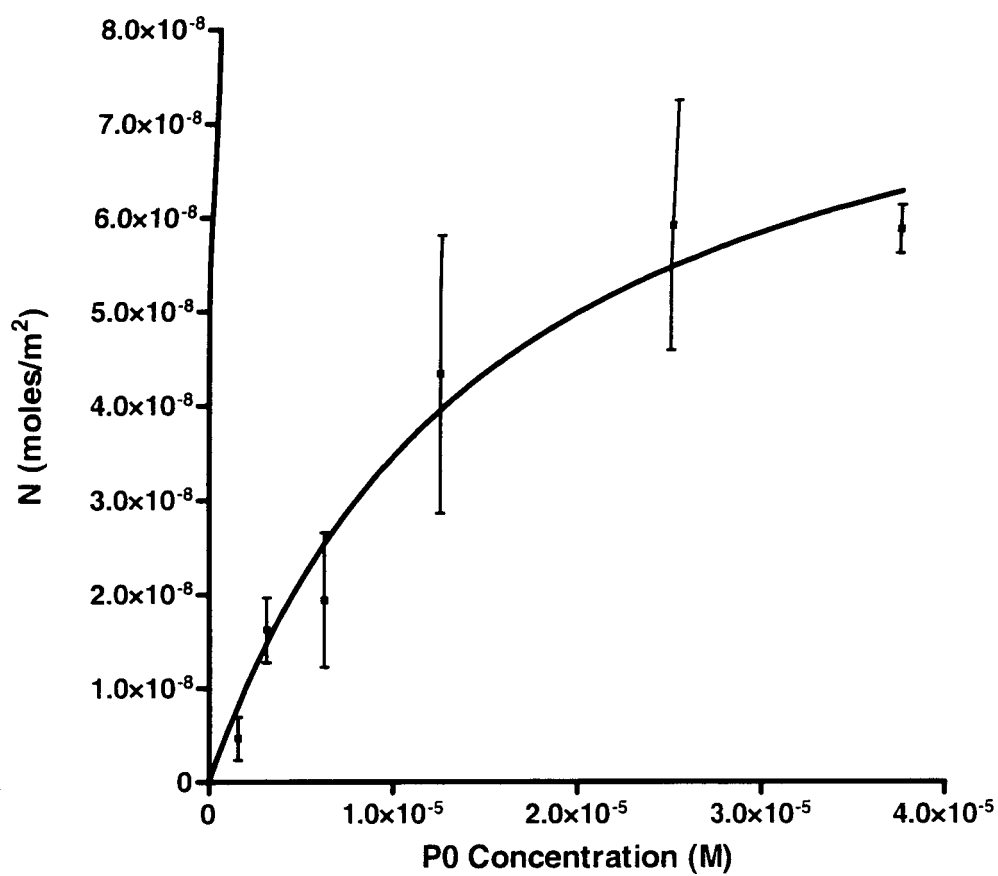


Figure 3.3 Equilibrium Adsorption Isotherm of rOPN.

Recombinant OPN was allowed to equilibrate in 0.5 mg HAP (1 mg/mL) in HEPES buffer at 37°C for 4 h. N_{\max} was observed to be $7.10 \pm 0.36 \times 10^{-8}$ mole rOPN per m^2 HAP and the $K_D = 3.55 \pm 0.46 \times 10^{-6}$. Data points were fit to a one-site binding model. $n = 2$.

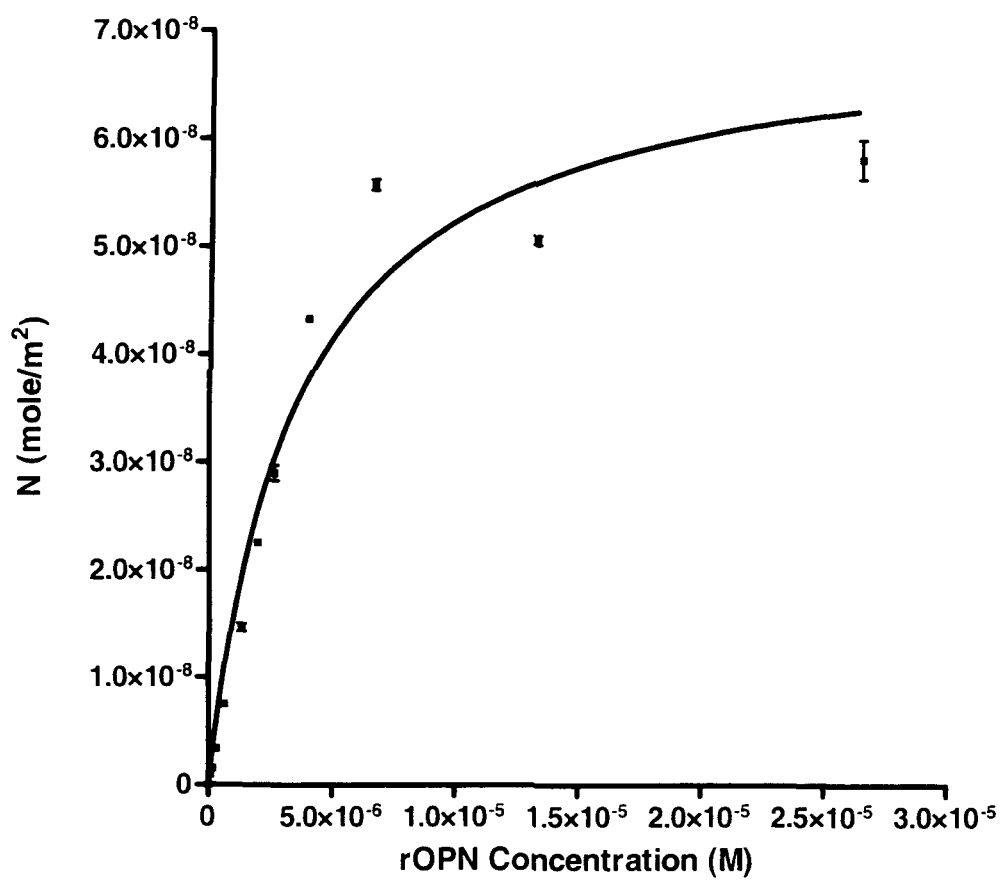


Figure 3.4 Equilibrium Adsorption Isotherm of poly-Asp.

Poly-Asp was allowed to equilibrate in 0.5 mg HAP (1 mg/mL) in HEPES buffer at 37°C for 4 h. N_{\max} was observed to be $7.35 \pm 0.53 \times 10^{-8}$ mole poly-Asp per m^2 HAP and the $K_D = 3.43 \pm 0.71 \times 10^{-6}$. Data points were fit to a one-site binding model. $n = 2$.

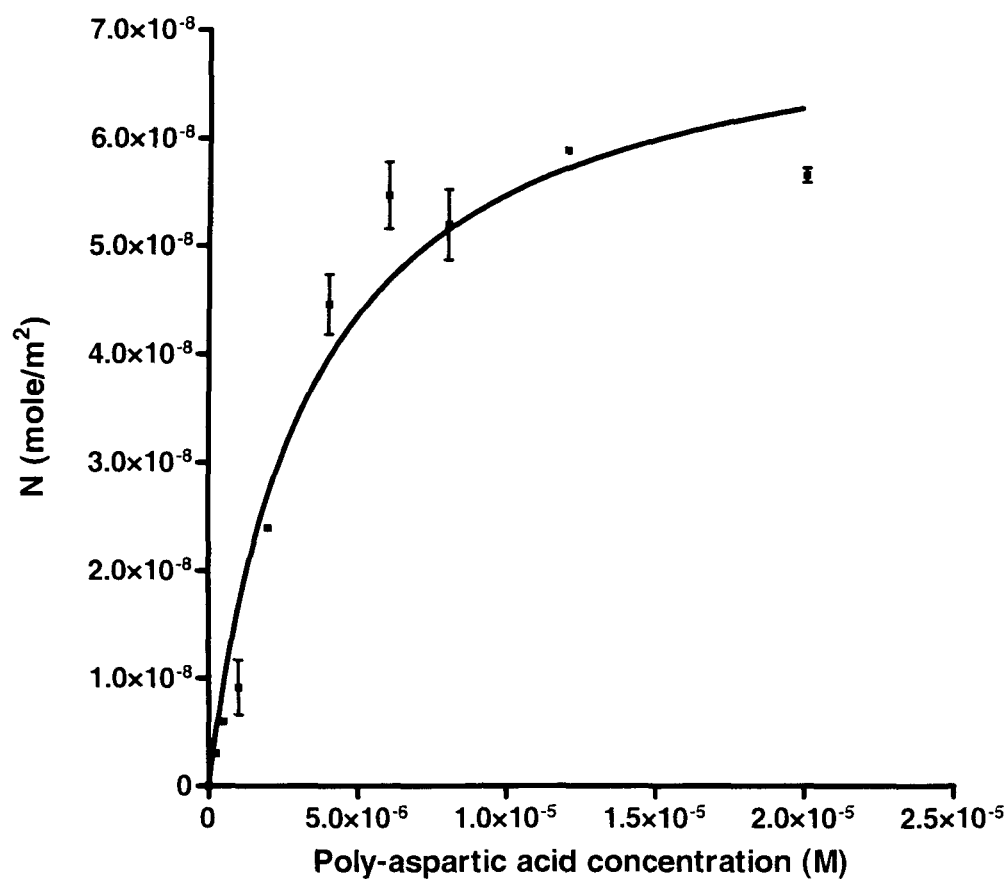


Table 3.1 Summary of equilibrium adsorption isotherm N_{\max} and K_D at 37°C for the peptides/proteins investigated.

Peptide/protein	N_{\max} (mole/m ²)	N_{\max} (μg/m ²)	K_D (M)
Poly-Asp	$7.35 \pm 0.53 \times 10^{-8}$	809 ± 68	$3.43 \pm 0.71 \times 10^{-6}$
rOPN	$7.10 \pm 0.36 \times 10^{-8}$	2361 ± 120	$3.55 \pm 0.46 \times 10^{-6}$
P0	$8.92 \pm 2.30 \times 10^{-8}$	157 ± 41	$1.58 \pm 0.93 \times 10^{-5}$
P3	$4.69 \pm 0.46 \times 10^{-7}$	921 ± 90	$2.94 \pm 0.71 \times 10^{-5}$

3.3.2 Isothermal titration calorimetry

Heats of reaction determined using isothermal titration calorimetry allow the Gibbs free energy (ΔG) to be calculated using the standard thermodynamic relationship [$\Delta G = -RT \cdot \ln K_b$] where T is the absolute temperature, R is the gas constant and K_b is the equilibrium constant (revealed by ITC). Direct measurement of the enthalpy then allows for the elucidation of the entropic (ΔS) contribution to the overall observed free energy using the Gibbs' equation, $\Delta G = \Delta H - T\Delta S$, thus providing a complete thermodynamic characterization of the adsorption process. This is important since the free energies of two interactions possessing identical affinities may have different enthalpic and entropic components.

In order to study the effects of phosphorylation of the peptides/proteins on the thermodynamics of adsorption onto HAP, we have used ITC to detect the heat exchanged during the titration of rOPN, mOPN, P3, and P0 into a HAP slurry. Due to limitations in protein quantity, an EAI of mOPN was not performed, thus the ITC experiments of mOPN were performed for qualitative analysis only.

Both rOPN and mOPN underwent an endothermic reaction with HAP (Figure 3.5 and 3.6). The rOPN titration exhibited an apparent endothermic heat of adsorption of approximately 28.4 kcal/mol and the detected heats decayed to zero after only approximately 10% of the EAI-calculated total number of binding sites were occupied (Figure 3.5). The largest observed heat of adsorption of the peptides/proteins studied was that of mOPN at ~548.5 kcal/mol; however, as described above an EAI could not be performed (Figure 3.6). Without the knowledge of the number of mOPN binding sites on HAP the percentage of total sites occupied at which enthalpy decreases

Figure 3.5 Calorimetric titration of HAP with rOPN.

The upper panel shows the heats for the injection of rOPN into HAP after correcting for the heat of dilution. These peaks were integrated and plotted as enthalpy per mole rOPN injected versus the molar ratio between total injected rOPN and total HAP adsorption sites. The solid line is a fit of the data to a one-site binding model. The calorimeter cell contained the HAP/HEPES slurry, and 10- μ l injections of rOPN (200 μ g/mL) were made at 7-min intervals. Recombinant OPN was dissolved in identical HEPES buffer as the equilibrated HAP slurry after the HAP was removed by filtration through a 0.2- μ m filter. The temperature was 37°C. $R^2 = 0.596$. $n = 2$.

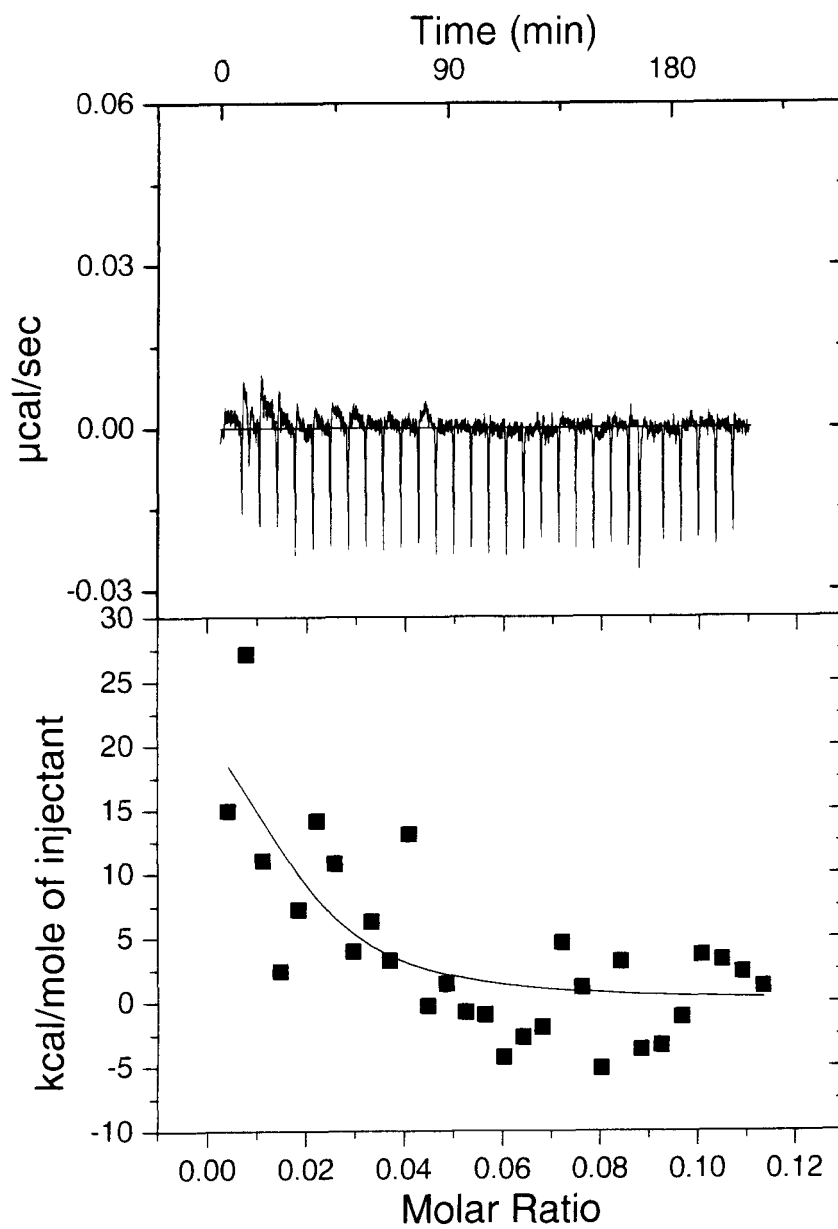
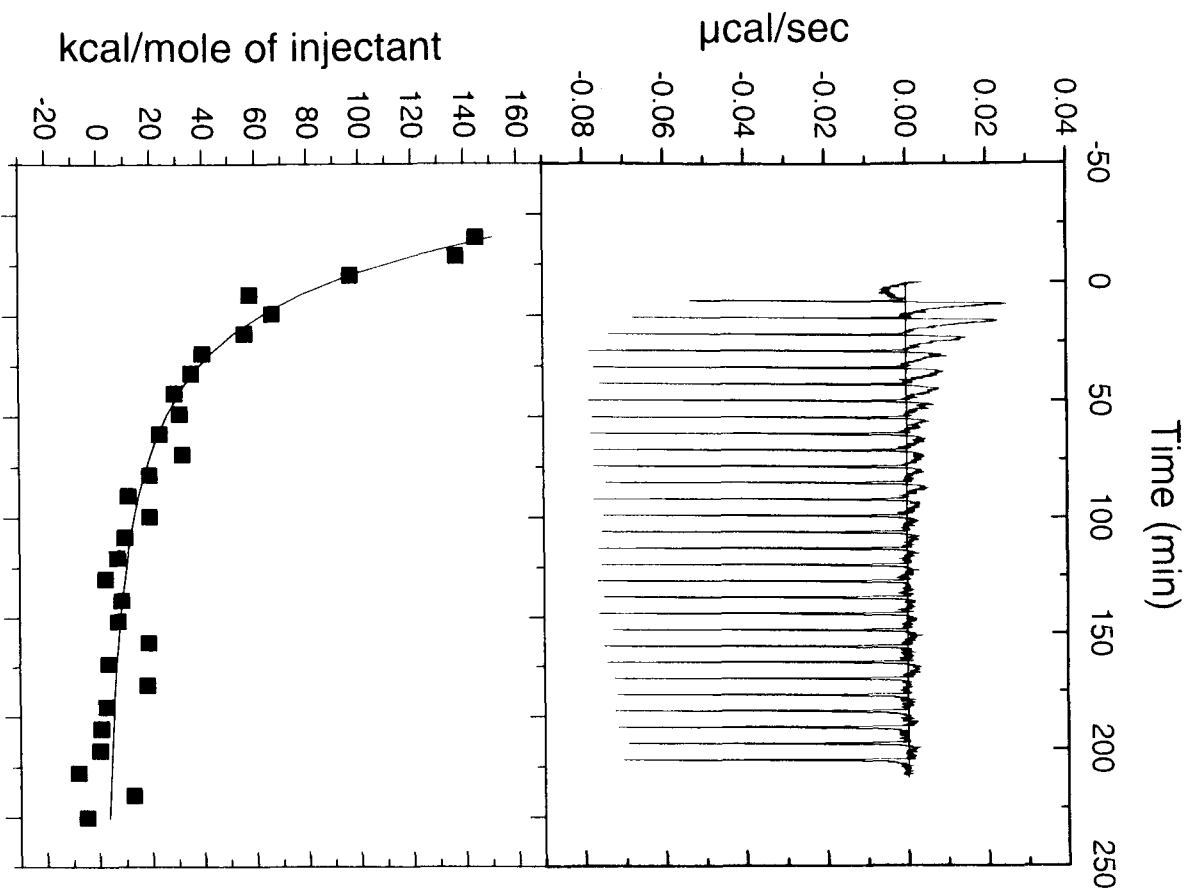


Figure 3.6 Calorimetric titration of HAP with mOPN.

The upper panel shows the heats for the injection of mOPN into HAP after correcting for the heat of dilution. These peaks were integrated and plotted as enthalpy per mole mOPN injected. The total number of HAP adsorption sites was not known for mOPN so the molar ratio between total injected mOPN and total HAP adsorption sites could not be calculated, thus the x-axis of lower panel was left blank. The solid line is a fit to the data to a one-site binding model (using the number of HAP binding sites found for rOPN). The calorimeter cell contained the HAP/HEPES slurry and 10- μ l injections of mOPN (100 μ g/mL) were made at 7-min intervals. Milk OPN was dissolved in identical HEPES buffer as the equilibrated HAP slurry after the HAP was removed by filtration through a 0.2- μ m filter. The temperature was 37°C. $R^2 = 0.955$. $n = 2$.



to zero could not be elucidated. The homopolymer poly-Asp possessed an observed heat of adsorption approximately ten-fold lower (~ 50 kcal/mol) than that of mOPN, and similar to rOPN, the measurable enthalpy decayed to zero when only a small fractional coverage ($\sim 5\%$) of the total HAP binding sites was achieved (Figure 3.7). Based on the ITC data, the apparent free energy of adsorption of rOPN and poly-Asp to HAP is approximately -10 kcal/mol (Table 3.2).

It is seen in Figure 3.8 that the enthalpy of adsorption of P3 is endothermic. The apparent free energy of P3 adsorption to HAP was observed to be approximately -8.9 kcal/mol, similar to the free energy of rOPN and poly-Asp adsorption (Table 3.2). Moreover, the enthalpy approaches zero after only enough P3 has been injected to occupy approximately 10% of the sites on the HAP as determined by the equilibrium adsorption isotherm. No detectable heat was observed for the remaining ~ 30 injections (Figure 3.8). In contrast, no heat of adsorption was observed when P0 was injected into the HAP slurry. The ITC profile of P0 remained identical to the HAP blank experiment even after the injection volume was doubled to ensure that the lack of a detectable enthalpy was not due to a lower heat signature compared to that observed for P3 (Figure 3.9).

Figure 3.7 Calorimetric titration of HAP with poly-Asp.

The upper panel shows the heats for the injection of poly-Asp into HAP after correcting for the heat of dilution. These peaks were integrated and plotted as enthalpy per mole poly-Asp injected versus the molar ratio between total injected poly-Asp and total HAP adsorption sites. The solid line is a fit to the data to a one-site binding model. The calorimeter cell contained the HAP/HEPES slurry and 10- μ l injections of poly-Asp (100 μ g/mL) were made at 8-min intervals. Poly-Asp (11,000 Da) was dissolved in identical HEPES buffer as the equilibrated HAP slurry after the HAP was removed by filtration through a 0.2- μ m filter. The temperature was 37°C. $R^2 = 0.962$. $n = 2$.

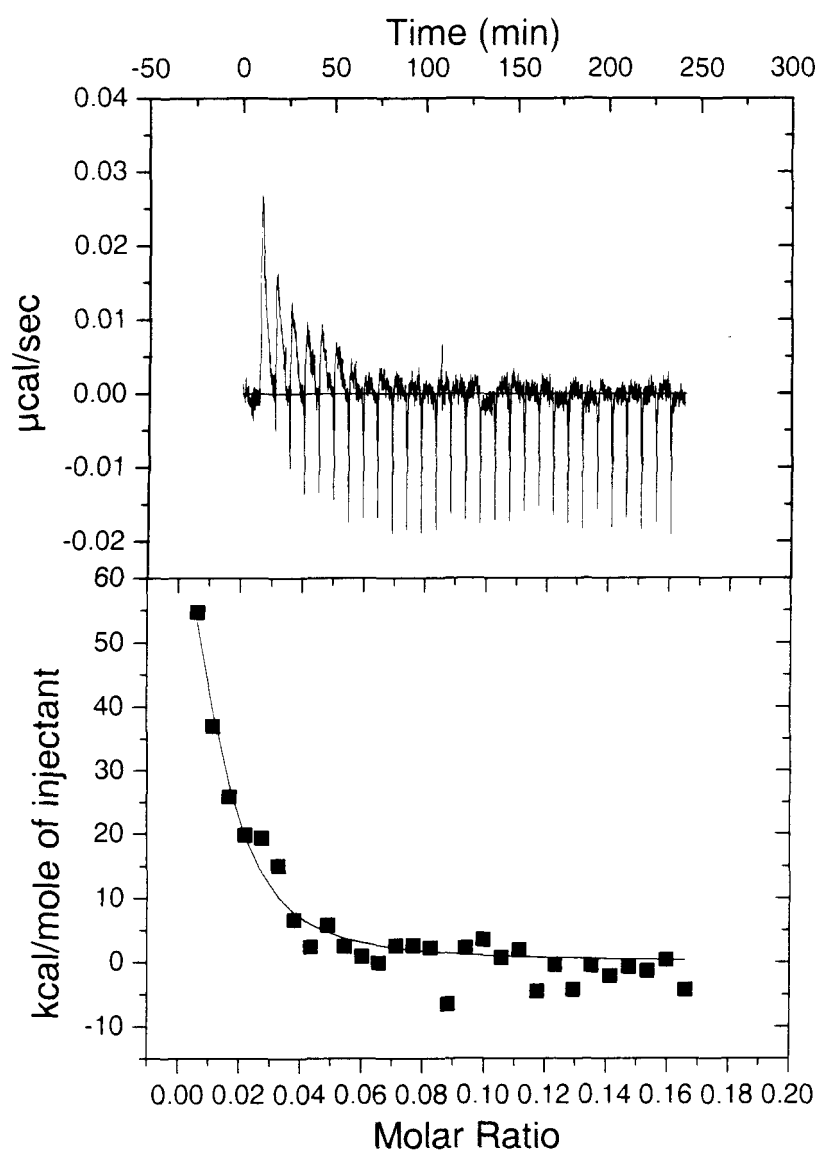


Figure 3.8 Calorimetric titration of HAP with P3.

The upper panel shows the heats for the injection of P3 into HAP after correcting for the heat of dilution. These peaks were integrated and plotted as enthalpy per mole P3 injected versus the molar ratio between total injected P3 and total HAP adsorption sites. The solid line is a fit to the data to a one-site binding model. The calorimeter cell contained the HAP/HEPES slurry and 5- μ l injections of P3 (100 μ g/mL) were made at 15-min intervals. P3 was dissolved in identical HEPES buffer as the equilibrated HAP slurry after the HAP was removed by filtration through a 0.2- μ m filter. The temperature was 37°C. $R^2 = 0.951$. $n = 2$.

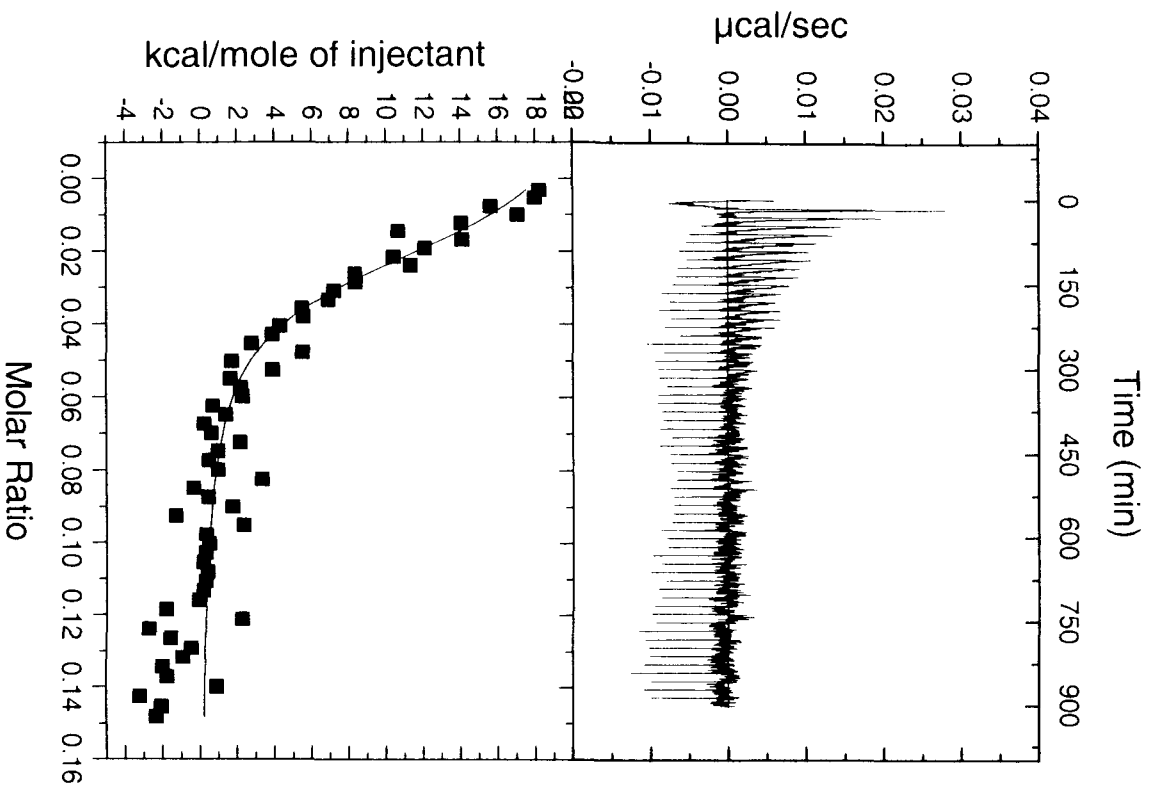


Figure 3.9 Calorimetric titration of HAP with P0.

The upper panel shows the heats for the injection of P0 into HAP after correcting for the heat of dilution. These peaks were integrated and plotted as enthalpy per mole P0 injected versus the molar ratio between total injected P0 and total HAP adsorption sites. The solid line is a fit to the data to a one-site binding model. The calorimeter cell contained the HAP/HEPES slurry and 10- μ l injections of P0 (100 μ g/mL) were made at 15-min intervals. P0 was dissolved in identical HEPES buffer as the equilibrated HAP slurry after the HAP was removed by filtration through a 0.2- μ m filter. The temperature was 37°C. $n = 2$.

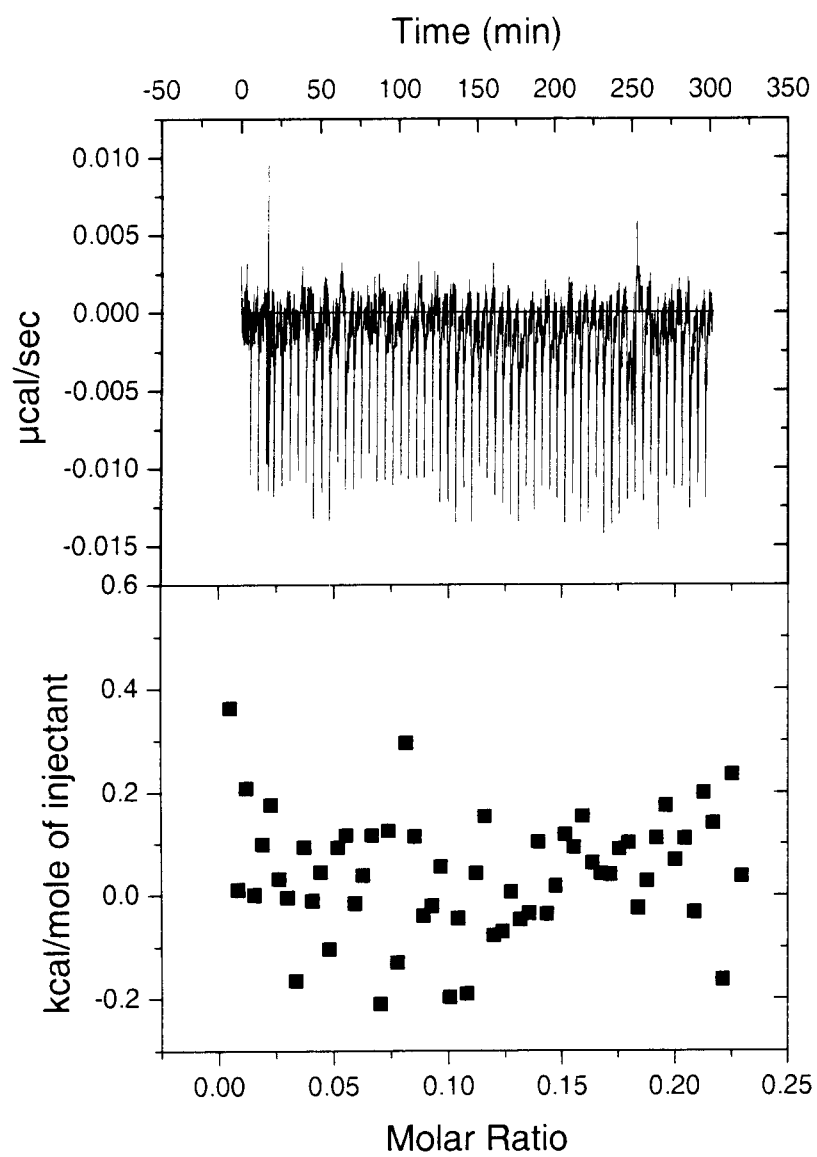


Table 3.2 Summary of the apparent thermodynamic parameters at 37°C for the peptides/proteins investigated using ITC

Protein / Peptide	K _D (M)	N ^ψ	ΔH _{obs} (kcal/mol)	TΔS _{obs} (kcal/mol)	ΔG _{app} (kcal/mol)
Poly- Asp	9.71 ± 3.89 × 10 ⁻⁸	0.012 ± 0.004	105.0 ± 35.6	115.0	-10.0
rOPN	9.17 ± 12.4 × 10 ⁻⁸	0.018 ± 0.011	28.4 ± 21.9	38.4	-10.0
mOPN	N/D	N/D	548.5 ± 380.3	N/D	N/D
P3	4.55 ± 1.30 × 10 ⁻⁷	0.027 ± 0.002	21.8 ± 2.1	30.8	-9.0
P0	N/D	N/D	N/D	N/D	N/D

ψ – Binding stoichiometry determined by ITC, polypeptide/HAP.

N/D – not determined.

Experiments were performed in HEPES buffer (10 mM HEPES, 100 mM NaCl, 10 mM KCl, pH 7.4).

3.4 Discussion

Examination of the EAI data reveals that at saturation, approximately six times more P3 molecules are bound to the surface of HAP than poly-Asp. This roughly correlates to the difference in mass between the two molecules, poly-Asp being approximately six times the mass of P3. Therefore, the amounts of each required to fully saturate the HAP surface were quite similar, with $904 \mu\text{g}/\text{m}^2$ of P3 required versus $798 \mu\text{g}/\text{m}^2$ of poly-Asp. This may suggest that both these molecules bind to similar features on HAP and adsorb through a similar mechanism, since the total mass of each molecule required to cover the surface of HAP was similar. Goldberg *et al.*, who also studied the adsorption of poly-Asp onto HAP found that $628 \mu\text{g}/\text{m}^2$ was required to saturate the crystal surface [309]. The difference in values obtained is likely due to a combination of several factors including variation in: the molecular weight of poly-Asp, the physical properties of the synthetic HAP and the experimental protocols (e.g. binding buffer, equilibration temperature and polypeptide labeling).

In contrast, despite the difference between the mass of rOPN and poly-Asp, the number of binding sites for these two molecules was found to be very similar to one another. Recombinant OPN, being about three times the length of poly-Asp, required $2358 \mu\text{g}/\text{m}^2$ compared to $798 \mu\text{g}/\text{m}^2$ for poly-Asp to fully saturate the HAP surface. Thus, rOPN, being three times more massive than poly-Asp, also required three times more mass to saturate the equivalent area of HAP. Since poly-Asp and P3 are both robust inhibitors of HAP growth and required the lowest masses to fully saturate the HAP surface, it is likely that more of each molecule is closely juxtaposed with the crystal surface compared to rOPN. Furthermore, the N_{max} of rOPN detected in this study, 2358

$\mu\text{g}/\text{m}^2$, was markedly greater than that measured by Goldberg *et al.*, $490 \mu\text{g}/\text{m}^2$ [309].

This discrepancy is likely due to use of recombinant OPN in this study, compared to native porcine OPN used in the previous analysis. The native OPN is expected to possess a higher affinity for the HAP surface than rOPN due to its post-translational phosphorylated residues. Indeed, the anticipated difference in the affinity for the HAP surface of the native compared to the recombinant protein was observed, with the K_D measured in this study, $3.55 \times 10^{-6} \text{ M}$, being approximately an order of magnitude lower than that reported by Goldberg *et al.*, $3.26 \times 10^{-7} \text{ M}$ [309].

In combination with the EAI data, the ITC experiments allowed for a complete thermodynamic characterization of adsorption to HAP for the polypeptides under study. This includes the values of ΔH_{obs} , $K_B (=1/K_D)$, ΔG_{obs} and ΔS_{obs} . The subscript 'obs' is used to designate that the 'observed' parameters determined using ITC include contributions from all of the events that might give out or take in heat during the adsorption process. K_B and the derived ΔG_{obs} provide a measure of the affinity of an interaction, ΔH_{obs} is derived from the net heats of making and breaking bonds, and ΔS_{obs} is a reporter of the net change in order of the system under study.

Analysis of the ITC data reveals several interesting trends. For the polypeptides for which the Gibbs free energy could be calculated – poly-Asp, rOPN and P3 – all were observed to be similar, ranging between approximately -9 to -10 kcal/mol. This coincides with the -10.1 kcal/mol observed by Goobes *et al.* for the free energy of statherin adsorbing to HAP [285]. Thus, the driving force for adsorption to HAP is quite similar for these molecules despite their differing amino acid sequences, MWs and physical properties. However, the enthalpies and entropies for the peptides and proteins

were quite distinct. For instance, the enthalpies of adsorption for P3, rOPN and poly-Asp were ~22, ~28 and ~105 kcal/mol, respectively. Furthermore, the observed enthalpy of adsorption of mOPN is substantially greater than that of poly-Asp. This distinction, besides being due to differences in peptide/protein MW, is possibly a result of variance in the fraction of each molecule coming into close proximity to the crystal surface during adsorption, since the entropic contribution to the free energy closely followed the magnitude of endothermic enthalpy. The large positive entropies observed likely originate from water molecules being released from the surface of the HAP crystals into the bulk solvent upon polypeptide adsorption [310, 311].

Furthermore, the ITC data reveal that the majority (>90%) of the binding sites that exist for each peptide/protein involve a completely entropic process. It is interesting to note that the enthalpically unfavourable (endothermic) binding sites are occupied first and thus must have a higher affinity for the peptides/proteins than the majority of the sites, which adsorb through a purely entropic process. A similar phenomenon has been previously observed by Goobes *et al.* for the binding of the salivary protein statherin to HAP [285]. This group referred to the enthalpically undetectable adsorption process as *thermo-neutral*.

The dissociation constants observed in the EAI experiments were much greater in magnitude than those observed in the ITC studies. This is due to the insensitivity of the ITC experiments to the purely entropic adsorption process, which accounts for the majority of the observed binding. This was also observed by Goobes *et al.* in their study of the thermodynamics of statherin adsorption to HAP [285].

The lack of enthalpy detected for what appears to be a purely entropic adsorption mechanism may be due to several reasons: 1) the thermodynamics of adsorption to these sites may in fact not possess an enthalpic component, 2) the microcalorimeter used may not possess the sensitivity required to measure what is an extremely diminutive enthalpy of adsorption, or 3) as mentioned by Goobes *et al.*, these adsorption sites may populate too slowly for detection by the calorimeter. It has been suggested that the solely entropic adsorption process may result from steric effects originating from altered polypeptide-mineral orientation at higher HAP surface coverage [285]. As the concentration of polypeptide in the solution increases there would be increased competition for the limited number of binding sites. Thus, initial adsorption may occur with the polypeptide parallel to the crystal surface, but as surface coverage increases the polypeptides may adsorb with a decreased fraction of their length being parallel to the crystal surface. This effect would result in a transition between a predominantly parallel/side-on adsorption to a *predominantly perpendicular orientation. The altered adsorption mechanism would increase the total number of molecules adsorbed to the crystal surface, yet decrease the average number of polypeptide-crystal contacts per individual polypeptide.* Furthermore, adsorption through this method would account for the enthalpically-neutral region of the titration curve as there would be no net absorption/release of heat as the total number of polypeptide-crystal contacts would remain relatively constant. It is unknown if a gradual transition between these two adsorption processes would create a noticeable ‘step’ in the EAI.

The creation of multiple layers of adsorbed peptide/protein on the crystal surface or a two-site binding model may also explain the observed ITC data [285, 312]. Yet, the

EAI's do not suggest either of these models. The formation of multiple layers would only be possible if subsequent layers adsorbed to the previous one with identical affinity as the initial layer adsorbing to the HAP surface. Furthermore, the negativity of the peptide/proteins would lead one to expect this intermolecular interaction to be unfavourable, and thus display a measureable enthalpy. The two-site model is also refuted by the curves obtained in the EAI experiments, unless again the affinity of each peptide/protein to both sites is identical.

All the strongly adsorbing polypeptides displayed a spontaneous adsorption process indicated by the negative Gibbs free energy of adsorption. The exact reason for the preferential adsorption of peptide/protein to the enthalpically detectable sites is currently unknown. Peptides/proteins which exhibited both a measureable positive enthalpy of adsorption and high surface coverage of the HAP possessed clusters of anionic residues. Thus, it appears that electrostatic interaction between the peptide/protein and HAP is required for the close association needed to exclude water molecules from the mineral surface. This entropic effect may be a common process utilized by mineral-binding proteins [284, 285]. Furthermore, it has been suggested that the preferential adsorption to the enthalpically detectable sites may represent adsorption to high-energy growth sites on the HAP surface such as steps or kinks [285].

The experimentally determined enthalpy of adsorption detected in these experiments includes the total heat evolved from the system. This includes the making/breaking of non-covalent bonds, as well as protonation/deprotonation events. Thus, the endothermic enthalpy change observed in the initial injections of peptide/protein in the HAP slurry may include buffer-ionization enthalpy (ΔH_{ion}). Future experiments should be performed

to determine the enthalpic contribution of the buffer and reveal if protonation events are involved in the adsorption process.

Chapter Four – Summary, Perspectives and Future Directions

4.1 Summary and Perspectives

Of the polypeptides utilized in this study, some were able to effectively inhibit HAP crystal growth, whereas others were able to decrease the growth rate only moderately. For example, at the highest concentrations tested, P3 was able to reduce the growth rate by ~80% whereas rOPN decreased growth only by 40%. This is presumably due to these molecules adsorbing to only a subset of growth sites on the surface of the crystal.

The strongest inhibitors observed were poly-Asp, P-OPAR, mOPN, P3 and OPAR. All strong inhibitors possess clusters of anionic residues, the 16mer peptides possessing anionic residues along their entire length and mOPN possessing many clusters of concentrated anionic charge. Poly-Asp, the most potent inhibitor, is a homopolymer composed of consecutive negatively charged residues. Ranking their inhibitory potency (IC_{50}) by $\mu\text{g/ml}$ versus μM reveals that inhibition likely occurs through a physical adsorption process as all the strong inhibitors required similar weight concentrations to impart similar inhibitory effects on crystal growth. Yet, analyzing their inhibitory potencies by μM reveals that the polypeptide length is important with respect to inhibition of HAP crystal growth. The three largest polypeptides, poly-Asp, rOPN and mOPN, each possesses a much lower molar IC_{50} than its model 16mer peptide. This implies that increasing the length of an inhibitor may also increase its inhibitory potency. The relatively low molar IC_{50} of the long polymers likely originates from the synergistic effect of the anionic clusters along their length. This effect of avidity likely also occurs in the 16mer peptides, through the multiple interacting residues along its length, although poly-Asp, rOPN and mOPN range from 6- to 19-fold longer. The increased number of anionic groups interacting with the crystal surface in the longer molecules is expected to

have a much greater effect on their respective avidities' compared to the shorter peptides. Of relevance, molecular dynamics studies of 16mer peptides have shown that they are able to make several contacts along their length with the surface of mineral crystals [283]. These multiple contacts are likely facilitated by their flexible/disordered structure. The findings that rOPN displays an endothermic heat of adsorption and that a high mass of protein per area is required to saturate the HAP surface corroborate the CCSG finding that rOPN is able to inhibit HAP growth albeit modestly, in contrast to the observations of Gericke *et al.* [52].

The mass of potent inhibitors required to effectively decrease HAP growth was found to be only a fraction of that required to fully saturate their binding sites in EAI experiments. This has been a frequently encountered phenomenon, in which 3 to 5 times less peptide/protein is required to completely inhibit HAP growth compared to that needed to saturate the HAP surface [276, 313]. This finding supports the notion that biological inhibitors possess a high affinity for the growth sites of crystals, such as steps or kinks [285, 314, 315]. Thus, these molecules are able to drastically decrease the crystal growth rate by selectively adsorbing to high-energy growth sites, even at low surface coverage [314, 315].

Of the polypeptides that were able to dose-dependently decrease the crystal growth rate, all displayed an endothermic enthalpy of adsorption. No heat of adsorption was observed for the weakest inhibitor tested, P0. Furthermore, EAI experiments reveal that P0 exhibits the lowest mass per area required to saturate its binding sites on the crystal surface. Thus, there appears to be a correlation between the amount of peptide/protein required to saturate the HAP surface, inhibitor strength, and endothermic enthalpy upon

binding. Strong inhibitors likely have the ability to bind to many sites on the heterogeneous HAP surface, whereas poor inhibitors may only bind to a subset of these sites. The results suggest that adsorption of approximately $800 \mu\text{g}/\text{m}^2$ is the optimal amount of adsorbed polypeptide for effective inhibition of HAP growth, with greater than or less than this amount (e.g. rOPN $2358 \mu\text{g}/\text{m}^2$ and P0 $154 \mu\text{g}/\text{m}^2$) indicating suboptimal inhibitory potency, although further experiments with a greater variety of inhibitors are required to corroborate this finding. The strong inhibitors may achieve maximum surface coverage by adsorbing in a side-on (parallel) orientation with respect to the crystal surface, thus maximizing the number of protein-crystal contacts. Weak inhibitors, in addition to possibly possessing fewer binding sites on the surface of HAP, likely adsorb with only a fraction of the molecule in close proximity to the crystal surface.

A flexible structure, often exhibited by mineral-binding proteins, may promote greater interaction with the mineral surface by enabling adsorption to structurally diverse surface features compared to a conformationally restricted protein. Furthermore, a compactly folded globular protein would possess only a fraction of its surface area available for interaction with the crystal surface compared to a disordered protein. Since the inhibitory process involves a physical adsorption process, much of a globular protein's surface would be too far from the crystal surface to impart an inhibitory effect. Thus, the flexible structure of these proteins is likely a selected property as it increases the available surface area of the mineral binding proteins and enables (in theory) the entire length of the molecule to come within close proximity to the crystal surface.

For the molecules for which the Gibbs free energy of adsorption could be calculated, poly-Asp, rOPN, and P3, all were similar, ranging from -9 to -10 kcal/mol. Thus, despite

the differences in their physical properties, they all experience a comparable driving force for adsorption to the HAP surface. Yet, their individual enthalpies and entropies of adsorption differ greatly, with differences in their endothermic enthalpy of adsorption being compensated for with proportionately larger entropy. The majority of the binding sites of all inhibitors tested are occupied by a completely entropic process. However, these sites appear to be occupied subsequent to the sites observed to possess an unfavourable endothermic enthalpy. This may be due to a transition from a mostly side-on (parallel) initial adsorption process that displays an endothermic enthalpy, to one in which less of the molecule is parallel to the crystal surface as coverage increases. Since this transition would involve no net change in the number of polypeptide-crystal contacts, it would be enthalpically neutral. Alternatively, the absorption of heat upon polypeptide adsorption may originate from a protonation event during the adsorption process. This effect has been reported for the adsorption of statherin to HAP, for which the heat of adsorption was observed to be strongly dependent on the buffer species in which the reaction took place [285].

The common characteristic of all the strongly inhibiting proteins that exhibit an enthalpic adsorption process is regions of concentrated negative charge, whether due to clusters of phosphorylated or anionic amino acid residues or both. It appears that it is negative charge density, rather than the presence of specific chemical groups, that determines the affinity of a polypeptide for the HAP surface. This phenomenon is also observed with the potent mineralization inhibitor MGP, which contains numerous negative-charge-bearing γ -carboxy-glutamate residues [241, 316]. Furthermore, this phenomenon extends to other calcium-containing mineral phases such as CaOx, the

predominant mineral found in kidney stones [202, 272]. The ability of these anionic proteins to inhibit several different types of mineral growth is exploited through the widespread expression of these proteins in bodily fluids supersaturated with respect to particular mineral phases. Although the importance of proteins bearing negative charge has been firmly established, recent molecular dynamics experiments reveal that beyond a certain magnitude of negative charge (~ -0.5 per residue), no further increase in peptide adsorption to the HAP mineral surface is observed [317]. This result is intriguing, as the reason for the limited effect of increasing negativity on accentuating inhibitory potency is currently unknown. This limiting effect may have been approached in the CCSG experiments as several inhibitors approached the inhibitory potency of the strongest inhibitor tested, poly-Asp, while possessing a lower net negative charge, although more highly charged inhibitors have yet to be tested.

4.2 Future Directions

Although several of the peptides/proteins were shown to be effective inhibitors of HAP growth, it would be of interest to analyze the effect of utilizing mixtures of different inhibitors. If each inhibitor possesses a high affinity for a subset of growth sites on the crystal surface, combinations of inhibitors may produce synergistic increases in crystal growth inhibition. This would decrease the overall concentration of inhibitor required to abolish crystal growth. Also, since length of the polypeptide may impact its ability to inhibit crystal growth, it would be interesting to compare the effects of peptide repeats of various lengths. Several iterations of this should provide a clear picture of the effect molecular length imparts on the inhibitory potency of polypeptides. For example, a

involvement of protonation/deprotonation during adsorption events of the inhibitors analyzed in this study. ITC is a direct method that can be utilized to elucidate proton flux during adsorption phenomenon [318, 319]. This is easily carried out by performing ITC experiments in a range of buffers with different ionization energies. If protonation/deprotonation events are involved, different buffers will produce different contributions to the enthalpy change of adsorption. A simple plot of the measured binding enthalpies (ΔH) versus the buffer dissociation enthalpy (ΔH_{ion}) yields a straight line with the slope corresponding to the number of protons absorbed or released during the adsorption event [320].

Extension of these ITC studies to other biologically important calcium-based mineral phases such as calcium oxalate and calcite would reveal if the entropic driving force of adsorption is a general phenomenon. Knowledge of the requirements for a molecule to effectively inhibit crystal growth and the mechanism of adsorption are critical to the disciplines of medicine and dentistry. A complete understanding of the mode of crystal adsorption/growth inhibition will ultimately lead to the rational design of molecules optimally suited for specific functions.

References

- 1 Knoll, H. A. (2003) Biomineralization and Evolutionary History. Reviews in Mineralogy and Geochemistry **54**, 329-356
- 2 Kirschvink, J. L. and Hagadorn, J. W. (2000) The Biomineralisation of Nano- and Micro-Structures. Wiley-VCH Verlag GmbH, Weinheim
- 3 Weiner, S. and Dove, P. M. (2003) An overview of biomineralization processes and the problem of the vital effect. Reviews in Mineralogy & Geochemistry **54**, 1-29
- 4 Lowenstam, H. A. (1981) Minerals formed by organisms. *Science* **211**, 1126-1131
- 5 Mann, S. (1983) Mineralization in biological systems. *Struct Bonding* **54**, 125-174
- 6 Fortin, D. (1997) Surface-mediated mineral development by bacteria. Reviews in Mineralogy & Geochemistry **54**
- 7 Tebo, B. M., Ghiorse, W. C., van Wassbergen, L. G., Siering, P. L. and Caspi, R. (1997) Bacterially mediated mineral formation: Insights into manganese(II) oxidation from molecular genetic and biochemical studies. Reviews in Mineralogy & Geochemistry **35**, 225-266
- 8 Wetherbee, R. (2002) Biomineralization. The diatom glasshouse. *Science* **298**, 547
- 9 Addadi, L., Joester, D., Nudelman, F. and Weiner, S. (2006) Mollusk shell formation: a source of new concepts for understanding biomineralization processes. *Chemistry* **12**, 980-987
- 10 Arakaki, A., Webb, J. and Matsunaga, T. (2003) A novel protein tightly bound to bacterial magnetic particles in *Magnetospirillum magneticum* strain AMB-1. *J Biol Chem* **278**, 8745-8750
- 11 Mann, S. (1988) Molecular recognition in biomineralization. *Nature* **332**, 119-124
- 12 Weiner, S. and Traub, W. (1980) X-ray diffraction study of the insoluble organic matrix of mollusk shells. *FEBS Lett* **111**, 311-316
- 13 Weiner, S., Traub, W. and Lowenstam, H. A. (1983) Organic matrix in calcified exoskeletons. D. Reidel Publishing Co., Dordrecht
- 14 Kroger, N., Lorenz, S., Brunner, E. and Sumper, M. (2002) Self-assembly of highly phosphorylated silaffins and their function in biosilica morphogenesis. *Science* **298**, 584-586
- 15 George, N. C., Killian, C. E. and Wilt, F. H. (1991) Characterization and expression of a gene encoding a 30.6-kDa *Strongylocentrotus purpuratus* spicule matrix protein. *Dev Biol* **147**, 334-342
- 16 Killian, C. E. and Wilt, F. H. (1996) Characterization of the proteins comprising the integral matrix of *Strongylocentrotus purpuratus* embryonic spicules. *J Biol Chem* **271**, 9150-9159
- 17 Franceschi, V. R. and Horner, H. T. (1980) Calcium oxalate crystals in plants. *Bot. Rev.* **46**, 361-427
- 18 Webb, M. A. (1999) Cell-mediated crystallization of calcium oxalate in plants. *Plant Cell* **11**, 751-761

- 19 Li, X., Zhang, D., Lynch-Holm, V. J., Okita, T. W. and Franceschi, V. R. (2003) Isolation of a crystal matrix protein associated with calcium oxalate precipitation in vacuoles of specialized cells. *Plant Physiol* **133**, 549-559
- 20 Hunter, G. K. and Goldberg, H. A. (1993) Nucleation of hydroxyapatite by bone sialoprotein. *Proc Natl Acad Sci U S A* **90**, 8562-8565
- 21 Gajjeraman, S., Narayanan, K., Hao, J., Qin, C. and George, A. (2007) Matrix macromolecules in hard tissues control the nucleation and hierarchical assembly of hydroxyapatite. *J Biol Chem* **282**, 1193-1204
- 22 Addadi, L. and Weiner, S. (1985) Interactions between acidic proteins and crystals: stereochemical requirements in biomineralization. *Proc Natl Acad Sci U S A* **82**, 4110-4114
- 23 Albeck, S., Addadi, I. and Weiner, S. (1996) Regulation of calcite crystal morphology by intracrystalline acidic proteins and glycoproteins. *Connect Tissue Res* **35**, 365-370
- 24 Michenfelder, M., Fu, G., Lawrence, C., Weaver, J. C., Wustman, B. A., Taranto, L., Evans, J. S. and Morse, D. E. (2003) Characterization of two molluscan crystal-modulating biomineralization proteins and identification of putative mineral binding domains. *Biopolymers* **70**, 522-533
- 25 Treccani, L., Mann, K., Heinemann, F. and Fritz, M. (2006) Perlwapin, an abalone nacre protein with three four-disulfide core (whey acidic protein) domains, inhibits the growth of calcium carbonate crystals. *Biophys J* **91**, 2601-2608
- 26 Gerbaud, V., Pignol, D., Loret, E., Bertrand, J. A., Berland, Y., Fontecilla-Camps, J. C., Canselier, J. P., Gabas, N. and Verdier, J. M. (2000) Mechanism of calcite crystal growth inhibition by the N-terminal undecapeptide of lithostathine. *J Biol Chem* **275**, 1057-1064
- 27 Schlesinger, D. H. and Hay, D. I. (1986) Complete covalent structure of a proline-rich phosphoprotein, PRP-2, an inhibitor of calcium phosphate crystal growth from human parotid saliva. *Int J Pept Protein Res* **27**, 373-379
- 28 Lamkin, M. S. and Oppenheim, F. G. (1993) Structural features of salivary function. *Crit Rev Oral Biol Med* **4**, 251-259
- 29 Kaiser, E. T. and Bock, S. C. (1989) Protein inhibitors of crystal growth. *J Urol* **141**, 750-752
- 30 Mo, L., Liaw, L., Evan, A. P., Sommer, A. J., Lieske, J. C. and Wu, X. R. (2007) Renal calcinosis and stone formation in mice lacking osteopontin, Tamm-Horsfall protein, or both. *Am J Physiol Renal Physiol* **293**, F1935-F1943
- 31 Gorski, J. P. (1992) Acidic phosphoproteins from bone matrix: a structural rationalization of their role in biomineralization. *Calcif Tissue Int* **50**, 391-396
- 32 Hunter, G. K., Hauschka, P. V., Poole, A. R., Rosenberg, L. C. and Goldberg, H. A. (1996) Nucleation and inhibition of hydroxyapatite formation by mineralized tissue proteins. *Biochem J* **317** (Pt 1), 59-64
- 33 Fisher, L. W. and Fedarko, N. S. (2003) Six genes expressed in bones and teeth encode the current members of the SIBLING family of proteins. *Connect Tissue Res* **44 Suppl 1**, 33-40
- 34 Rittling, S. R. and Denhardt, D. T. (1999) Osteopontin function in pathology: lessons from osteopontin-deficient mice. *Exp Nephrol* **7**, 103-113

- 35 Qin, C., Baba, O. and Butler, W. T. (2004) Post-translational modifications of sibling proteins and their roles in osteogenesis and dentinogenesis. *Crit Rev Oral Biol Med* **15**, 126-136
- 36 Boskey, A. L., Maresca, M., Ullrich, W., Doty, S. B., Butler, W. T. and Prince, C. W. (1993) Osteopontin-hydroxyapatite interactions in vitro: inhibition of hydroxyapatite formation and growth in a gelatin-gel. *Bone Miner* **22**, 147-159
- 37 Hunter, G. K., Kyle, C. L. and Goldberg, H. A. (1994) Modulation of crystal formation by bone phosphoproteins: structural specificity of the osteopontin-mediated inhibition of hydroxyapatite formation. *Biochem J* **300** (Pt 3), 723-728
- 38 Jono, S., Peinado, C. and Giachelli, C. M. (2000) Phosphorylation of osteopontin is required for inhibition of vascular smooth muscle cell calcification. *J Biol Chem* **275**, 20197-20203
- 39 Tye, C. E., Rattray, K. R., Warner, K. J., Gordon, J. A., Sodek, J., Hunter, G. K. and Goldberg, H. A. (2003) Delineation of the hydroxyapatite-nucleating domains of bone sialoprotein. *J Biol Chem* **278**, 7949-7955
- 40 Senger, D. R., Wirth, D. F. and Hynes, R. O. (1979) Transformed mammalian cells secrete specific proteins and phosphoproteins. *Cell* **16**, 885-893
- 41 Franzen, A. and Heinegard, D. (1985) Isolation and characterization of two sialoproteins present only in bone calcified matrix. *Biochem J* **232**, 715-724
- 42 Prince, C. W., Oosawa, T., Butler, W. T., Tomana, M., Bhowan, A. S., Bhowan, M. and Schrohenloher, R. E. (1987) Isolation, characterization, and biosynthesis of a phosphorylated glycoprotein from rat bone. *J Biol Chem* **262**, 2900-2907
- 43 Prince, C. W. (1989) Secondary structure predictions for rat osteopontin. *Connect Tissue Res* **21**, 15-20
- 44 Oldberg, A., Franzen, A. and Heinegard, D. (1986) Cloning and sequence analysis of rat bone sialoprotein (osteopontin) cDNA reveals an Arg-Gly-Asp cell-binding sequence. *Proc Natl Acad Sci U S A* **83**, 8819-8823
- 45 Oldberg, A., Franzen, A. and Heinegard, D. (1988) The primary structure of a cell-binding bone sialoprotein. *J Biol Chem* **263**, 19430-19432
- 46 Keykhosravi, M., Doherty-Kirby, A., Zhang, C., Brewer, D., Goldberg, H. A., Hunter, G. K. and Lajoie, G. (2005) Comprehensive identification of post-translational modifications of rat bone osteopontin by mass spectrometry. *Biochemistry* **44**, 6990-7003
- 47 Fisher, L. W., Hawkins, G. R., Tuross, N. and Termine, J. D. (1987) Purification and partial characterization of small proteoglycans I and II, bone sialoproteins I and II, and osteonectin from the mineral compartment of developing human bone. *J Biol Chem* **262**, 9702-9708
- 48 Smith, J. H. and Denhardt, D. T. (1987) Molecular cloning of a tumor promoter-inducible mRNA found in JB6 mouse epidermal cells: induction is stable at high, but not at low, cell densities. *J Cell Biochem* **34**, 13-22
- 49 Fisher, L. W., Torchia, D. A., Fohr, B., Young, M. F. and Fedarko, N. S. (2001) Flexible structures of SIBLING proteins, bone sialoprotein, and osteopontin. *Biochem Biophys Res Commun* **280**, 460-465
- 50 Gorski, J. P., Kremer, E., Ruiz-Perez, J., Wise, G. E. and Artigues, A. (1995) Conformational analyses on soluble and surface bound osteopontin. *Ann N Y Acad Sci* **760**, 12-23

- 51 Li, X., Romero, P., Rani, M., Dunker, A. K. and Obradovic, Z. (1999) Predicting Protein Disorder for N-, C-, and Internal Regions. *Genome Inform Ser Workshop Genome Inform* **10**, 30-40
- 52 Gericke, A., Qin, C., Spevak, L., Fujimoto, Y., Butler, W. T., Sorensen, E. S. and Boskey, A. L. (2005) Importance of phosphorylation for osteopontin regulation of biomineralization. *Calcif Tissue Int* **77**, 45-54
- 53 Haylock, D. N. and Nilsson, S. K. (2006) Osteopontin: a bridge between bone and blood. *Br J Haematol* **134**, 467-474
- 54 Kaartinen, M. T., Pirhonen, A., Linnala-Kankkunen, A. and Maenpaa, P. H. (1999) Cross-linking of osteopontin by tissue transglutaminase increases its collagen binding properties. *J Biol Chem* **274**, 1729-1735
- 55 Denhardt, D. T., Noda, M., O'Regan, A. W., Pavlin, D. and Berman, J. S. (2001) Osteopontin as a means to cope with environmental insults: regulation of inflammation, tissue remodeling, and cell survival. *J Clin Invest* **107**, 1055-1061
- 56 Kazanecki, C. C., Uzwiak, D. J. and Denhardt, D. T. (2007) Control of osteopontin signaling and function by post-translational phosphorylation and protein folding. *J Cell Biochem* **102**, 912-924
- 57 Brown, L. F., Berse, B., Van de Water, L., Papadopoulos-Sergiou, A., Perruzzi, C. A., Manseau, E. J., Dvorak, H. F. and Senger, D. R. (1992) Expression and distribution of osteopontin in human tissues: widespread association with luminal epithelial surfaces. *Mol Biol Cell* **3**, 1169-1180
- 58 Denhardt, D. T. and Guo, X. (1993) Osteopontin: a protein with diverse functions. *Faseb J* **7**, 1475-1482
- 59 Yoon, K., Buenaga, R. and Rodan, G. A. (1987) Tissue specificity and developmental expression of rat osteopontin. *Biochem Biophys Res Commun* **148**, 1129-1136
- 60 Nomura, S., Wills, A. J., Edwards, D. R., Heath, J. K. and Hogan, B. L. (1988) Developmental expression of 2ar (osteopontin) and SPARC (osteonectin) RNA as revealed by in situ hybridization. *J Cell Biol* **106**, 441-450
- 61 Butler, W. T. (1989) The nature and significance of osteopontin. *Connect Tissue Res* **23**, 123-136
- 62 Young, M. F., Kerr, J. M., Termine, J. D., Wewer, U. M., Wang, M. G., McBride, O. W. and Fisher, L. W. (1990) cDNA cloning, mRNA distribution and heterogeneity, chromosomal location, and RFLP analysis of human osteopontin (OPN). *Genomics* **7**, 491-502
- 63 Craig, A. M. and Denhardt, D. T. (1991) The murine gene encoding secreted phosphoprotein 1 (osteopontin): promoter structure, activity, and induction in vivo by estrogen and progesterone. *Gene* **100**, 163-171
- 64 Mazzali, M., Kipari, T., Ophascharoensuk, V., Wesson, J. A., Johnson, R. and Hughes, J. (2002) Osteopontin--a molecule for all seasons. *Qjm* **95**, 3-13
- 65 Patarca, R., Freeman, G. J., Singh, R. P., Wei, F. Y., Durfee, T., Blattner, F., Regnier, D. C., Kozak, C. A., Mock, B. A., Morse, H. C., 3rd and et al. (1989) Structural and functional studies of the early T lymphocyte activation 1 (Eta-1) gene. Definition of a novel T cell-dependent response associated with genetic resistance to bacterial infection. *J Exp Med* **170**, 145-161

- 66 Goold, R. D., diSibio, G. L., Xu, H., Lang, D. B., Dadgar, J., Magrane, G. G., Dugaiczky, A., Smith, K. A., Cox, D. R., Masters, S. B. and et al. (1993) The development of sequence-tagged sites for human chromosome 4. *Hum Mol Genet* **2**, 1271-1288
- 67 Kiefer, M. C., Bauer, D. M. and Barr, P. J. (1989) The cDNA and derived amino acid sequence for human osteopontin. *Nucleic Acids Res* **17**, 3306
- 68 Crosby, A. H., Edwards, S. J., Murray, J. C. and Dixon, M. J. (1995) Genomic organization of the human osteopontin gene: exclusion of the locus from a causative role in the pathogenesis of dentinogenesis imperfecta type II. *Genomics* **27**, 155-160
- 69 Merry, K., Dodds, R., Littlewood, A. and Gowen, M. (1993) Expression of osteopontin mRNA by osteoclasts and osteoblasts in modelling adult human bone. *J Cell Sci* **104** (Pt 4), 1013-1020
- 70 Ducy, P., Zhang, R., Geoffroy, V., Ridall, A. L. and Karsenty, G. (1997) *Osf2/Cbfa1*: a transcriptional activator of osteoblast differentiation. *Cell* **89**, 747-754
- 71 Nakashima, K., Zhou, X., Kunkel, G., Zhang, Z., Deng, J. M., Behringer, R. R. and de Crombrughe, B. (2002) The novel zinc finger-containing transcription factor *osterix* is required for osteoblast differentiation and bone formation. *Cell* **108**, 17-29
- 72 Komori, T., Yagi, H., Nomura, S., Yamaguchi, A., Sasaki, K., Deguchi, K., Shimizu, Y., Bronson, R. T., Gao, Y. H., Inada, M., Sato, M., Okamoto, R., Kitamura, Y., Yoshiki, S. and Kishimoto, T. (1997) Targeted disruption of *Cbfa1* results in a complete lack of bone formation owing to maturational arrest of osteoblasts. *Cell* **89**, 755-764
- 73 Yucha, C. and Guthrie, D. (2003) Renal homeostasis of calcium. *Nephrol Nurs J* **30**, 621-626; quiz 627-628
- 74 Prince, C. W. and Butler, W. T. (1987) 1,25-Dihydroxyvitamin D3 regulates the biosynthesis of osteopontin, a bone-derived cell attachment protein, in clonal osteoblast-like osteosarcoma cells. *Cell Relat Res* **7**, 305-313
- 75 Oldberg, A., Jirskog-Hed, B., Axelsson, S. and Heinegard, D. (1989) Regulation of bone sialoprotein mRNA by steroid hormones. *J Cell Biol* **109**, 3183-3186
- 76 Chang, P. L. and Prince, C. W. (1991) 1 alpha,25-dihydroxyvitamin D3 stimulates synthesis and secretion of nonphosphorylated osteopontin (secreted phosphoprotein 1) in mouse JB6 epidermal cells. *Cancer Res* **51**, 2144-2150
- 77 Fatherazi, S., Matsa-Dunn, D., Foster, B. L., Rutherford, R. B., Somerman, M. J. and Presland, R. B. (2009) Phosphate regulates osteopontin gene transcription. *J Dent Res* **88**, 39-44
- 78 Guo, H., Cai, C. Q., Schroeder, R. A. and Kuo, P. C. (2001) Osteopontin is a negative feedback regulator of nitric oxide synthesis in murine macrophages. *J Immunol* **166**, 1079-1086
- 79 Patarca, R., Saavedra, R. A. and Cantor, H. (1993) Molecular and cellular basis of genetic resistance to bacterial infection: the role of the early T-lymphocyte activation-1/osteopontin gene. *Crit Rev Immunol* **13**, 225-246
- 80 Yu, X. Q., Fan, J. M., Nikolic-Paterson, D. J., Yang, N., Mu, W., Pichler, R., Johnson, R. J., Atkins, R. C. and Lan, H. Y. (1999) IL-1 up-regulates osteopontin

- expression in experimental crescentic glomerulonephritis in the rat. *Am J Pathol* **154**, 833-841
- 81 Ricardo, S. D., Franzoni, D. F., Roesener, C. D., Crisman, J. M. and Diamond, J. R. (2000) Angiotensinogen and AT(1) antisense inhibition of osteopontin translation in rat proximal tubular cells. *Am J Physiol Renal Physiol* **278**, F708-716
- 82 Noda, M. and Rodan, G. A. (1989) Transcriptional regulation of osteopontin production in rat osteoblast-like cells by parathyroid hormone. *J Cell Biol* **108**, 713-718
- 83 Hullinger, T. G., Pan, Q., Viswanathan, H. L. and Somerman, M. J. (2001) TGFbeta and BMP-2 activation of the OPN promoter: roles of smad- and hox-binding elements. *Exp Cell Res* **262**, 69-74
- 84 Diamond, J. R., Kreisberg, R., Evans, R., Nguyen, T. A. and Ricardo, S. D. (1998) Regulation of proximal tubular osteopontin in experimental hydronephrosis in the rat. *Kidney Int* **54**, 1501-1509
- 85 Ashizawa, N., Graf, K., Do, Y. S., Nunohiro, T., Giachelli, C. M., Meehan, W. P., Tuan, T. L. and Hsueh, W. A. (1996) Osteopontin is produced by rat cardiac fibroblasts and mediates A(II)-induced DNA synthesis and collagen gel contraction. *J Clin Invest* **98**, 2218-2227
- 86 Takemoto, M., Yokote, K., Yamazaki, M., Ridall, A. L., Butler, W. T., Matsumoto, T., Tamura, K., Saito, Y. and Mori, S. (2000) Enhanced expression of osteopontin by high glucose. Involvement of osteopontin in diabetic macroangiopathy. *Ann N Y Acad Sci* **902**, 357-363
- 87 Sodhi, C. P., Phadke, S. A., Batlle, D. and Sahai, A. (2001) Hypoxia and high glucose cause exaggerated mesangial cell growth and collagen synthesis: role of osteopontin. *Am J Physiol Renal Physiol* **280**, F667-674
- 88 Zohar, R., Suzuki, N., Suzuki, K., Arora, P., Glogauer, M., McCulloch, C. A. and Sodek, J. (2000) Intracellular osteopontin is an integral component of the CD44-ERM complex involved in cell migration. *J Cell Physiol* **184**, 118-130
- 89 Suzuki, K., Zhu, B., Rittling, S. R., Denhardt, D. T., Goldberg, H. A., McCulloch, C. A. and Sodek, J. (2002) Colocalization of intracellular osteopontin with CD44 is associated with migration, cell fusion, and resorption in osteoclasts. *J Bone Miner Res* **17**, 1486-1497
- 90 Zhu, B., Suzuki, K., Goldberg, H. A., Rittling, S. R., Denhardt, D. T., McCulloch, C. A. and Sodek, J. (2004) Osteopontin modulates CD44-dependent chemotaxis of peritoneal macrophages through G-protein-coupled receptors: evidence of a role for an intracellular form of osteopontin. *J Cell Physiol* **198**, 155-167
- 91 Junaid, A., Moon, M. C., Harding, G. E. and Zahradka, P. (2007) Osteopontin localizes to the nucleus of 293 cells and associates with polo-like kinase-1. *Am J Physiol Cell Physiol* **292**, C919-926
- 92 Shinohara, M. L., Kim, H. J., Kim, J. H., Garcia, V. A. and Cantor, H. (2008) Alternative translation of osteopontin generates intracellular and secreted isoforms that mediate distinct biological activities in dendritic cells. *Proc Natl Acad Sci U S A* **105**, 7235-7239

- 93 Weber, G. F. and Ashkar, S. (2000) Molecular mechanisms of tumor dissemination in primary and metastatic brain cancers. *Brain Res Bull* **53**, 421-424
- 94 Weber, G. F. and Ashkar, S. (2000) Stress response genes: the genes that make cancer metastasize. *J Mol Med* **78**, 404-408
- 95 He, B., Mirza, M. and Weber, G. F. (2006) An osteopontin splice variant induces anchorage independence in human breast cancer cells. *Oncogene* **25**, 2192-2202
- 96 Mirza, M., Shaughnessy, E., Hurley, J. K., Vanpatten, K. A., Pestano, G. A., He, B. and Weber, G. F. (2008) Osteopontin-c is a selective marker of breast cancer. *Int J Cancer* **122**, 889-897
- 97 Panda, D., Kundu, G. C., Lee, B. I., Peri, A., Fohl, D., Chackalaparampil, I., Mukherjee, B. B., Li, X. D., Mukherjee, D. C., Seides, S., Rosenberg, J., Stark, K. and Mukherjee, A. B. (1997) Potential roles of osteopontin and α V β 3 integrin in the development of coronary artery restenosis after angioplasty. *Proc Natl Acad Sci U S A* **94**, 9308-9313
- 98 Senger, D. R., Perruzzi, C. A., Papadopoulos, A. and Tenen, D. G. (1989) Purification of a human milk protein closely similar to tumor-secreted phosphoproteins and osteopontin. *Biochim Biophys Acta* **996**, 43-48
- 99 Kohri, K., Nomura, S., Kitamura, Y., Nagata, T., Yoshioka, K., Iguchi, M., Yamate, T., Umekawa, T., Suzuki, Y., Sinohara, H. and et al. (1993) Structure and expression of the mRNA encoding urinary stone protein (osteopontin). *J Biol Chem* **268**, 15180-15184
- 100 McKee, M. D. and Nanci, A. (1996) Osteopontin at mineralized tissue interfaces in bone, teeth, and osseointegrated implants: ultrastructural distribution and implications for mineralized tissue formation, turnover, and repair. *Microsc Res Tech* **33**, 141-164
- 101 Radivojac, P., Iakoucheva, L. M., Oldfield, C. J., Obradovic, Z., Uversky, V. N. and Dunker, A. K. (2007) Intrinsic disorder and functional proteomics. *Biophys J* **92**, 1439-1456
- 102 Rangaswami, H., Bulbule, A. and Kundu, G. C. (2006) Osteopontin: role in cell signaling and cancer progression. *Trends Cell Biol* **16**, 79-87
- 103 Tatusova, T. A. and Madden, T. L. (1999) BLAST 2 Sequences, a new tool for comparing protein and nucleotide sequences. *FEMS Microbiol Lett* **174**, 247-250
- 104 Butler, W. T. (1995) Structural and functional domains of osteopontin. *Ann N Y Acad Sci* **760**, 6-11
- 105 Sorensen, E. S., Hojrup, P. and Petersen, T. E. (1995) Posttranslational modifications of bovine osteopontin: identification of twenty-eight phosphorylation and three O-glycosylation sites. *Protein Sci* **4**, 2040-2049
- 106 Christensen, B., Nielsen, M. S., Haselmann, K. F., Petersen, T. E. and Sorensen, E. S. (2005) Post-translationally modified residues of native human osteopontin are located in clusters: identification of 36 phosphorylation and five O-glycosylation sites and their biological implications. *Biochem J* **390**, 285-292
- 107 Sorensen, E. S. and Petersen, T. E. (1995) Phosphorylation, glycosylation, and transglutaminase sites in bovine osteopontin. *Ann N Y Acad Sci* **760**, 363-366

- 108 Christensen, B., Petersen, T. E. and Sorensen, E. S. (2008) Post-translational modification and proteolytic processing of urinary osteopontin. *Biochem J* **411**, 53-61
- 109 Zetina, C. R. (2001) A conserved helix-unfolding motif in the naturally unfolded proteins. *Proteins* **44**, 479-483
- 110 Steinmetz, M. O., Jahnke, W., Towbin, H., Garcia-Echeverria, C., Voshol, H., Muller, D. and van Oostrum, J. (2001) Phosphorylation disrupts the central helix in Op18/stathmin and suppresses binding to tubulin. *EMBO Rep* **2**, 505-510
- 111 Wright, P. E. and Dyson, H. J. (1999) Intrinsically unstructured proteins: re-assessing the protein structure-function paradigm. *J Mol Biol* **293**, 321-331
- 112 Kriwacki, R. W., Hengst, L., Tennant, L., Reed, S. I. and Wright, P. E. (1996) Structural studies of p21Waf1/Cip1/Sdi1 in the free and Cdk2-bound state: conformational disorder mediates binding diversity. *Proc Natl Acad Sci U S A* **93**, 11504-11509
- 113 Tompa, P. (2005) The interplay between structure and function in intrinsically unstructured proteins. *FEBS Lett* **579**, 3346-3354
- 114 Oldfield, C. J., Cheng, Y., Cortese, M. S., Brown, C. J., Uversky, V. N. and Dunker, A. K. (2005) Comparing and combining predictors of mostly disordered proteins. *Biochemistry* **44**, 1989-2000
- 115 Nemir, M., DeVouge, M. W. and Mukherjee, B. B. (1989) Normal rat kidney cells secrete both phosphorylated and nonphosphorylated forms of osteopontin showing different physiological properties. *J Biol Chem* **264**, 18202-18208
- 116 Singh, K., DeVouge, M. W. and Mukherjee, B. B. (1990) Physiological properties and differential glycosylation of phosphorylated and nonphosphorylated forms of osteopontin secreted by normal rat kidney cells. *J Biol Chem* **265**, 18696-18701
- 117 Salih, E., Wang, J., Mah, J. and Fluckiger, R. (2002) Natural variation in the extent of phosphorylation of bone phosphoproteins as a function of in vivo new bone formation induced by demineralized bone matrix in soft tissue and bony environments. *Biochem J* **364**, 465-474
- 118 Salih, E., Zhou, H. Y. and Glimcher, M. J. (1996) Phosphorylation of purified bovine bone sialoprotein and osteopontin by protein kinases. *J Biol Chem* **271**, 16897-16905
- 119 Neame, P. J. and Butler, W. T. (1996) Posttranslational modification in rat bone osteopontin. *Connect Tissue Res* **35**, 145-150
- 120 Sorensen, S., Justesen, S. J. and Johnsen, A. H. (2003) Purification and characterization of osteopontin from human milk. *Protein Expr Purif* **30**, 238-245
- 121 Larkin, M. A., Blackshields, G., Brown, N. P., Chenna, R., McGettigan, P. A., McWilliam, H., Valentin, F., Wallace, I. M., Wilm, A., Lopez, R., Thompson, J. D., Gibson, T. J. and Higgins, D. G. (2007) Clustal W and Clustal X version 2.0. *Bioinformatics* **23**, 2947-2948
- 122 Meggio, F., Marchiori, F., Borin, G., Chessa, G. and Pinna, L. A. (1984) Synthetic peptides including acidic clusters as substrates and inhibitors of rat liver casein kinase TS (type-2). *J Biol Chem* **259**, 14576-14579
- 123 Marin, O., Meggio, F., Marchiori, F., Borin, G. and Pinna, L. A. (1986) Site specificity of casein kinase-2 (TS) from rat liver cytosol. A study with model peptide substrates. *Eur J Biochem* **160**, 239-244

- 124 Marin, O., Meggio, F., Draetta, G. and Pinna, L. A. (1992) The consensus sequences for cdc2 kinase and for casein kinase-2 are mutually incompatible. A study with peptides derived from the beta-subunit of casein kinase-2. *FEBS Lett* **301**, 111-114
- 125 Mercier, J. C. (1981) Phosphorylation of caseins, present evidence for an amino acid triplet code posttranslationally recognized by specific kinases. *Biochimie* **63**, 1-17
- 126 Lasa-Benito, M., Marin, O., Meggio, F. and Pinna, L. A. (1996) Golgi apparatus mammary gland casein kinase: monitoring by a specific peptide substrate and definition of specificity determinants. *FEBS Lett* **382**, 149-152
- 127 Lasa, M., Chang, P. L., Prince, C. W. and Pinna, L. A. (1997) Phosphorylation of osteopontin by Golgi apparatus casein kinase. *Biochem Biophys Res Commun* **240**, 602-605
- 128 Sodek, J., Ganss, B. and McKee, M. D. (2000) Osteopontin. *Crit Rev Oral Biol Med* **11**, 279-303
- 129 Prince, C. W., Dickie, D. and Krumdieck, C. L. (1991) Osteopontin, a substrate for transglutaminase and factor XIII activity. *Biochem Biophys Res Commun* **177**, 1205-1210
- 130 Sorensen, E. S., Rasmussen, L. K., Moller, L., Jensen, P. H., Hojrup, P. and Petersen, T. E. (1994) Localization of transglutaminase-reactive glutamine residues in bovine osteopontin. *Biochem J* **304** (Pt 1), 13-16
- 131 Kaartinen, M. T., El-Maadawy, S., Rasanen, N. H. and McKee, M. D. (2002) Tissue transglutaminase and its substrates in bone. *J Bone Miner Res* **17**, 2161-2173
- 132 Beninati, S., Senger, D. R., Cordella-Miele, E., Mukherjee, A. B., Chackalaparampil, I., Shanmugam, V., Singh, K. and Mukherjee, B. B. (1994) Osteopontin: its transglutaminase-catalyzed posttranslational modifications and cross-linking to fibronectin. *J Biochem* **115**, 675-682
- 133 Zhang, Q., Domenicucci, C., Goldberg, H. A., Wrana, J. L. and Sodek, J. (1990) Characterization of fetal porcine bone sialoproteins, secreted phosphoprotein I (SPPI, osteopontin), bone sialoprotein, and a 23-kDa glycoprotein. Demonstration that the 23-kDa glycoprotein is derived from the carboxyl terminus of SPPI. *J Biol Chem* **265**, 7583-7589
- 134 Senger, D. R., Perruzzi, C. A. and Papadopoulos, A. (1989) Elevated expression of secreted phosphoprotein I (osteopontin, 2ar) as a consequence of neoplastic transformation. *Anticancer Res* **9**, 1291-1299
- 135 Agnihotri, R., Crawford, H. C., Haro, H., Matrisian, L. M., Havrda, M. C. and Liaw, L. (2001) Osteopontin, a novel substrate for matrix metalloproteinase-3 (stromelysin-1) and matrix metalloproteinase-7 (matrilysin). *J Biol Chem* **276**, 28261-28267
- 136 Gao, Y. A., Agnihotri, R., Vary, C. P. and Liaw, L. (2004) Expression and characterization of recombinant osteopontin peptides representing matrix metalloproteinase proteolytic fragments. *Matrix Biol* **23**, 457-466
- 137 Barry, S. T., Ludbrook, S. B., Murrison, E. and Horgan, C. M. (2000) Analysis of the alpha4beta1 integrin-osteopontin interaction. *Exp Cell Res* **258**, 342-351

- 138 Bayless, K. J., Meininger, G. A., Scholtz, J. M. and Davis, G. E. (1998) Osteopontin is a ligand for the $\alpha 4 \beta 1$ integrin. *J Cell Sci* **111** (Pt 9), 1165-1174
- 139 Bayless, K. J. and Davis, G. E. (2001) Identification of dual $\alpha 4 \beta 1$ integrin binding sites within a 38 amino acid domain in the N-terminal thrombin fragment of human osteopontin. *J Biol Chem* **276**, 13483-13489
- 140 Levy, R. J., Schoen, F. J., Levy, J. T., Nelson, A. C., Howard, S. L. and Oshry, L. J. (1983) Biologic determinants of dystrophic calcification and osteocalcin deposition in glutaraldehyde-preserved porcine aortic valve leaflets implanted subcutaneously in rats. *Am J Pathol* **113**, 143-155
- 141 Boskey, A. L., Spevak, L., Paschalis, E., Doty, S. B. and McKee, M. D. (2002) Osteopontin deficiency increases mineral content and mineral crystallinity in mouse bone. *Calcif Tissue Int* **71**, 145-154
- 142 Yoshitake, H., Rittling, S. R., Denhardt, D. T. and Noda, M. (1999) Osteopontin-deficient mice are resistant to ovariectomy-induced bone resorption. *Proc Natl Acad Sci U S A* **96**, 8156-8160
- 143 Ishijima, M., Rittling, S. R., Yamashita, T., Tsuji, K., Kurosawa, H., Nifuji, A., Denhardt, D. T. and Noda, M. (2001) Enhancement of osteoclastic bone resorption and suppression of osteoblastic bone formation in response to reduced mechanical stress do not occur in the absence of osteopontin. *J Exp Med* **193**, 399-404
- 144 Ihara, H., Denhardt, D. T., Furuya, K., Yamashita, T., Muguruma, Y., Tsuji, K., Hruska, K. A., Higashio, K., Enomoto, S., Nifuji, A., Rittling, S. R. and Noda, M. (2001) Parathyroid hormone-induced bone resorption does not occur in the absence of osteopontin. *J Biol Chem* **276**, 13065-13071
- 145 Rittling, S. R., Matsumoto, H. N., McKee, M. D., Nanci, A., An, X. R., Novick, K. E., Kowalski, A. J., Noda, M. and Denhardt, D. T. (1998) Mice lacking osteopontin show normal development and bone structure but display altered osteoclast formation in vitro. *J Bone Miner Res* **13**, 1101-1111
- 146 Denhardt, D. T. and Noda, M. (1998) Osteopontin expression and function: role in bone remodeling. *J Cell Biochem Suppl* **30-31**, 92-102
- 147 Mark, M. P., Prince, C. W., Oosawa, T., Gay, S., Bronckers, A. L. and Butler, W. T. (1987) Immunohistochemical demonstration of a 44-KD phosphoprotein in developing rat bones. *J Histochem Cytochem* **35**, 707-715
- 148 Mark, M. P., Prince, C. W., Gay, S., Austin, R. L., Bhowan, M., Finkelman, R. D. and Butler, W. T. (1987) A comparative immunocytochemical study on the subcellular distributions of 44 kDa bone phosphoprotein and bone gamma-carboxyglutamic acid (Gla)-containing protein in osteoblasts. *J Bone Miner Res* **2**, 337-346
- 149 Walker, C. G., Ito, Y., Dangaria, S., Luan, X. and Diekwisch, T. G. (2008) RANKL, osteopontin, and osteoclast homeostasis in a hyperocclusion mouse model. *Eur J Oral Sci* **116**, 312-318
- 150 Ross, F. P., Chappel, J., Alvarez, J. I., Sander, D., Butler, W. T., Farach-Carson, M. C., Mintz, K. A., Robey, P. G., Teitelbaum, S. L. and Cheresch, D. A. (1993) Interactions between the bone matrix proteins osteopontin and bone sialoprotein

- and the osteoclast integrin α v β 3 potentiate bone resorption. *J Biol Chem* **268**, 9901-9907
- 151 van Dijk, S., D'Errico, J. A., Somerman, M. J., Farach-Carson, M. C. and Butler, W. T. (1993) Evidence that a non-RGD domain in rat osteopontin is involved in cell attachment. *J Bone Miner Res* **8**, 1499-1506
 - 152 Reinholt, F. P., Hultenby, K., Oldberg, A. and Heinegard, D. (1990) Osteopontin-a possible anchor of osteoclasts to bone. *Proc Natl Acad Sci U S A* **87**, 4473-4475
 - 153 Yamate, T., Mocharla, H., Taguchi, Y., Igietseme, J. U., Manolagas, S. C. and Abe, E. (1997) Osteopontin expression by osteoclast and osteoblast progenitors in the murine bone marrow: demonstration of its requirement for osteoclastogenesis and its increase after ovariectomy. *Endocrinology* **138**, 3047-3055
 - 154 Fukushima, O., Bekker, P. J. and Gay, C. V. (1991) Characterization of the Functional Stages of Osteoclasts by Enzyme-Histochemistry and Electron-Microscopy. *Anatomical Record* **231**, 298-315
 - 155 Holtrop, M. E. and Raisz, L. G. (1979) Comparison of the Effects of 1,25-Dihydroxycholecalciferol, Prostaglandin-E2, and Osteoclast-Activating Factor with Parathyroid-Hormone on the Ultrastructure of Osteoclasts in Cultured Long Bones of Fetal Rats. *Calcified Tissue International* **29**, 201-205
 - 156 Hirata, A., Sugahara, T. and Nakamura, H. (2009) Localization of Runx2, Osterix, and Osteopontin in Tooth Root Formation in Rat Molars. *J Histochem Cytochem*
 - 157 O'Regan, A. W., Nau, G. J., Chupp, G. L. and Berman, J. S. (2000) Osteopontin (Eta-1) in cell-mediated immunity: teaching an old dog new tricks. *Immunol Today* **21**, 475-478
 - 158 Shinohara, M. L., Lu, L., Bu, J., Werneck, M. B., Kobayashi, K. S., Glimcher, L. H. and Cantor, H. (2006) Osteopontin expression is essential for interferon-alpha production by plasmacytoid dendritic cells. *Nat Immunol* **7**, 498-506
 - 159 Shinohara, M. L., Jansson, M., Hwang, E. S., Werneck, M. B., Glimcher, L. H. and Cantor, H. (2005) T-bet-dependent expression of osteopontin contributes to T cell polarization. *Proc Natl Acad Sci U S A* **102**, 17101-17106
 - 160 Diao, H., Kon, S., Iwabuchi, K., Kimura, C., Morimoto, J., Ito, D., Segawa, T., Maeda, M., Hamuro, J., Nakayama, T., Taniguchi, M., Yagita, H., Van Kaer, L., Onoe, K., Denhardt, D., Rittling, S. and Uede, T. (2004) Osteopontin as a mediator of NKT cell function in T cell-mediated liver diseases. *Immunity* **21**, 539-550
 - 161 Weber, G. F. and Cantor, H. (1996) The immunology of Eta-1/osteopontin. *Cytokine Growth Factor Rev* **7**, 241-248
 - 162 Ashkar, S., Weber, G. F., Panoutsakopoulou, V., Sanchirico, M. E., Jansson, M., Zawaideh, S., Rittling, S. R., Denhardt, D. T., Glimcher, M. J. and Cantor, H. (2000) Eta-1 (osteopontin): an early component of type-1 (cell-mediated) immunity. *Science* **287**, 860-864
 - 163 Patarca, R., Wei, F. Y., Singh, P., Morasso, M. I. and Cantor, H. (1990) Dysregulated expression of the T cell cytokine Eta-1 in CD4-8- lymphocytes during the development of murine autoimmune disease. *J Exp Med* **172**, 1177-1183

- 164 Singh, R. P., Patarca, R., Schwartz, J., Singh, P. and Cantor, H. (1990) Definition of a specific interaction between the early T lymphocyte activation 1 (Eta-1) protein and murine macrophages in vitro and its effect upon macrophages in vivo. *J Exp Med* **171**, 1931-1942
- 165 Weber, G. F., Zawaideh, S., Hikita, S., Kumar, V. A., Cantor, H. and Ashkar, S. (2002) Phosphorylation-dependent interaction of osteopontin with its receptors regulates macrophage migration and activation. *J Leukoc Biol* **72**, 752-761
- 166 Fedarko, N. S., Fohr, B., Robey, P. G., Young, M. F. and Fisher, L. W. (2000) Factor H binding to bone sialoprotein and osteopontin enables tumor cell evasion of complement-mediated attack. *J Biol Chem* **275**, 16666-16672
- 167 Hanahan, D. and Weinberg, R. A. (2000) The hallmarks of cancer. *Cell* **100**, 57-70
- 168 Craig, A. M., Smith, J. H. and Denhardt, D. T. (1989) Osteopontin, a transformation-associated cell adhesion phosphoprotein, is induced by 12-O-tetradecanoylphorbol 13-acetate in mouse epidermis. *J Biol Chem* **264**, 9682-9689
- 169 El-Tanani, M. K., Campbell, F. C., Kurisetty, V., Jin, D., McCann, M. and Rudland, P. S. (2006) The regulation and role of osteopontin in malignant transformation and cancer. *Cytokine Growth Factor Rev* **17**, 463-474
- 170 Furger, K. A., Menon, R. K., Tuck, A. B., Bramwell, V. H. and Chambers, A. F. (2001) The functional and clinical roles of osteopontin in cancer and metastasis. *Curr Mol Med* **1**, 621-632
- 171 Bellahcene, A. and Castronovo, V. (1997) Expression of bone matrix proteins in human breast cancer: potential roles in microcalcification formation and in the genesis of bone metastases. *Bull Cancer* **84**, 17-24
- 172 Agrawal, D., Chen, T., Irby, R., Quackenbush, J., Chambers, A. F., Szabo, M., Cantor, A., Coppola, D. and Yeatman, T. J. (2002) Osteopontin identified as lead marker of colon cancer progression, using pooled sample expression profiling. *J Natl Cancer Inst* **94**, 513-521
- 173 Chaplet, M., Waltregny, D., Detry, C., Fisher, L. W., Castronovo, V. and Bellahcene, A. (2006) Expression of dentin sialophosphoprotein in human prostate cancer and its correlation with tumor aggressiveness. *Int J Cancer* **118**, 850-856
- 174 Chen, J., Rodriguez, J. A., Barnett, B., Hashimoto, N., Tang, J. and Yoneda, T. (2003) Bone sialoprotein promotes tumor cell migration in both in vitro and in vivo models. *Connect Tissue Res* **44 Suppl 1**, 279-284
- 175 Sung, V., Stubbs, J. T., 3rd, Fisher, L., Aaron, A. D. and Thompson, E. W. (1998) Bone sialoprotein supports breast cancer cell adhesion proliferation and migration through differential usage of the alpha(v)beta3 and alpha(v)beta5 integrins. *J Cell Physiol* **176**, 482-494
- 176 Agrawal, D., Chen, T., Irby, R., Quackenbush, J., Chambers, A. F., Szabo, M., Cantor, A., Coppola, D. and Yeatman, T. J. (2003) Osteopontin identified as colon cancer tumor progression marker. *C R Biol* **326**, 1041-1043
- 177 Lecrone, V., Li, W., Devoll, R. E., Logothetis, C. and Farach-Carson, M. C. (2000) Calcium signals in prostate cancer cells: specific activation by bone-matrix proteins. *Cell Calcium* **27**, 35-42

- 178 El-Tanani, M. K., Campbell, F. C., Crowe, P., Erwin, P., Harkin, D. P., Pharoah, P., Ponder, B. and Rudland, P. S. (2006) BRCA1 suppresses osteopontin-mediated breast cancer. *J Biol Chem* **281**, 26587-26601
- 179 Rudland, P. S., Platt-Higgins, A., El-Tanani, M., De Silva Rudland, S., Barraclough, R., Winstanley, J. H., Howitt, R. and West, C. R. (2002) Prognostic significance of the metastasis-associated protein osteopontin in human breast cancer. *Cancer Res* **62**, 3417-3427
- 180 Khodavirdi, A. C., Song, Z., Yang, S., Zhong, C., Wang, S., Wu, H., Pritchard, C., Nelson, P. S. and Roy-Burman, P. (2006) Increased expression of osteopontin contributes to the progression of prostate cancer. *Cancer Res* **66**, 883-888
- 181 Oates, A. J., Barraclough, R. and Rudland, P. S. (1996) The identification of osteopontin as a metastasis-related gene product in a rodent mammary tumour model. *Oncogene* **13**, 97-104
- 182 Bell, W. R. (1996) The fibrinolytic system in neoplasia. *Semin Thromb Hemost* **22**, 459-478
- 183 Price, J. T. and Thompson, E. W. (2002) Mechanisms of tumour invasion and metastasis: emerging targets for therapy. *Expert Opin Ther Targets* **6**, 217-233
- 184 Teramoto, H., Castellone, M. D., Malek, R. L., Letwin, N., Frank, B., Gutkind, J. S. and Lee, N. H. (2005) Autocrine activation of an osteopontin-CD44-Rac pathway enhances invasion and transformation by H-RasV12. *Oncogene* **24**, 489-501
- 185 Takafuji, V., Forgues, M., Unsworth, E., Goldsmith, P. and Wang, X. W. (2007) An osteopontin fragment is essential for tumor cell invasion in hepatocellular carcinoma. *Oncogene* **26**, 6361-6371
- 186 Fedarko, N. S., Jain, A., Karadag, A. and Fisher, L. W. (2004) Three small integrin binding ligand N-linked glycoproteins (SIBLINGs) bind and activate specific matrix metalloproteinases. *Faseb J* **18**, 734-736
- 187 Cui, R., Takahashi, F., Ohashi, R., Gu, T., Yoshioka, M., Nishio, K., Ohe, Y., Tominaga, S., Takagi, Y., Sasaki, S., Fukuchi, Y. and Takahashi, K. (2007) Abrogation of the interaction between osteopontin and α v β 3 integrin reduces tumor growth of human lung cancer cells in mice. *Lung Cancer* **57**, 302-310
- 188 Tang, H., Wang, J., Bai, F., Hong, L., Liang, J., Gao, J., Zhai, H., Lan, M., Zhang, F., Wu, K. and Fan, D. (2007) Inhibition of osteopontin would suppress angiogenesis in gastric cancer. *Biochem Cell Biol* **85**, 103-110
- 189 Bao, L. H., Sakaguchi, H., Fujimoto, J. and Tamaya, T. (2007) Osteopontin in metastatic lesions as a prognostic marker in ovarian cancers. *J Biomed Sci* **14**, 373-381
- 190 Mack, P. C., Redman, M. W., Chansky, K., Williamson, S. K., Farneth, N. C., Lara, P. N., Jr., Franklin, W. A., Le, Q. T., Crowley, J. J. and Gandara, D. R. (2008) Lower osteopontin plasma levels are associated with superior outcomes in advanced non-small-cell lung cancer patients receiving platinum-based chemotherapy: SWOG Study S0003. *J Clin Oncol* **26**, 4771-4776
- 191 Patani, N., Jiang, W. and Mokbel, K. (2008) Osteopontin C mRNA expression is associated with a poor clinical outcome in human breast cancer. *Int J Cancer* **122**, 2646

- 192 Chang, Y. S., Kim, H. J., Chang, J., Ahn, C. M., Kim, S. K. and Kim, S. K. (2007) Elevated circulating level of osteopontin is associated with advanced disease state of non-small cell lung cancer. *Lung Cancer* **57**, 373-380
- 193 Coe, F. L. and Parks, J. H. (2000) Pathogenesis and treatment of nephrolithiasis. In *The Kidney* (Seldin, D. and Giebisch, G., eds.), pp. 1841-1867, Lippincott Williams & Wilkins, Philadelphia
- 194 Brown, C. M. and Purich, D. L. (1992) Physical-chemical processes in kidney stone formation. In *Disorders of bone and mineral metabolism*, pp. 613-624, Raven Press, New York
- 195 Evan, A. P., Lingeman, J. E., Coe, F. L., Parks, J. H., Bledsoe, S. B., Shao, Y., Sommer, A. J., Paterson, R. F., Kuo, R. L. and Grynpsas, M. (2003) Randall's plaque of patients with nephrolithiasis begins in basement membranes of thin loops of Henle. *J Clin Invest* **111**, 607-616
- 196 Kim, S. C., Coe, F. L., Tinmouth, W. W., Kuo, R. L., Paterson, R. F., Parks, J. H., Munch, L. C., Evan, A. P. and Lingeman, J. E. (2005) Stone formation is proportional to papillary surface coverage by Randall's plaque. *J Urol* **173**, 117-119; discussion 119
- 197 Coe, F. L., Evan, A. and Worcester, E. (2005) Kidney stone disease. *J Clin Invest* **115**, 2598-2608
- 198 Grases, F., Costa-Bauza, A., Ramis, M., Montesinos, V. and Conte, A. (2002) Simple classification of renal calculi closely related to their micromorphology and etiology. *Clin Chim Acta* **322**, 29-36
- 199 McKee, M. D., Nanci, A. and Khan, S. R. (1995) Ultrastructural immunodetection of osteopontin and osteocalcin as major matrix components of renal calculi. *J Bone Miner Res* **10**, 1913-1929
- 200 Nakagawa, Y., Abram, V., Kezdy, F. J., Kaiser, E. T. and Coe, F. L. (1983) Purification and characterization of the principal inhibitor of calcium oxalate monohydrate crystal growth in human urine. *J Biol Chem* **258**, 12594-12600
- 201 Edyvane, K. A., Hibberd, C. M., Harnett, R. M., Marshall, V. R. and Ryall, R. L. (1987) Macromolecules inhibit calcium oxalate crystal growth and aggregation in whole human urine. *Clin Chim Acta* **167**, 329-338
- 202 Asplin, J. R., Arsenault, D., Parks, J. H., Coe, F. L. and Hoyer, J. R. (1998) Contribution of human uropontin to inhibition of calcium oxalate crystallization. *Kidney Int* **53**, 194-199
- 203 Stapleton, A. M. and Ryall, R. L. (1995) Blood coagulation proteins and urolithiasis are linked: crystal matrix protein is the F1 activation peptide of human prothrombin. *Br J Urol* **75**, 712-719
- 204 Marengo, S. R., Resnick, M. I., Yang, L. and Chung, J. Y. (1998) Differential expression of urinary inter-alpha-trypsin inhibitor trimers and dimers in normal compared to active calcium oxalate stone forming men. *J Urol* **159**, 1444-1450
- 205 Pillay, S. N., Asplin, J. R. and Coe, F. L. (1998) Evidence that calgranulin is produced by kidney cells and is an inhibitor of calcium oxalate crystallization. *Am J Physiol* **275**, F255-261
- 206 Hess, B., Nakagawa, Y., Parks, J. H. and Coe, F. L. (1991) Molecular abnormality of Tamm-Horsfall glycoprotein in calcium oxalate nephrolithiasis. *Am J Physiol* **260**, F569-578

- 207 Lian, J. B., Prien, E. L., Jr., Glimcher, M. J. and Gallop, P. M. (1977) The presence of protein-bound gamma-carboxyglutamic acid in calcium-containing renal calculi. *J Clin Invest* **59**, 1151-1157
- 208 Spector, A. R., Gray, A. and Prien, E. L., Jr. (1976) Kidney stone matrix. Differences in acidic protein composition. *Invest Urol* **13**, 387-389
- 209 Nakagawa, Y., Ahmed, M., Hall, S. L., Deganello, S. and Coe, F. L. (1987) Isolation from human calcium oxalate renal stones of nephrocalcin, a glycoprotein inhibitor of calcium oxalate crystal growth. Evidence that nephrocalcin from patients with calcium oxalate nephrolithiasis is deficient in gamma-carboxyglutamic acid. *J Clin Invest* **79**, 1782-1787
- 210 Kleinman, J. G., Beshensky, A., Worcester, E. M. and Brown, D. (1995) Expression of osteopontin, a urinary inhibitor of stone mineral crystal growth, in rat kidney. *Kidney Int* **47**, 1585-1596
- 211 Beshensky, A. M., Wesson, J. A., Worcester, E. M., Sorokina, E. J., Snyder, C. J. and Kleinman, J. G. (2001) Effects of urinary macromolecules on hydroxyapatite crystal formation. *J Am Soc Nephrol* **12**, 2108-2116
- 212 Ohri, R., Tung, E., Rajachar, R. and Giachelli, C. M. (2005) Mitigation of ectopic calcification in osteopontin-deficient mice by exogenous osteopontin. *Calcif Tissue Int* **76**, 307-315
- 213 Chalko, C., Krishna, G., Hoyer, J. R. and Goldfarb, S. (1991) Characterization of urinary uropontin excretion in humans. *J. Am. Soc. Nephrol.* **3**, 681
- 214 Min, W., Shiraga, H., Chalko, C., Goldfarb, S., Krishna, G. G. and Hoyer, J. R. (1998) Quantitative studies of human urinary excretion of uropontin. *Kidney Int* **53**, 189-193
- 215 Hoyer, J. R., Pietrzyk, R. A., Liu, H. and Whitson, P. A. (1999) Effects of microgravity on urinary osteopontin. *J Am Soc Nephrol* **10 Suppl 14**, S389-393
- 216 Shiraga, H., Min, W., VanDusen, W. J., Clayman, M. D., Miner, D., Terrell, C. H., Sherbotie, J. R., Foreman, J. W., Przysiecki, C., Neilson, E. G. and et al. (1992) Inhibition of calcium oxalate crystal growth in vitro by uropontin: another member of the aspartic acid-rich protein superfamily. *Proc Natl Acad Sci U S A* **89**, 426-430
- 217 Johnson, R. C., Leopold, J. A. and Loscalzo, J. (2006) Vascular calcification: pathobiological mechanisms and clinical implications. *Circ Res* **99**, 1044-1059
- 218 Anthea, M., Jean Hopkins, R. L., McLaughlin, C. W., Johnson, S., Warner, M. Q., LaHart, D. and Wright, J. D. (1993) *Human Biology and Health*. Prentice Hall, New Jersey
- 219 Blumenthal, H. T., A.I., L. and P.A., W. (1944) Calcification of the media of the human aorta and its relationship to intimal arteriosclerosis, again and disease. *Am J Pathol* **20**, 665-687
- 220 O'Keefe, J. H., Jr., Lavie, C. J., Nishimura, R. A. and Edwards, W. D. (1991) Degenerative aortic stenosis. One effect of the graying of America. *Postgrad Med* **89**, 143-146,151-144
- 221 Schoen, F. J., Harasaki, H., Kim, K. M., Anderson, H. C. and Levy, R. J. (1988) Biomaterial-associated calcification: pathology, mechanisms, and strategies for prevention. *J Biomed Mater Res* **22**, 11-36

- 222 Schoen, F. J. and Hobson, C. E. (1985) Anatomic analysis of removed prosthetic heart valves: causes of failure of 33 mechanical valves and 58 bioprostheses, 1980 to 1983. *Hum Pathol* **16**, 549-559
- 223 Schoen, F. J., Kujovich, J. L., Levy, R. J. and Sutton, M. S. (1988) Bioprosthetic valve failure. *Cardiovasc Clin* **18**, 289-317
- 224 Bini, A., Mann, K. G., Kudryk, B. J. and Schoen, F. J. (1999) Noncollagenous bone matrix proteins, calcification, and thrombosis in carotid artery atherosclerosis. *Arterioscler Thromb Vasc Biol* **19**, 1852-1861
- 225 Dhore, C. R., Cleutjens, J. P., Lutgens, E., Cleutjens, K. B., Geusens, P. P., Kitslaar, P. J., Tordoir, J. H., Spronk, H. M., Vermeer, C. and Daemen, M. J. (2001) Differential expression of bone matrix regulatory proteins in human atherosclerotic plaques. *Arterioscler Thromb Vasc Biol* **21**, 1998-2003
- 226 Farzaneh-Far, A., Proudfoot, D., Shanahan, C. and Weissberg, P. L. (2001) Vascular and valvar calcification: recent advances. *Heart* **85**, 13-17
- 227 Asou, Y., Rittling, S. R., Yoshitake, H., Tsuji, K., Shinomiya, K., Nifuji, A., Denhardt, D. T. and Noda, M. (2001) Osteopontin facilitates angiogenesis, accumulation of osteoclasts, and resorption in ectopic bone. *Endocrinology* **142**, 1325-1332
- 228 Giachelli, C. M., Bae, N., Almeida, M., Denhardt, D. T., Alpers, C. E. and Schwartz, S. M. (1993) Osteopontin is elevated during neointima formation in rat arteries and is a novel component of human atherosclerotic plaques. *J Clin Invest* **92**, 1686-1696
- 229 Giachelli, C. M., Liaw, L., Murry, C. E., Schwartz, S. M. and Almeida, M. (1995) Osteopontin expression in cardiovascular diseases. *Ann N Y Acad Sci* **760**, 109-126
- 230 O'Brien, E. R., Garvin, M. R., Stewart, D. K., Hinohara, T., Simpson, J. B., Schwartz, S. M. and Giachelli, C. M. (1994) Osteopontin is synthesized by macrophage, smooth muscle, and endothelial cells in primary and restenotic human coronary atherosclerotic plaques. *Arterioscler Thromb* **14**, 1648-1656
- 231 Ikeda, T., Shirasawa, T., Esaki, Y., Yoshiki, S. and Hirokawa, K. (1993) Osteopontin mRNA is expressed by smooth muscle-derived foam cells in human atherosclerotic lesions of the aorta. *J Clin Invest* **92**, 2814-2820
- 232 Hirota, S., Imakita, M., Kohri, K., Ito, A., Morii, E., Adachi, S., Kim, H. M., Kitamura, Y., Yutani, C. and Nomura, S. (1993) Expression of osteopontin messenger RNA by macrophages in atherosclerotic plaques. A possible association with calcification. *Am J Pathol* **143**, 1003-1008
- 233 Fitzpatrick, L. A., Severson, A., Edwards, W. D. and Ingram, R. T. (1994) Diffuse calcification in human coronary arteries. Association of osteopontin with atherosclerosis. *J Clin Invest* **94**, 1597-1604
- 234 Giachelli, C. M., Scatena, M. and Wada, T. (1997) Osteopontin: potential roles in vascular function and dystrophic calcification. *J. Bone Miner. Metab.* **15**, 179-183
- 235 O'Brien, K. D., Kuusisto, J., Reichenbach, D. D., Ferguson, M., Giachelli, C., Alpers, C. E. and Otto, C. M. (1995) Osteopontin is expressed in human aortic valvular lesions. *Circulation* **92**, 2163-2168

- 236 Shen, M., Marie, P., Farge, D., Carpentier, S., De Pollak, C., Hott, M., Chen, L., Martinet, B. and Carpentier, A. (1997) Osteopontin is associated with bioprosthetic heart valve calcification in humans. *C R Acad Sci III* **320**, 49-57
- 237 Srivatsa, S. S., Harrity, P. J., Maercklein, P. B., Kleppe, L., Veinot, J., Edwards, W. D., Johnson, C. M. and Fitzpatrick, L. A. (1997) Increased cellular expression of matrix proteins that regulate mineralization is associated with calcification of native human and porcine xenograft bioprosthetic heart valves. *J Clin Invest* **99**, 996-1009
- 238 Ohmori, R., Momiyama, Y., Taniguchi, H., Takahashi, R., Kusuhara, M., Nakamura, H. and Ohsuzu, F. (2003) Plasma osteopontin levels are associated with the presence and extent of coronary artery disease. *Atherosclerosis* **170**, 333-337
- 239 Kadoglou, N. P., Gerasimidis, T., Golemati, S., Kapelouzou, A., Karayannacos, P. E. and Liapis, C. D. (2008) The relationship between serum levels of vascular calcification inhibitors and carotid plaque vulnerability. *J Vasc Surg* **47**, 55-62
- 240 Burke, A. P., Taylor, A., Farb, A., Malcom, G. T. and Virmani, R. (2000) Coronary calcification: insights from sudden coronary death victims. *Z Kardiol* **89 Suppl 2**, 49-53
- 241 Speer, M. Y., McKee, M. D., Guldberg, R. E., Liaw, L., Yang, H. Y., Tung, E., Karsenty, G. and Giachelli, C. M. (2002) Inactivation of the osteopontin gene enhances vascular calcification of matrix Gla protein-deficient mice: evidence for osteopontin as an inducible inhibitor of vascular calcification in vivo. *J Exp Med* **196**, 1047-1055
- 242 De Yoreo, J. J. and Vekilov, P. G. (2003) Principles of Crystal Nucleation and Growth. *Reviews in Mineralogy & Geochemistry* **54**, 57-93
- 243 Fletcher, N. H. (1958) Size Effect in Heterogeneous Nucleation. *The Journal of Chemical Physics* **3**, 572-576
- 244 Chernov, A. A. (1961) The Spiral Growth of Crystals. *Physics-Uspekhi* **4**, 116-148
- 245 Land, T. A., De Yoreo, J. J. and Lee, J. J. (1997) *In situ* AFM investigation of canavalin crystallization kinetics. *Surf Sci* **384**, 136
- 246 Frank, F. C. (1949) Influence of Dislocations on Crystal Growth. *Discussions of the Faraday Society* **5**, 48-54
- 247 Cabrera, N. and Vermileya, D. A. (1959) *Growth and Perfection of Crystals*. John Wiley & Sons, New York
- 248 Williams, R. J. P. (1984) An Introduction to Biominerals and the Role of Organic Molecules in Their Formation. *Philosophical Transactions of the Royal Society of London* **304**, 411-424
- 249 Currey, J. D. (1999) The design of mineralised hard tissues for their mechanical functions. *J Exp Biol* **202**, 3285-3294
- 250 Thiele, H. and Awad, A. (1969) Nucleation and oriented crystallization apatite in ionotropic gels. *J Biomed Mater Res* **3**, 431-441
- 251 Crenshaw, M. A. and Ristedt, H. (1975) Histochemical and structural study of nautiloid septal nacre. *Biomineralization* **8**, 1-8
- 252 Lowenstam, H. A. and Weiner, S. (1989) *On Biomineralization*. Oxford University Press, USA

- 253 Nudelman, F., Gotliv, B. A., Addadi, L. and Weiner, S. (2006) Mollusk shell formation: mapping the distribution of organic matrix components underlying a single aragonitic tablet in nacre. *J Struct Biol* **153**, 176-187
- 254 Gilbert, P. U. P. A., Abrecht, M. and Frazer, B. H. (2005) The Organic-Mineral Interface in Biomaterials. *Reviews in Mineralogy & Geochemistry* **59**, 157-185
- 255 Kamat, S., Su, X., Ballarini, R. and Heuer, A. H. (2000) Structural basis for the fracture toughness of the shell of the conch *Strombus gigas*. *Nature* **405**, 1036-1040
- 256 Currey, J. D. (2005) Materials science. Hierarchies in biomineral structures. *Science* **309**, 253-254
- 257 Krause, J. W. (2005) *Krause's Essential Human Histology for Medical Students*. Universal-Publishers
- 258 Falini, G., Albeck, S., Weiner, S. and Addadi, L. (1996) Control of aragonite or calcite polymorphism by mollusk shell macromolecules. *Science* **271**, 67-69
- 259 He, G., Dahl, T., Veis, A. and George, A. (2003) Dentin matrix protein 1 initiates hydroxyapatite formation in vitro. *Connect Tissue Res* **44 Suppl 1**, 240-245
- 260 He, G., Dahl, T., Veis, A. and George, A. (2003) Nucleation of apatite crystals in vitro by self-assembled dentin matrix protein 1. *Nat Mater* **2**, 552-558
- 261 Kasugai, S., Nagata, T. and Sodek, J. (1992) Temporal studies on the tissue compartmentalization of bone sialoprotein (BSP), osteopontin (OPN), and SPARC protein during bone formation in vitro. *J Cell Physiol* **152**, 467-477
- 262 Tye, C. E., Hunter, G. K. and Goldberg, H. A. (2005) Identification of the type I collagen-binding domain of bone sialoprotein and characterization of the mechanism of interaction. *J Biol Chem* **280**, 13487-13492
- 263 Wang, A., Martin, J. A., Lembke, L. A. and Midura, R. J. (2000) Reversible suppression of in vitro biomineralization by activation of protein kinase A. *J Biol Chem* **275**, 11082-11091
- 264 Fernandez, M. S., Escobar, C., Lavelin, I., Pines, M. and Arias, J. L. (2003) Localization of osteopontin in oviduct tissue and eggshell during different stages of the avian egg laying cycle. *J Struct Biol* **143**, 171-180
- 265 Pines, M., Knopov, V. and Bar, A. (1995) Involvement of osteopontin in egg shell formation in the laying chicken. *Matrix Biol* **14**, 765-771
- 266 Richardson, C. F., Johnsson, M., Raj, P. A., Levine, M. J. and Nancollas, G. H. (1993) The Influence of Histatin-5 Fragments on the Mineralization of Hydroxyapatite. *Archives of Oral Biology* **38**, 997-1002
- 267 Hincke, M. T. and St. Maurice, M. (2000) *Chemical Biology of Mineralized Tissues*. American Academy of Orthopaedic Surgeons, Rosemont, Illinois
- 268 Worcester, E. M., Blumenthal, S. S., Beshensky, A. M. and Lewand, D. L. (1992) The calcium oxalate crystal growth inhibitor protein produced by mouse kidney cortical cells in culture is osteopontin. *J Bone Miner Res* **7**, 1029-1036
- 269 Pampana, D. A., Robertson, K. A., Litvinova, O., Lajoie, G., Goldberg, H. A. and Hunter, G. K. (2004) Inhibition of hydroxyapatite formation by osteopontin phosphopeptides. *Biochem J* **378**, 1083-1087
- 270 Wada, T., McKee, M. D., Steitz, S. and Giachelli, C. M. (1999) Calcification of vascular smooth muscle cell cultures: inhibition by osteopontin. *Circ Res* **84**, 166-178

- 271 Mo, L., Huang, H. Y., Zhu, X. H., Shapiro, E., Hasty, D. L. and Wu, X. R. (2004) Tamm-Horsfall protein is a critical renal defense factor protecting against calcium oxalate crystal formation. *Kidney Int* **66**, 1159-1166
- 272 Hoyer, J. R., Asplin, J. R. and Otvos, L. (2001) Phosphorylated osteopontin peptides suppress crystallization by inhibiting the growth of calcium oxalate crystals. *Kidney Int* **60**, 77-82
- 273 Taller, A., Grohe, B., Rogers, K. A., Goldberg, H. A. and Hunter, G. K. (2007) Specific adsorption of osteopontin and synthetic polypeptides to calcium oxalate monohydrate crystals. *Biophys J* **93**, 1768-1777
- 274 McDiarmid, R. and Doty, P. (1966) The spectrophotometric titration of polyacrylic, poly-L-aspartic, and poly-L-glutamic acids. *J Phys Chem* **70**, 2620-2627
- 275 Goldberg, H. A. and Hunter, G. K. (1995) The inhibitory activity of osteopontin on hydroxyapatite formation in vitro. *Ann N Y Acad Sci* **760**, 305-308
- 276 Tsortos, A. and Nancollas, G. H. (2002) The role of polycarboxylic acids in calcium phosphate mineralization. *J Colloid Interface Sci* **250**, 159-167
- 277 Fujisawa, R., Kuboki, Y. and Sasaki, S. (1986) Changes in interaction of bovine dentin phosphophoryn with calcium and hydroxyapatite by chemical modifications. *Calcif Tissue Int* **39**, 248-251
- 278 Romberg, R. W., Werness, P. G., Riggs, B. L. and Mann, K. G. (1986) Inhibition of hydroxyapatite crystal growth by bone-specific and other calcium-binding proteins. *Biochemistry* **25**, 1176-1180
- 279 Wikiel, K., Burke, E. M., Perich, J. W., Reynolds, E. C. and Nancollas, G. H. (1994) Hydroxyapatite Mineralization and Demineralization in the Presence of Synthetic Phosphorylated Pentapeptides. *Archives of Oral Biology* **39**, 715-721
- 280 Lenstrup, E. (1926) The Phosphorous Content of Human Milk and Cow's Milk. *J Biol Chem* **70**, 193-202
- 281 Verma, I. S. and Sommer, H. H. (1957) The Study of the Naturally Occurring Salts in Milk. *The Journal of Dairy Science* **40**, 331-335
- 282 Langdon, A., Wignall, G. R., Rogers, K., Sorensen, E. S., Denstedt, J., Grohe, B., Goldberg, H. A. and Hunter, G. K. (2009) Kinetics of calcium oxalate crystal growth in the presence of osteopontin isoforms: an analysis by scanning confocal interference microscopy. *Calcif Tissue Int* **84**, 240-248
- 283 Grohe, B., O'Young, J., Ionescu, D. A., Lajoie, G., Rogers, K. A., Karttunen, M., Goldberg, H. A. and Hunter, G. K. (2007) Control of calcium oxalate crystal growth by face-specific adsorption of an osteopontin phosphopeptide. *J Am Chem Soc* **129**, 14946-14951
- 284 Moreno, E. C., Kresak, M. and Hay, D. I. (1984) Adsorption of molecules of biological interest onto hydroxyapatite. *Calcif Tissue Int* **36**, 48-59
- 285 Goobes, R., Goobes, G., Campbell, C. T. and Stayton, P. S. (2006) Thermodynamics of statherin adsorption onto hydroxyapatite. *Biochemistry* **45**, 5576-5586
- 286 Nancollas, G. H. and Mohan, M. S. (1970) The growth of hydroxyapatite crystals. *Arch Oral Biol* **15**, 731-745
- 287 Tomson, M. B. and Nancollas, G. H. (1978) Mineralization Kinetics: A Constant Composition Approach. *Science* **200**, 1059-1060

- 288 Nancollas, G. H. and Tomazic, B. (1974) Growth of calcium phosphate on hydroxyapatite crystals. Effect of supersaturation and ionic medium. *J. Phys. Chem.* **78**, 2218-2225
- 289 Sorensen, E. S. and Petersen, T. E. (1993) Purification and characterization of three proteins isolated from the proteose peptone fraction of bovine milk. *J Dairy Res* **60**, 189-197
- 290 Johnson, W. C. (1999) Analyzing protein circular dichroism spectra for accurate secondary structures. *Proteins* **35**, 307-312
- 291 Provencher, S. W. and Glockner, J. (1981) Estimation of globular protein secondary structure from circular dichroism. *Biochemistry* **20**, 33-37
- 292 Vogel, H. J. (1989) Phosphorus-31 nuclear magnetic resonance of phosphoproteins. *Methods Enzymol* **177**, 263-282
- 293 Robitaille, P. L., Robitaille, P. A., Brown Jr., G. G. and Brown, G. G. (1991) An analysis of the pH-dependent chemical-shift behavior of phosphorus-containing metabolites. *Journal of Magnetic Resonance* (1969) **92**, 73-84
- 294 Wojciechowski, M., Grycuk, T., Antosiewicz, J. M. and Lesyng, B. (2003) Prediction of secondary ionization of the phosphate group in phosphotyrosine peptides. *Biophys J* **84**, 750-756
- 295 Nielsen, A. E. and Christoffersen, J. (1982) The mechanism of crystallization and dissolution. Dahlem Konferenzen, Berlin, Germany
- 296 Burton, W. K., Cabrera, N. and Frank, F. C. (1951) The Growth of Crystals and the Equilibrium Structure of their Surfaces. *Philosophical Transactions of the Royal Society of London* **243**, 299-358
- 297 Nancollas, G. H. and Zawacki, S. J. (1984) Inhibitors of crystallization and dissolution. Elsevier, Amsterdam
- 298 Gilman, H. and Hukins, D. W. (1994) Seeded growth of hydroxyapatite in the presence of dissolved albumin at constant composition. *J Inorg Biochem* **55**, 31-39
- 299 Finn, B. E., Evenas, J., Drakenberg, T., Waltho, J. P., Thulin, E. and Forsen, S. (1995) Calcium-induced structural changes and domain autonomy in calmodulin. *Nat Struct Biol* **2**, 777-783
- 300 Penel, S., Morrison, R. G., Mortishire-Smith, R. J. and Doig, A. J. (1999) Periodicity in alpha-helix lengths and C-capping preferences. *J Mol Biol* **293**, 1211-1219
- 301 Shoemaker, K. R., Kim, P. S., Brems, D. N., Marqusee, S., York, E. J., Chaiken, I. M., Stewart, J. M. and Baldwin, R. L. (1985) Nature of the charged-group effect on the stability of the C-peptide helix. *Proc Natl Acad Sci U S A* **82**, 2349-2353
- 302 Sreerama, N. and Woody, R. W. (2000) Estimation of protein secondary structure from circular dichroism spectra: comparison of CONTIN, SELCON, and CDSSTR methods with an expanded reference set. *Anal Biochem* **287**, 252-260
- 303 Greenfield, N. J. (1996) Methods to estimate the conformation of proteins and polypeptides from circular dichroism data. *Anal Biochem* **235**, 1-10
- 304 Nemethy, G. and Printz, M. P. (1972) The γ Turn, a Possible Folded Conformation of the Polypeptide Chain. Comparison with the β Turn. *Macromolecules* **5**, 755-758
- 305 Voet, D. and Voet, J. G. (2004) *Biochemistry*. J. Wiley & Sons, Hoboken, NJ

- 306 Pelton, J. T. and McLean, L. R. (2000) Spectroscopic methods for analysis of
protein secondary structure. *Anal Biochem* **277**, 167-176
- 307 Pierce, M. M., Raman, C. S. and Nall, B. T. (1999) Isothermal titration
calorimetry of protein-protein interactions. *Methods* **19**, 213-221
- 308 Goobes, R., Goobes, G., Shaw, W. J., Drobny, G. P., Campbell, C. T. and
Stayton, P. S. (2007) Thermodynamic roles of basic amino acids in statherin
recognition of hydroxyapatite. *Biochemistry* **46**, 4725-4733
- 309 Goldberg, H. A., Warner, K. J., Li, M. C. and Hunter, G. K. (2001) Binding of
bone sialoprotein, osteopontin and synthetic polypeptides to hydroxyapatite.
Connect Tissue Res **42**, 25-37
- 310 Robinson, G. W. and Cho, C. H. (1999) Role of hydration water in protein
unfolding. *Biophys J* **77**, 3311-3318
- 311 Privalov, P. L. and Makhatadze, G. I. (1993) Contribution of hydration to protein
folding thermodynamics. II. The entropy and Gibbs energy of hydration. *J Mol
Biol* **232**, 660-679
- 312 Radtchenko, I. L., Sukhorukov, G. B., Leporatti, S., Khomutov, G. B., Donath, E.
and Mohwald, H. (2000) Assembly of Alternated Multivalent Ion/Polyelectrolyte
Layers on Colloidal Particles. Stability of the Multilayers and Encapsulation of
Macromolecules into Polyelectrolyte Capsules. *J Colloid Interface Sci* **230**, 272-
280
- 313 Nancollas, G. H. and Budz, J. A. (1990) Analysis of particle size distribution of
hydroxyapatite crystallites in the presence of synthetic and natural polymers. *J
Dent Res* **69**, 1678-1685
- 314 Raj, P. A., Johnsson, M., Levine, M. J. and Nancollas, G. H. (1992) Salivary
Statherin - Dependence on Sequence, Charge, Hydrogen-Bonding Potency, and
Helical Conformation for Adsorption to Hydroxyapatite and Inhibition of
Mineralization. *Journal of Biological Chemistry* **267**, 5968-5976
- 315 Johnsson, M., Richardson, C. F., Bergey, E. J., Levine, M. J. and Nancollas, G. H.
(1991) The effects of human salivary cystatins and statherin on hydroxyapatite
crystallization. *Arch Oral Biol* **36**, 631-636
- 316 Kaartinen, M. T., Murshed, M., Karsenty, G. and McKee, M. D. (2007)
Osteopontin upregulation and polymerization by transglutaminase 2 in calcified
arteries of Matrix Gla protein-deficient mice. *J Histochem Cytochem* **55**, 375-386
- 317 O'Young, J., Karttunen, M., Goldberg, H. A. and Hunter, G. K. (2009) Charge
and Conformation in Adsorption of Osteopontin to Hydroxyapatite. In
IADR/AADR/CADR 87th General Session and Exhibition, pp. 83, International
Association of Dental Research, Miami, FL
- 318 Flogel, M. and Biltonen, R. L. (1975) The pH dependence of the thermodynamics
of the interaction of 3'-cytidine monophosphate with ribonuclease A.
Biochemistry **14**, 2610-2615
- 319 Morin, P. E. and Freire, E. (1991) Direct calorimetric analysis of the enzymatic
activity of yeast cytochrome c oxidase. *Biochemistry* **30**, 8494-8500
- 320 Beschiaschvili, G. and Seelig, J. (1992) Peptide binding to lipid bilayers.
Nonclassical hydrophobic effect and membrane-induced pK shifts. *Biochemistry*
31, 10044-10053